THE CLASSICAL-LIMIT S-MATRIX FOR HEAVY ION SCATTERING

Raul Jose Donangelo
(Ph. D. thesis)

January 1977

Prepared for the U. S. Energy Research and
Development Administration under Contract W-7405-ENG-48

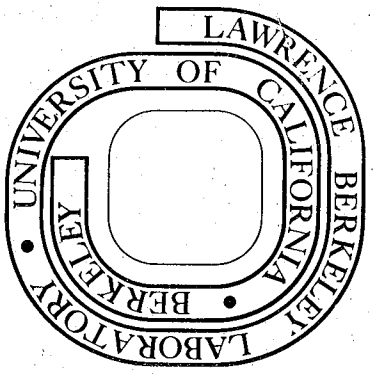

TABLE OF CONTENTS

ACKNOWLEDGMENTS

I wish to express my sincere gratitude to Professor John O. Rasmussen, who directed this research work. His guidance, encouragement and strong support in all phases of this work were essential to make it possible.

Much of the material included in this thesis is the result of a most fruitful collaboration with Drs. Jean-Paul Boisson and Mike W. Guidry. Our work together was a most enjoyable experience to me.

I thank Dr. Herbert Massmann for his invaluable help in getting me started into the topic of this research. In the late stages of this work I benefited greatly from discussions with my fellow graduate student Luiz F. Oliveira whose fresh look served to polish several points in the presentation. I am also indebted to Professor William H. Miller and Drs. Frank S. Stephens and Wladislaw Swiatecki for stimulating discussions and suggestions.

The fine typing of Mrs. Paula Bjork and the excellent drawing of Mrs. Nancy Monroe are deeply appreciated.

I would like to express a sincere debt of gratitude to a multitude of other people, too numerous to mention by name, who with their teaching and friendship have helped me to take all the steps needed to reach this goal.

In particular my wife, Carmen, and my children, Ines and Andres, were a source of cheerfulness and motivation during this work. To them and to my parents is dedicated this thesis.

I gratefully acknowledge financial support from a Fulbright Fellowship and an International Atomic Energy Agency Fellowship during different stages of this work. This research was done under the auspices of the U.S. Energy Research and Development Administration.

The Classical-Limit S-Matrix for Heavy Ion Scattering

by

Raul Jose Donangelo

ABSTRACT

An integral representation for the classical limit of the quantum mechanical S-matrix is developed and applied to heavy-ion Coulomb excitation and Coulomb-nuclear interference.

The method combines the quantum principle of superposition with exact classical dynamics to describe the projectile-target system. A detailed consideration of the classical trajectories and of the dimensionless parameters that characterize the system is carried out.

The results are compared, where possible, to exact quantum mechanical calculations and to conventional semiclassical calculations. We find that in the case of backscattering the classical limit S-matrix method is able to almost exactly reproduce the quantum-mechanical S-matrix elements, and therefore the transition probabilities, even for projectiles as light as protons. The results also suggest that this approach should be a better approximation for heavy-ion multiple Coulomb excitation than earlier semiclassical methods, due to a more accurate description of the classical orbits in the electromagnetic field of the target nucleus.

Calculations using this method indicate that the rotational excitation probabilities in the Coulomb-nuclear interference region should be very sensitive to the details of the potential at the surface of the nucleus, suggesting that heavy-ion rotational excitation could constitute a sensitive probe of the nuclear potential in this region.

The application to other problems as well as the present limits of applicability of the formalism are also discussed.

I. INTRODUCTION

The collective low-lying states of the nucleus are amenable to a classical description in terms of oscillations in the shape of the nuclear surface or of rotations of the nuclear body.

In the study of these states the fact that they can be excited by the electromagnetic field of charged projectiles was first pointed out by Mottelson[1,2] in the early 1950's, and very shortly after experimentally verified.[3,4] This process, generally carried out at energies below the Coulomb barrier and known as Coulomb excitation, became an important tool in the study of nuclear structure. One of the strongest reasons for this is the good understanding of the nature of electromagnetic interactions, whereas the strong interactions manifested in the short-range nuclear force are less well known.

Initially only light ions were available as projectiles to the experimenters, so that only the lowest energy collective states were excited by the electromagnetic field, and the theory developed by Alder et al.[5] could explain the experimental results in full detail. More recently the construction of heavy ion accelerators made feasible the study of multiple Coulomb excitation processes, in which through the strong electric field of the heavy projectile the target nucleus absorbs several quanta, and many nuclear states can be populated. This pushed the old theoretical methods to their limits. Thus, stimulated by the world-wide interest in heavy ion induced reactions, theorists attacked this more complex problem by different methods.

It was soon seen that the purely quantum mechanical methods, such as the coupled-channel Born approximation, which could describe fairly accurately the collision process in the case of light projectiles could not handle the case of heavy ions due to the much larger number of partial waves and channels involved in the calculation. The most sophisticated coupled-channel computer code available now[6] can handle only cases for which the Sommerfeld parameter η is less than 30 (the number of partial waves that need to be included in the calculation is proportional to η), while with the heavy ion beams available today Coulomb excitation experiments for which η is about 400 are already performed, and in the near future it will be possible to use ^{238}U beams to perform these experiments, which will raise the value of η to about 550. For these cases a coupled-channel quantum mechanical calculation is completely impossible at the present time.

However, this increase in the value of η, which makes the problem intractable by quantum mechanical methods, brings it closer to the realm of classical mechanics, since the Sommerfeld parameter is inversely proportional to the de Broglie wavelength.

This fact is the basis for the different semiclassical theories that were used to find approximate solutions to the problem. In the method of Alder and Winther[7] the relative motion of projectile and target is described classically, and the trajectory of the projectile is assumed to be a hyperbola. The target is described in quantum mechanical terms by means of coupled-channel equations relating the different excited states. This method is the foundation for the

Winther-de Boer code for Coulomb excitation,[8] the most widely used at present to analyze experimental data.

A new approach appeared a few years ago, which can be derived from Feynman's path integral formulation of Quantum Mechanics; it is known under the name Uniform Semiclassical Approximation (USCA), and was developed mostly by W. H. Miller[10-18] to study atomic and molecular collisions. More recently it was applied to the nuclear case[19-22] and more specifically, also to the problem of Coulomb excitation[23-25] and Coulomb-nuclear interference.[26] In this method one evaluates Feynman's path integral for the S-matrix by means of stationary phase integration. It is easily seen[10] that the trajectories for which the integrand in Feynman's expression for the S-matrix is stationary are, for a given transition, those classical trajectories that satisfy the quantized boundary conditions for the transition studied. For example, for the Coulomb excitation of a deformed even-even nucleus in its ground state, to find the S-matrix between the ground state and, say, the 4^+ state, one has to find the classical trajectories which have initial value of the nuclear spin equal to zero, and final value of the nuclear spin equal to that of the 4^+ state. This implies that to obtain these trajectories one has to search for the initial values of the internal degrees of freedom of the target (its orientation relative to the beam axis in our example), which evolve into the desired final boundary conditions (the final spin in our example). After this is done, the evaluation of Feynman's path integral by stationary phase methods is rather straightforward.

This method is obviously restricted to cases for which a classical model can be formulated to describe the system. From what we pointed out at the beginning, this restriction does not exclude the collective, low lying states that are excited in the Coulomb excitation process.

Almost simultaneously with the introduction of the USCA, R. A. Marcus[27-36] and W. H. Miller,[10-18] among others, found another way of evaluating by classical methods the S-matrix. In this formulation classical mechanical trajectories are used to construct the wavefunction of the system in the asymptotic region. The elements of the S-matrix are then obtained by projecting the system wavefunction onto the final channels. This leads to another integral expression for the S-matrix but where now the integral is not over all possible paths as in Feynman's expression, but over the initial values of the internal degrees of freedom of the target, so that in this form it is possible to evaluate directly the integral instead of approximating it by stationary phase methods. This has the practical advantage that eliminates the need for a root search, which may become extremely difficult when the target has several internal degrees of freedom and/or when the transitions being considered are not classically allowed (this means that for no real initial value of the internal degrees of freedom the final boundary conditions are satisfied), and in which cases the root search has to be extended to complex initial values.

In order to avoid confusion when referring to these methods we will keep the name USCA for the root search method derived from Feynman's expression for the S-matrix, and we will follow Miller in using the designation Classical-Limit S-Matrix (CLSM) for the integral

expression based upon the wavefunction constructed using classical trajectories. The practical application of these methods is rather different, but the theoretical bases are related. Figure I-1 shows schematically how they are connected, and describes also the essentials of the semiclassical Alder-Winther (A-W) method, which will also be extensively referred to in this work.

The main objective of this thesis is the application of the CLSM formalism to several scattering problems in nuclear physics.

In Chapter II we will develop the CLSM formalism for the case of Coulomb excitation of rotational states of deformed nuclei by back-scattering of heavy ions. This will imply the study of the classical trajectories followed by this system and the dimensionless quantities that govern them. The connection with the USCA and the discussion of a limiting case where analytical solutions exist for the CLSM, Alder-Winther and quantum mechanical methods is also included in this chapter. An extensive comparison of the CLSM formalism (Chapter II) to the Alder-Winther semiclassical theory and to quantum mechanics is carried out in Chapter III. The effect of the approximate dynamics employed by the A-W method and the region of applicability of the CLSM formalism are discussed for this case.

In Chapter IV we extend the CLSM formalism for this problem to include a complex nuclear interaction between the projectile and the deformed target. This will imply the use of complex classical trajectories, but it is shown that the CLSM formalism may be used without changes. The study of the Coulomb-nuclear interference pattern of the excitation probabilities for a particular system suggests that

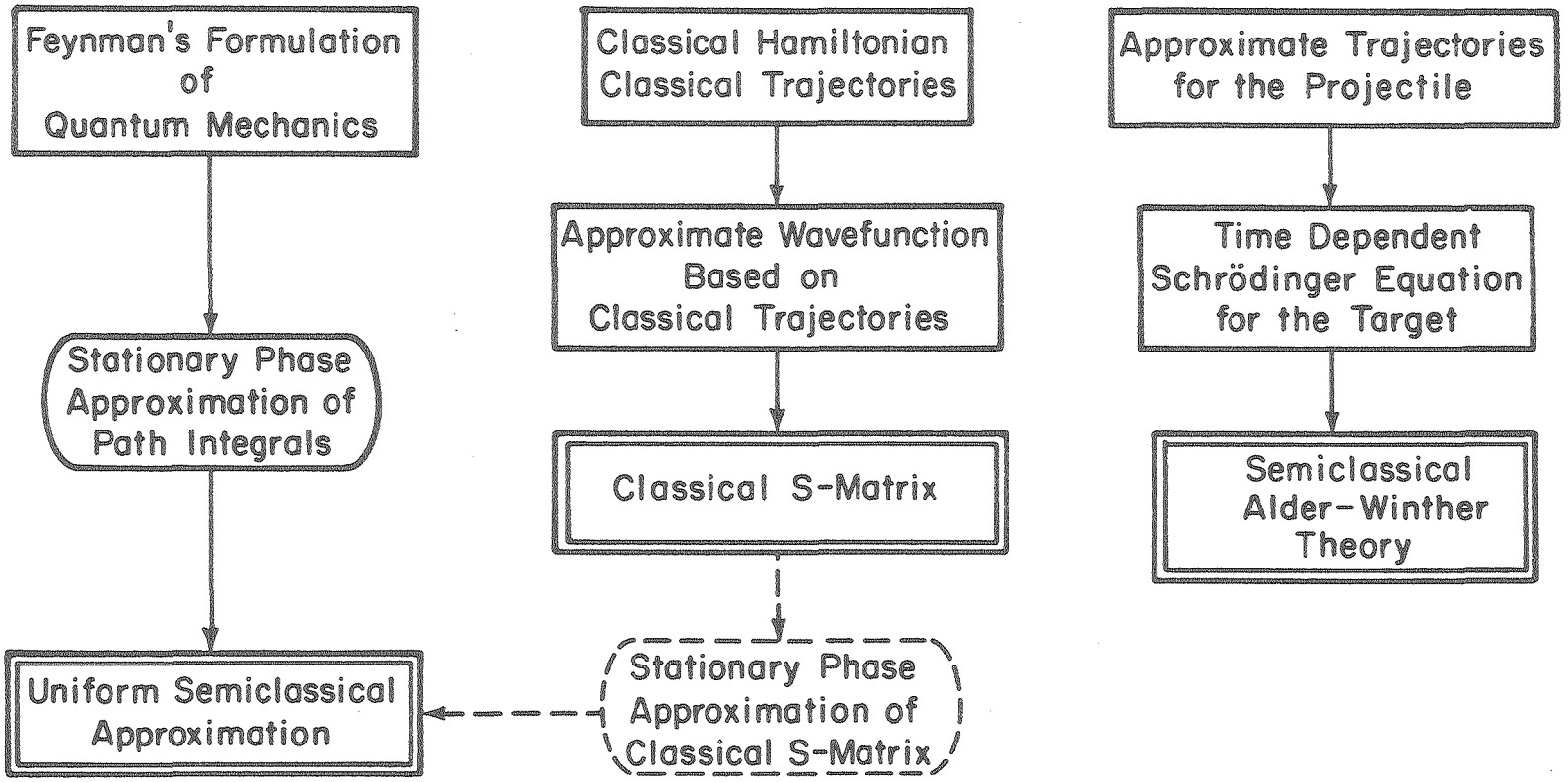

Fig. I-1 Diagram showing the calculational steps used in the different approaches and the connection between the USCA and CLSM methods.

XBL 775-8584

experiments of this sort could provide detailed information on the potential in the nuclear surface region.

Chapter V discusses the application of the CLSM method to several scattering problems and their present status. Included here are the generalization to non-backward angles of the formalism presented in Chapter II, the study of the Coulomb excitation of the K = 0 octupole vibration-rotation band in ^{238}U, and finally the problem of one-nucleon and cluster transfer in the collision of two nuclei, one of which is deformed, at energies about the Coulomb barrier.

In Chapter VI we present our conclusions.

Appendices A and B briefly summarize the USCA and Alder-Winther theories to which frequent references are made.

II. THE CLASSICAL-LIMIT S-MATRIX FOR COULOMB EXCITATION OF ROTATIONAL STATES

1. Introduction

The collective model is able to account for the large values of the electric quadrupole moment found in many nuclei by assuming that these nuclei have a permanent non-spherical shape. In this chapter we will focus our attention on the excitation of the rotational states of these deformed nuclei through the electromagnetic interaction with a nuclear projectile.

We shall especially consider even-even nuclei with an axially symmetric shape. If we denote by $\mathcal{J}$ the moment of inertia of such a nucleus with respect to an axis perpendicular to the symmetry axis, and by $\vec{I}$ the angular momentum operator, the Hamiltonian is simply given by

$$H = \frac{\hbar^2 \vec{I}^2}{2\mathcal{J}} \tag{1}$$

The eigenfunctions and eigenvalues of this Hamiltonian are given by

$$\phi_{IM} = Y_{IM}(\theta,\phi)$$
$$E_I = \frac{\hbar^2 I(I+1)}{2\mathcal{J}} \tag{2}$$

where Y_{IM} is the spherical harmonic function, I and M the total and magnetic angular momentum quantum numbers, and θ and ϕ the polar angles of the symmetry axis in a laboratory-fixed frame.

Since our nucleus is invariant under a rotation by π about any axis perpendicular to the symmetry axis, its wavefunction should be invariant under the transformation

$$\theta \to \pi - \theta, \quad \phi \to \pi + \phi$$

therefore, only states with even I are allowed.

For simplicity we will restrict ourselves in this chapter to the head-on-case, namely the case for which the relative motion angular momentum is initially equal to zero. The target nucleus is initially in its ground state, so that its angular momentum is zero. In these conditions the relative motion takes place in a plane; the angular momenta of the relative motion and of the target nucleus have a sum always equal to zero and are both of them perpendicular to this plane. By taking the Z-axis in this plane the projection M of the target angular momentum on this axis will be always zero, so we will not need to consider it in our calculations. To simplify the notation we will omit the subindex $M = 0$ in what follows.

We are interested in knowing the final state of the target, after the interaction has taken place. At the present time we cannot think of solving the Schrödinger equation for this system since it is a partial differential equation in four or more variables. This equation is reducible to a system of coupled channel radial equations, which can be numerically solved for systems such that the number of channels and states involved is not too high. In practice this reduces the present range of applicability of the coupled channel method in the study of Coulomb excitation to "light" systems, meaning by light systems those

for which the Sommerfeld parameter (to be defined in the next section) is less or equal to 30, and the excitation of states with spin larger than 10 can be neglected. Therefore it cannot be applied to study those cases of most practical interest, in which a heavy projectile excites high angular momentum states of an also heavy target nucleus.

Our approach to this problem will be to construct an approximate wavefunction, based on the study of the classical trajectories for this multidimensional system, and by means of it to evaluate the elements of the scattering matrix (S-matrix in what follows). The range of applicability of this approach will be seen to be quite wide.

2. Expression for the Classical-limit S-matrix[41]

We will take as coordinates to describe our system the following: χ , the angle defined by the symmetry axis of the target and the line joining the centers of projectile and target, and r , the distance between these centers. We denote by p_χ the angular momentum of the target and by v the relative velocity. Figure II-1 illustrates. Since the motion takes place in a plane, as we pointed out in the previous section, we do not need an additional azimuthal angle to determine the system.

Let ψ^+ be the scattered part of the eigenstate of the system corresponding to the initial conditions already mentioned (zero angular momentum for both the relative motion and the target).

The usual definition of the S-matrix (Ref. 37. 121 ff or many other quantum mechanics textbooks) gives

$$S_{0 \to I}\, \delta(E - E') = \langle IE' | \psi^+ \rangle \qquad (3)$$

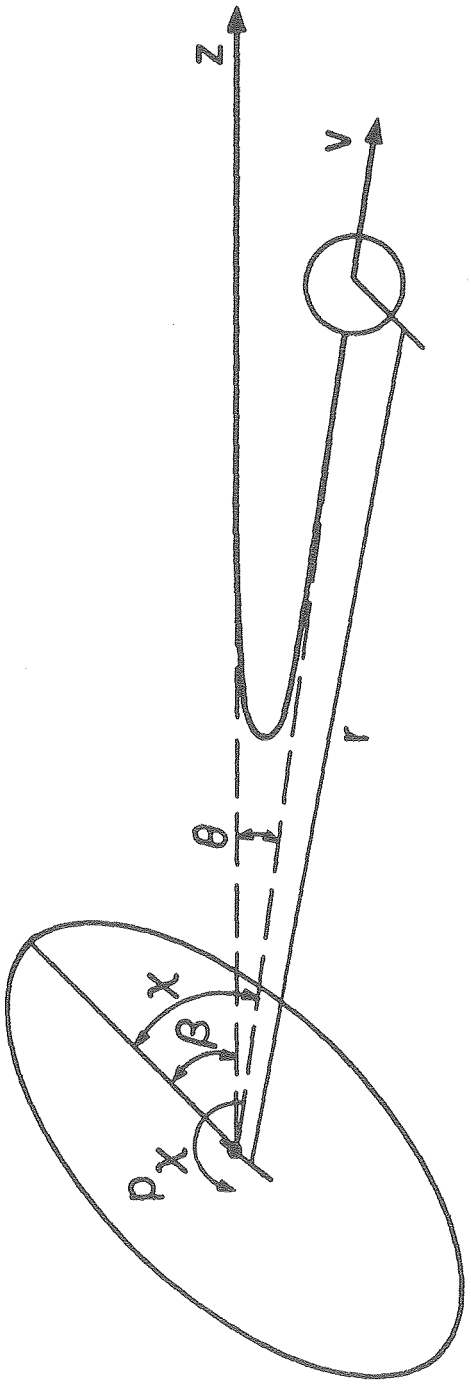

XBL 774-8297

Fig. II-1 Coordinates describing the geometry of the physical system.

where E is the energy of the state ψ^+ and $|IE'>$ is an eigenstate corresponding to a spin I of the target and an energy E' of the Hamiltonian of the system consisting only of the kinetic energy and monopole-monopole Coulomb interaction terms.

Taking χ and r as coordinates to represent the wavefuntions (it will be shown later that the Hamiltonian is depending only upon χ, r and their conjugate momenta)

$$<IE'|\psi^+> = \iint \Phi_I^*(\chi,r)\ \psi^+(\chi,r)\ 2\pi r^2 \sin\chi\ d\chi\ dr \tag{4}$$

The eigenfunction $\Phi_I(\chi,r)$ can be separated as the product of a spherical harmonic $Y_{I0}(\cos\chi)$ and a Coulomb wave function. In particular in the asymptotic region (for large values of r) it will be given by

$$\Phi_I(\chi,r) \sim \frac{1}{\sqrt{2\pi}} \sqrt{\frac{v_I}{v_0}}\, Y_{I0}(\cos\chi)\ \frac{1}{r}\, e^{-i[p_{r_I} r/\hbar - \eta_I \ell n(2p_{r_I} r/\hbar) + \sigma_I(\eta_I)]} \tag{5}$$

where v_0 is the initial asymptotic velocity, v_I is the final asymptotic velocity corresponding to a spin quantum number I, p_{r_I} the relative radial momentum in this case, and η_I the Sommerfeld parameter

$$\eta_I = \frac{Z_p Z_T e^2}{\hbar\, v_I} \tag{6}$$

Here Z_p and Z_T are the atomic numbers of projectile and target, respectively, and e the electronic charge. $\sigma_I(\eta_I) = \mathrm{Arg}[1 + I + i\eta_I]$ is the usual Coulomb phaseshift.

We write the wavefunction $\psi^+(\chi,r)$ in the following way:

$$\psi^+(\chi,r) = A(\chi,r) \exp\{i\phi(\chi,r)/\hbar\} \tag{7}$$

By making the short wavelength assumption in the usual way, (see Refs. 27,38) we obtain that the amplitude $A(\chi,r)$ satisfies an equation for conservation of amplitude flux, while the phase $\phi(\chi,r)$ verifies the classical Hamilton-Jacobi equation,

$$H(\chi, \frac{\partial\phi}{\partial\chi}, r, \frac{\partial\phi}{\partial r}) = E \tag{8}$$

To obtain the quantities $A(\chi,r)$ and $\phi(\chi,r)$ the following procedure is followed: we run classical trajectories for a given total energy E with the initial conditions $r = r_0$ large, $\chi = \chi_0$ (various arbitrary values), $p_r = p_{r_0} = -\sqrt{2m(E - Z_p Z_T e^2/r_0)}$, $p_{\chi_0} = 0$. From the values of the dynamical variables in the final asymptotic region, r_f, χ_f, p_{r_f}, p_{χ_f}, we can determine A and ϕ as follows:

Since A satisfies conservation of probability flux, if we consider the trajectories which initial value of χ are in the interval $[\chi_0, \chi_0 + d\chi_0]$, they will lead finally to an interval $[\chi_f, \chi_f + d\chi_f]$. The amplitude A must then satisfy:

$$A^2(\chi_f,r_f)\, v_f\, r_f^2 \sin\chi_f\, d\chi_f = A^2(\chi_0,r_0)\, v_0\, r_0^2 \sin\chi_0\, d\chi_0 \tag{9}$$

Since all initial orientations χ_0 are equally probable, $A(\chi_0,r_0)$ is independent of χ_0 and it is easily shown by using the normalization of ψ^+ that $A^2(\chi_0, r_0)\, r_0^2 = 1/2$.

Therefore,

$$A(\chi,r)=\sqrt{\frac{1}{2}\frac{v_0}{v}\frac{\sin\chi_0}{\sin\chi}\frac{d\chi_0}{d\chi}}\cdot\frac{1}{r} \tag{10}$$

where we have dropped the subindex f .

Since it is well known from classical mechanics that the classical action is a solution of the Hamilton-Jacobi equation (see Refs. 39 pp. 273-276, and 10) the expression for ϕ that satisfies Eq. (8) is

$$\phi(r,\chi) = -\int [r(t)\, dp_r(t) + \chi(t)\, dp_\chi(t)] + r\, p_r + \chi p_\chi + \hbar\sigma_0\,(\eta_0) \tag{11}$$

where the integral is performed along the trajectory and $\sigma_0(\eta_0)$ is the Coulomb phase shift for spin 0 and for the initial velocity v_0.

The wavefunction $\psi^+(\chi,r)$ as defined by Eqs. (7), (10) and (11) cannot be used to evaluate the S-matrix; it is immediately clear that we would obtain an expression for the S-matrix which is dependent on the distance r at which the final values of all magnitudes are evaluated.

To surmount this difficulty it is necessary to perform a canonical transformation of the set of variables (χ,r) to a new one where this situation does not occur. We choose the transformation to the new set $(\bar{\chi},\tau)$, in a way which is analogous to that employed by R. A. Marcus in Ref. 32, that is using a so-called "Uniformization with elastic collision trajectories".

The generating function we consider is

$$F_2(\chi,r,p_\chi,\bar{E}) \equiv p_\chi\chi + \int_{\tilde{r}_T}^{r} \tilde{p}_r(\tilde{r},p_\chi,\bar{E})\, d\tilde{r} \tag{12}$$

where $\tilde{p}_r$ is the radial momentum along an elastic trajectory governed by the monopole part of the Coulomb potential $Z_p Z_T e^2/r$, such that the energy $\bar{E}$ along this elastic trajectory equals the sum of the kinetic plus Coulomb energies at the point r at which F_2 is evaluated. Since the energy left to the particle depends on the energy that was transferred to the target, $\tilde{p}_r$ will depend on p_χ, the spin of the target at a distance r, as it is shown explicitly in Eq. (12). Finally, $\tilde{r}$ is the position along the elastic trajectory at which $\tilde{p}_r$ is evaluated, and $\tilde{r}_T$ is the turning point of the radial motion in the elastic collision, that is $\tilde{p}_r(\tilde{r}_T, p, \bar{E}) = 0$.

From Eq. (12) and the equations shown in Ref. 22, p. 241, we obtain the new coordinates $\bar{\chi}$ and τ

$$\bar{\chi} = \frac{\partial F_2}{\partial p_\chi} = \chi + \int_{\tilde{r}_T}^{r} \frac{\partial \tilde{p}_r}{\partial p_\chi} d\tilde{r}$$

$$\tau = \frac{\partial F_2}{\partial \bar{E}} = \int_{\tilde{r}_T}^{r} \frac{\partial \tilde{p}_r}{\partial \bar{E}} d\tilde{r} \qquad (13)$$

The derivates that appear here are easily evaluated from the expression of the Hamiltonian (Eq. 29, in the next section), and the definition of $\bar{E}$. From them we get

$$\bar{E} = \frac{\tilde{p}_r^2}{2m} + \frac{1}{2}\left(\frac{1}{m\tilde{r}^2} + \frac{1}{\mathcal{I}}\right) p_\chi^2 + \frac{Z_p Z_T e^2}{\tilde{r}} \qquad (14)$$

where m is the reduced mass of the system and $\mathcal{I}$ the moment of inertia of the target.

From Eq. (14)

$$\frac{\partial \tilde{p}_r}{\partial p_\chi} = -m \frac{p_\chi}{\tilde{p}_r}\left(\frac{1}{m\tilde{r}^2} + \frac{1}{\mathcal{I}}\right)$$

$$\frac{\partial \tilde{p}_r}{\partial \bar{E}} = \frac{m}{\tilde{p}_r} \qquad (15)$$

Replacing in Eq. (13) we find

$$\bar{\chi} = \chi - \int_{\tilde{r}_T}^{r} \frac{m p_\chi}{\tilde{p}_r}\left(\frac{1}{m\tilde{r}^2} + \frac{1}{\mathcal{I}}\right) d\tilde{r}$$

$$\tau = \int_{\tilde{r}_T}^{r} \frac{m}{\tilde{p}_r}\, d\tilde{r} \qquad (13')$$

τ can be physically interpreted as the time it takes for the particle to go from the turning point of the elastic trajectory to the final distance r . $\bar{\chi}$ can be seen by differentiation of Eq. (13') to be constant in the final asymptotic region; in that region it can be written as $\bar{\chi} = \chi - \omega\tau$, where $\omega = p_\chi/\mathcal{I}$ is the angular velocity of the target.

It is interesting to point out to the fact that this transformation of variables we made here is closely related to the transformation into the interaction representation in Quantum Mechanics (see for example Ref. 40, pp. 722 ff).

Transforming wavefunctions ϕ_I and ψ^+ by means of the canonical transformations given by Eq. (7), and replacing in the expression for the S-matrix (Eq. (3)) we obtain:

$$\psi^+(\bar{\chi},\tau) = \sqrt{\frac{1}{2}\,\frac{\sin\chi_0}{\sin\bar{\chi}}\,\frac{d\chi_0}{d\bar{\chi}}}\ \exp\{i\phi'/\hbar\} \tag{16}$$

where

$$\begin{aligned}\phi' = -\int\!\!\int\Big[r(t)\,dp_r(t) + \chi(t)\,dp_\chi(t)\Big] + \bar{E}\,\tau + \bar{\chi}\,p_\chi \\ + \int_0^{p_r} \tilde{r}\,d\tilde{p}_r + \hbar\sigma_0(\eta_0)\end{aligned} \tag{17}$$

and

$$\phi_I(\bar{\chi},\tau) = \frac{1}{\sqrt{2\pi}}\,Y_{I0}\,(\cos\bar{\chi})\,\exp\{i\phi''/\hbar\} \tag{18}$$

where $\phi'' = \bar{E}'\,\tau - \hbar\sigma_I(\eta_I)$ (19)

Finally, from Eq. (3)

$$\begin{aligned}S_{0\to I}\,\delta(E-E') = \int\!\!\int\sqrt{\frac{1}{2}\,\frac{\sin\chi_0}{\sin\bar{\chi}}\,\frac{d\chi_0}{d\bar{\chi}}}\cdot\frac{1}{\sqrt{2\pi}}\,Y_{I0}\,(\cos\bar{\chi}) \\ \cdot\exp\{i(E-\bar{E}')\,\tau/\hbar\}\,\exp(i\Delta/\hbar)\,2\pi\sin\bar{\chi}\,d\bar{\chi}\,d\tau\end{aligned} \tag{20}$$

where

$$\Delta = -\int [r(t)\, dp_r(t) + \chi(t)\, dp_\chi(t)] + \bar{\chi}\, p_\chi + \int_0^{p_r} \tilde{r}\, d\, \tilde{p}_r + \hbar[\sigma_0(\eta_0) + \sigma_I(\eta_I)] \tag{21}$$

The integral with respect to τ in (20) can be performed[32] and shown that the result is a δ-function in $(\bar{E}-\bar{E}')$. This reduces the expression for the S-matrix to a one-dimensional integral

$$S_{0\to I} = \int_0^{\pi} \sqrt{\frac{1}{4\pi} \frac{\sin\chi_0}{\sin\bar{\chi}} \frac{d\chi_0}{d\bar{\chi}}}\; Y_{I0}(\cos\bar{\chi})\; \exp(i\Delta/\hbar)\; 2\pi \sin\bar{\chi}\, d\bar{\chi} \tag{22}$$

Taking χ_0 as our variable of integration and replacing $Y_{I0}(\cos\bar{\chi})$ by $\sqrt{(2I+1)/4\pi}\; P_I(\cos\bar{\chi})$, where P_I is an ordinary Legendre polynomial, we obtain

$$S_{0\to I} = \frac{\sqrt{2I+1}}{2} \int_0^{\pi} \sqrt{\sin\chi_0 \sin\bar{\chi} \frac{d\bar{\chi}}{d\chi_0}}\; P_I(\cos\bar{\chi})\; \exp(i\Delta/\hbar)\; d\chi_0 \tag{23}$$

This expression will be applied to several physical systems, and then results discussed in the next Chapters, but before going into its applications let us consider the classical equations of motion which must be solved in order to evaluate the quantities appearing in Eq. (23).

3. Equations of Motion

We refer again to Fig. II-1 for a geometrical description of our system.

The kinetic energy is given by

$$K = \frac{1}{2} m\dot{r}^2 + \frac{1}{2} mr^2 \dot{\theta}^2 + \frac{1}{2} \mathcal{I} \dot{\beta}^2 \tag{24}$$

where m is the reduced mass of the system and $\mathcal{I}$ the moment of inertia of the target.

The potential energy is given by

$$V = \frac{Z_p Z_T e^2}{r} + \sum_{\substack{\lambda \text{even} \\ \lambda \geq 2}} \frac{Z_p Q_0^{(\lambda)} e^2}{2\, r^{\lambda+1}} P_\lambda(\cos\chi) \tag{25}$$

where χ is defined by $\chi \equiv \beta - \theta$, P_λ is the Legendre polynomial of order λ, $Z_p e$, $Z_T e$ are the charges of projectile and target, respectively, and $Q_0^{(\lambda)} e$ the multipole moment of order λ, defined by

$$Q_0^{(\lambda)} e = 2 \int r^\lambda P_\lambda(\cos\theta)\, \rho(r,\theta)\, d^3 r \tag{26}$$

where $\rho(r,\theta)$ is the density of electric charge.

We have already taken into account when writing Eq. 25 that the target nucleus we are considering has both reflection and axial symmetry.

Primarily for the sake of simplicity and since it is by far the most important contribution, we will consider only the first term in the sum appearing in Eq. (25). When later in this work we will need to include terms higher than the quadrupole term, it will be quite straightforward to do so.

From Eqs. (24) and (25) we can construct the Lagrangian for the interaction. Conservation of the total angular momentum implies that

$$\mathcal{J}\dot{\beta} + mr^2\,\dot{\theta} = 0 \tag{27}$$

for the head on case.

Then the Lagrangian takes the form:

$$\mathcal{L}(X,\dot{X},r,\dot{r}) = \frac{1}{2}\,m\dot{r}^2 + \frac{1}{2}\,\frac{mr^2\mathcal{J}}{mr^2+\mathcal{J}}\,\dot{X}^2 \tag{28}$$

$$- \frac{Z_p Z_T e^2}{r} - \frac{Z_p Q_0^{(2)} e^2}{2r^3}\,P_2(\cos X)$$

where X is the angle $\beta - \theta$, as previously defined.

From the definition of the canonical momenta, $p_q \equiv \frac{\partial \mathcal{L}}{\partial \dot{q}}$ we have: $p_r = m\dot{r}$ and $p_X = mr^2\mathcal{J}\,\dot{X}/(mr^2+\mathcal{J})$. We are now in condition of writing the Hamiltonian H.

$$H(X,p_X,r,p_r) = \frac{p_r^2}{2m} + \frac{1}{2}\left(\frac{1}{\mathcal{J}} + \frac{1}{mr^2}\right)p_X^2 \tag{29}$$

$$+ \frac{Z_p Z_T e^2}{r} + \frac{Z_p Q_0^{(2)} e^2}{2r^3}\,P_2(\cos X)$$

From the expression for p_X we observe that $p_X = \mathcal{J}\dot{\beta}$, the rotational angular momentum of the target.

Before proceeding to write Hamilton's equations of motion it will be convenient to write this Hamiltonian in dimensionless coordinates. To this effect we define the dimensionless variables

$$\hat{I} \equiv \frac{p_\chi}{\hbar}$$

$$\hat{r} \equiv \frac{mv_0^2\, r}{Z_p Z_T e^2} \quad ; \quad \hat{p}_r \equiv \frac{p_r}{mv_0} \tag{30}$$

$$\hat{t} \equiv \frac{mv_0^3\, t}{Z_p Z_T e^2} \quad ;$$

and the following quantities:

$$\eta_0 \equiv \frac{Z_p Z_T e^2}{\hbar\, v_0} \qquad \text{(Sommerfeld parameter)}$$

$$\xi \equiv \frac{3\hbar^2 \eta_0}{mv_0^2 \mathscr{S}} \qquad \text{(adiabaticity parameter)} \tag{31}$$

$$a \equiv \frac{Z_p Z_t e^2}{mv_0^2} \qquad \text{(half distance of closest approach)}$$

$$q_2 \equiv \frac{Z_p Q_0^{(2)} e^2}{4\hbar\, v_0 a^2} \qquad \text{(quadrupole strength parameter)}$$

here v_0 is the initial relative velocity at large distance where the interaction is negligible. We note that $\hat{r}$ is the measure of r in units of a, $\hat{p}_r$ measures p_r taking as unit its initial value

(in magnitude), $\hat{t}$ is the time in the unit a/v_0, and the meaning of $\hat{I}$ is obvious.

Then:

$$\hat{H}(\hat{\chi},\hat{I},\hat{r},\hat{p}_r) = \frac{\hat{p}_r^{\,2}}{2} + \frac{1}{2}\left(\frac{\xi}{3n_0} + \frac{1}{n_0^{\,2}\hat{r}^2}\right)\hat{I}^2 + \frac{1}{\hat{r}} + \frac{2q_2\, P_2(\cos\chi)}{n_0\,\hat{r}^3} \tag{32}$$

Hamilton's equations of motion are then:

$$\frac{d\hat{r}}{d\hat{t}} = \hat{p}_r$$

$$\frac{d\hat{p}_r}{d\hat{t}} = \frac{\hat{I}^2}{n_0^{\,2}\,\hat{r}^3} + \frac{1}{\hat{r}^2} + \frac{6q_2\, P_2(\cos\chi)}{n_0\,\hat{r}^4} \tag{33}$$

$$\frac{d\chi}{d\hat{t}} = \left(\frac{\xi}{3} + \frac{1}{n_0\,\hat{r}^2}\right)\hat{I}$$

$$\frac{d\hat{I}}{d\hat{t}} = 3q_2\,\frac{\sin 2\chi}{\hat{r}^3}$$

and the phase $\hat{\phi}$ is evaluated using the relation

$$\frac{d\hat{\phi}}{d\hat{t}} = -\,n_0\,\hat{r}\,\frac{d\hat{p}_r}{d\hat{t}} - \chi\,\frac{d\hat{I}}{d\hat{t}} \tag{33'}$$

In Fig. II-2 we plot the solutions of this system of equations for a realistic case, for several values of the initial orientation angle . The results show some characteristics that are present in a larger or smaller extent in the trajectories followed by all systems which study we are pursuing, and which are therefore worth mentioning now. One first observation is that the angular momentum is communicated to the target mostly in a small time interval around the point of closest approach. In this interval the radial distance does not change much: most of the angular momentum exchange takes place for distances $\hat{r} \leq 3$, while the minimum distance is $\hat{r} \approx 2$. During this time interval the orientation angle χ does not change much either: this means that during the most important part of the collision the system retains memory of its initial orientation. This is the basis for the sudden approximation, to be discussed in a later section.

Another characteristic we would like to point out appears in the last case shown in Fig. II-2 in which the angular momentum imparted to the target is so high that before the projectile has had time to recede very much, $\hat{\chi}$ has increased beyond 90^{o} and the torque on the target has reversed in direction. This is seen as a slight decrease in the angular momentum function $\hat{I}$ followed later when χ has gone through 180^{o} by an even slighter increase. Such adiabatic effects are more evident for more massive projectiles.

Figure II-3 shows the final value of the angular momentum $\hat{I}$ plotted as a function of the initial orientation χ_0 , for the same system considered in Fig. II-2. $\hat{I}(\chi_0)$ reaches a maximum for an initial

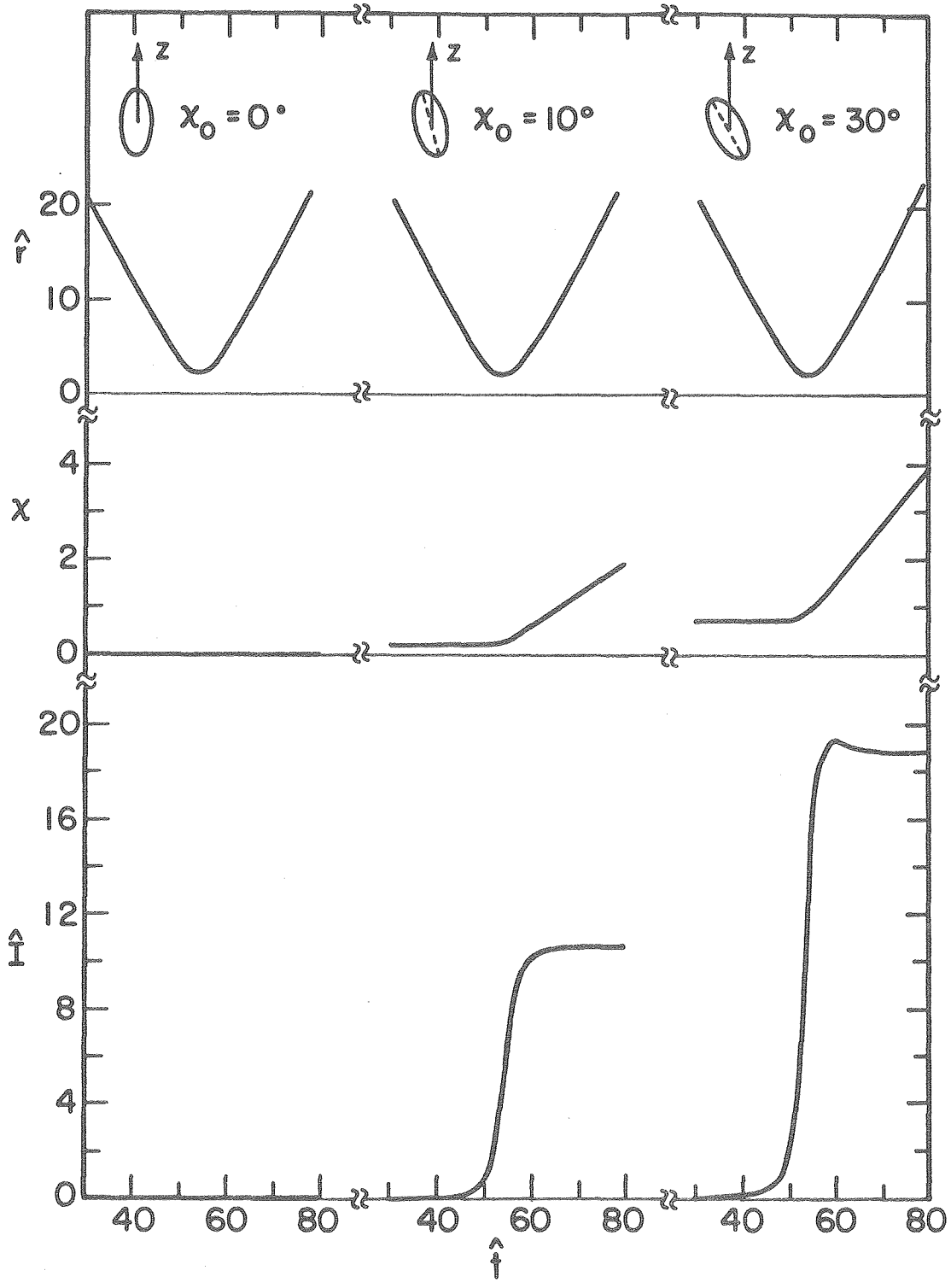

Fig. II-2

XBL 774-8299

Fig. II-2 Values of the functions $\hat{r}(\hat{t})$, $\chi(\hat{t})$ and $\hat{I}(\hat{t})$ (see text for definitions) for three different initial angles χ_o . The case shown is ^{86}Kr at 400 MeV lab energy on ^{238}U, which quadrupole moment was taken to be $Q_0^{(2)} = 11.12b$, with an energy of the 2^+ state $E_{2^+} = 0.0449$ MeV.

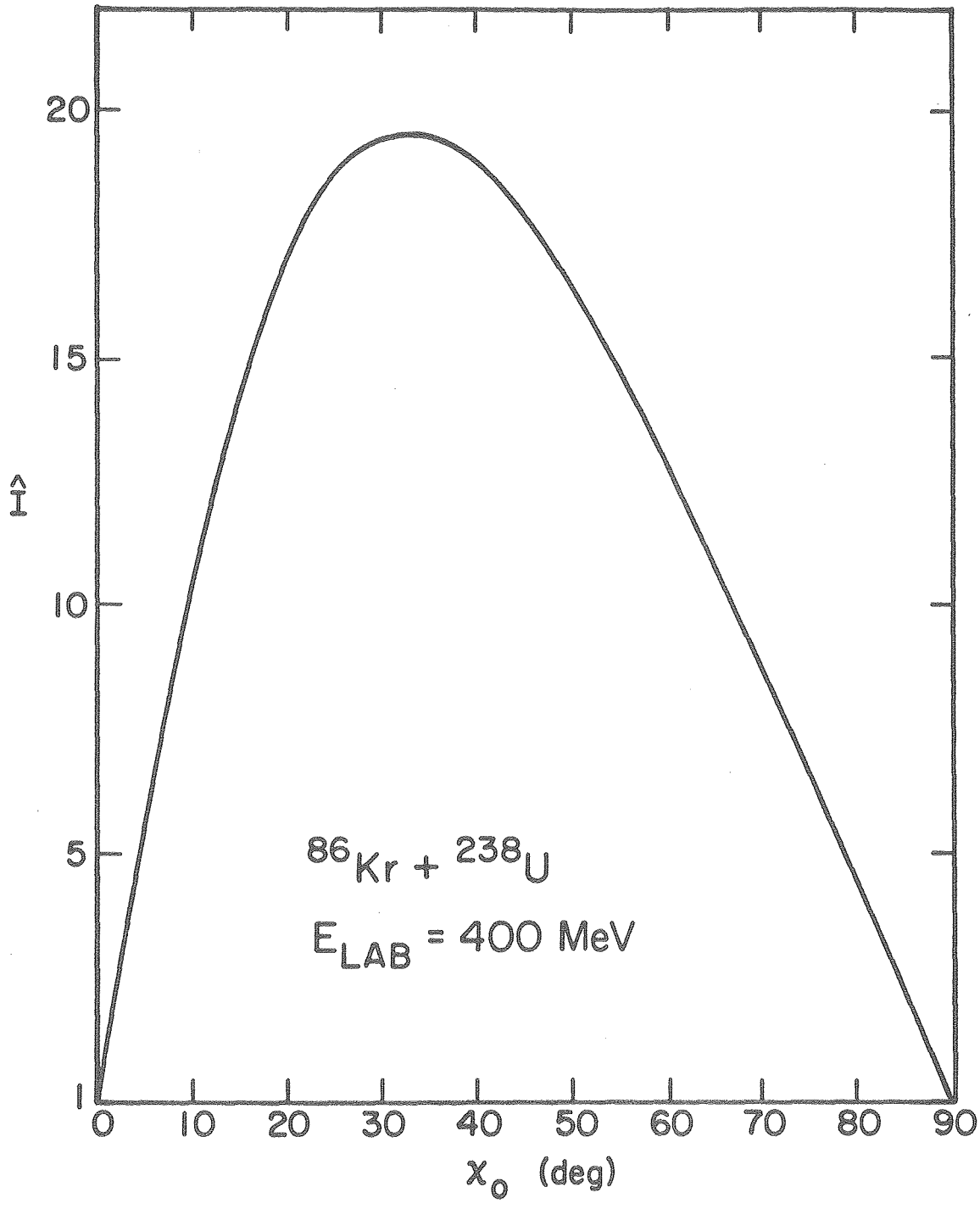

Fig. II-3 Function $\hat{I}(\chi_0)$ for the same physical system as in Fig. II-2.

orientation angle of $\approx 33^{o}$. On the other hand since Eq. (33) shows that $d\hat{I}/d\hat{t}$ is proportional to $\sin 2\chi$, we know that the quadrupole torque is maximum at $\chi = 45^{o}$. The fact that the maximum is shifted down from 45^{o} is a dynamical effect: for a trajectory with initial $\chi_0 \approx 33^{o}$ the quadrupole torque sets the target in motion in such a way that at the point of closest approach, when the torque is strongest, the orientation angle approaches 45^{o}. For $\chi_0 > 33^{o}$ the orientation angle at the point of closest approach is larger than 45^{o}, and the quadrupole torque is then smaller. This shift of the maximum towards smaller angles is also an effect that is more marked for heavier projectiles. In the sudden approximation we will see that $\hat{I}$ takes its maximum value at $\chi_0 = 45^{o}$, and besides that in this case $I(\chi_0) = 2q_2 \sin 2\chi_0$.

Using Fig. II-3 we can illustrate the procedure to be followed in order to evaluate the S-matrix according to the Uniform Semiclassical Approximation, described in general in Appendix A and in Refs. 24 and 25 for the case of Coulomb excitation. In this method one finds the trajectories leading to the final spin I of the state we want to consider. This means, one has to perform a search for those values of the initial parameters of the physical system (the angle χ_0 in our case) that lead to the spin I we are interested in. Actually in Refs. 23-25 the final angular momentum of the target is chosen to be 0.5, 2.5, 4.5,.... , instead of 0.0, 2.0, 4.0, ... or 0.0, $\sqrt{2\times 3}$, $\sqrt{4\times 5}$, ... Ref. 25 documents several reasons for doing so and in a later section of this chapter we will show how this choice appears naturally from the formalism we are developing here.

From the form of the function $\hat{I}(\chi_0)$ shown in Fig. II-3 we see that for values of I less than the maximum there are two initial angles χ_0 that lead to this final spin.

If the transition we are interested in is for I larger than the maximum of $\hat{I}(\chi_0)$ it can be seen that there are two complex values of χ_0 that satisfy the equation $\hat{I}(\chi_0) = I$. In this case the equations of motion will involve complex dynamical variables, but this is no major obstacle as we will see in the following chapters.

After the roots of $\hat{I}(\chi_0) = I$ have been determined, the S-matrix is given by an analytical formula (see Eqs. A-13 and A-15). We will show how these formulas relate to the expression derived here (Eq. 23).

4. Relationship Between the Classical-limit S-Matrix and the USCA Formulas

If we replace the Legendre polynomial appearing in the expression for the classical-limit S-matrix (CLSM) Eq. (23) by its asymptotic expression:

$$P_I(\cos\chi) \approx \frac{2\cos[(I+1/2)\bar{\chi} - \pi/4]}{\sqrt{(2I+1)\pi\sin\chi}} = \frac{e^{i[\ ]} + e^{-i[\ ]}}{\sqrt{(2I+1)\pi\sin\chi}} \qquad (34)$$

we can rewrite Eq. (23) in the form:

$$S_{0\to I} \cong \frac{1}{2\sqrt{\pi}} \left\{ \int_0^{\pi} dX_0 \sqrt{\sin X_0 \frac{d\bar{X}}{dX_0}}\; e^{i[\Delta/\hbar + (I+1/2)\bar{X} - \frac{\pi}{4}]} \right. \tag{35}$$

$$\left. + \int_0^{\pi} dX_0 \sqrt{\sin X_0 \frac{d\bar{X}}{dX_0}}\; e^{i[\Delta/\hbar - (I+1/2)X + \frac{\pi}{4}]} \right\}$$

If we change the variable of integration in the first integral of Eq. (35) from X_0 to $\pi - X_0$, all other quantities appearing in that equation remain unchanged except $\bar{X}$ which changes into $\pi - \bar{X}$. Then Eq. (35) becomes

$$S_{0\to I} \cong \frac{1}{2\sqrt{\pi}} \int_0^{\pi} dX_0 \sqrt{\sin X_0 \frac{d\bar{X}}{dX_0}} \left\{ e^{i[\Delta/\hbar + (I+1/2)(\pi - \bar{X}) - \frac{\pi}{4}]} \right.$$

$$\left. + e^{i[\Delta/\hbar - (I+1/2)\bar{X} + \frac{\pi}{4}]} \right\}$$

$$= \frac{1}{2\sqrt{\pi}} \int_0^{\pi} dX_0 \sqrt{\sin X_0 \frac{d\bar{X}}{dX_0}}\; e^{i[\Delta/\hbar - (I+1/2)\bar{X} + \frac{\pi}{4}]}$$

$$\times \left\{ 1 + e^{i\,2\pi I} \right\}$$

Then, since I is even

$$S_{0\to I} = \frac{1}{\sqrt{\pi}} \int_0^{\pi} dX_0 \sqrt{\sin X_0 \frac{d\bar{X}}{dX_0}}\; e^{i[\Delta/\hbar - (I+1/2)\bar{X} + \frac{\pi}{4}]} \tag{36}$$

The evaluation of this integral by stationary phase methods results in the USCA expression used in Refs. 24 and 25. It is not hard to show that the points of stationary phase satisfy the equation:

$$\hat{I}(\chi_0) = I + 1/2 \tag{37}$$

It is worth observing that the weighting factor $\sqrt{\sin \chi_0}$ that was introduced by geometrical considerations there, appears more naturally in this formalism even if the physical reason is obviously the same. Also the use of the $I + 1/2$ spin quantization condition which Refs. 23-25 use in an almost empirical way is here seen to appear as a direct consequence of the approximation done in obtaining Eq. (36), i.e., of having replaced the Legendre polynomial by its asymptotic expression (34).

The close relationship between the CLSM and the USCA expressions we have shown here, does not imply, though, that the procedure to obtain numerical results is similar and this fact makes a difference from a practical viewpoint. We will show in Ch. IV how the introduction of other terms in the Hamiltonian for our system, even simple terms like the hexadecapolar electric potential, increases the number of points of stationary phase in Eq. (36). This fact alone makes USCA expressions much more difficult to use on two counts: (1) There are more roots to be found, and unless the system can be very well analyzed from the beginning, one does not know the exact number beforehand. Therefore the search for the points of stationary phase may become very long and frustrating. (2) The expressions themselves are much more complicated, unless one neglects the reciprocate interaction

between stationary trajectories and uses less accurate expressions of the type of Eq. (A-12).

The numerical calculations using the CLSM are very similar if one adds more terms to the Hamiltonian: only Hamilton's equations of motion have to be rewritten to include these new terms.

Finally, we would like to point out that in the USCA there is a difference between "allowed" and "forbidden" transitions, meaning by allowed transitions those for which their final spin can be reached through classical trajectories, in the usual sense. For example, in the case shown in Fig. II-3 allowed transitions are those for which the final spin is less than the maximum, that is $I \leq 18$. The transitions for which $I \geq 20$ are forbidden in the classical sense. The stationary points of the integral appearing in Eq. (36), which are solution of Eq. (37) are complex numbers in the forbidden case. This means that the initial conditions for the equations of motion, Eq. (33), will be complex, and so will become the dynamical variables during the subsequent integration.

In contrast the CLSM makes no distinction between allowed and forbidden transitions, and the dynamical variables are real unless the Hamiltonian itself is complex, as it will be in the case in Ch. IV.

It could appear surprising at first sight that especially for high spin states where the roots of Eq. (37) are well into the complex X_0 plane, the CLSM and the USCA expressions were equivalent, apart from the approximations mentioned before, since those stationary phase points employed in the USCA are far from the real axis on which the integration leading to the CLSM is performed. However, since the

integrand in Eq. (23) is an analytic function it is possible to deform the path of integration in the way shown in Fig. II-4 so that it passes through the points of stationary phase for the transition considered. The relationship between both expressions is then clear also in this case.

For this same case of high spin final states the rapid decrease in excitation probability with increasing spin (illustrated by several examples in the next chapter) takes different forms in these two methods: in the USCA it is due to an increasing value of the imaginary part of the phase, while in the CLSM the Legendre polynomial $P_I(\cos\bar{\chi})$ oscillates more and more rapidly with increase I, thus bringing down the value of the integral in Eq. (23). Nevertheless from the preceding considerations we must take these as two different mathematical forms of the same representation of the physical process.

5. The $\xi = 0$ and $\eta_0 = \infty$ limit

Let us consider the special case in which the dimensionless parameters ξ and η_0, defined in Eq. (31), approach the limiting case $\xi = 0$ and $\eta_0 = \infty$. This case is particularly interesting to discuss because Biedenharn and Class have shown[42] that the quantum mechanical treatment can be completely solved in analytical terms.

We will first discuss the physical implications of taking $\xi = 0$ and $\eta_0 = \infty$. From the equations of motion, Eq. (33), it is clear that for $\eta_0 = \infty$ the trajectory of the projectile is a hyperbola (a straight line in the particular case of a head-on collision we

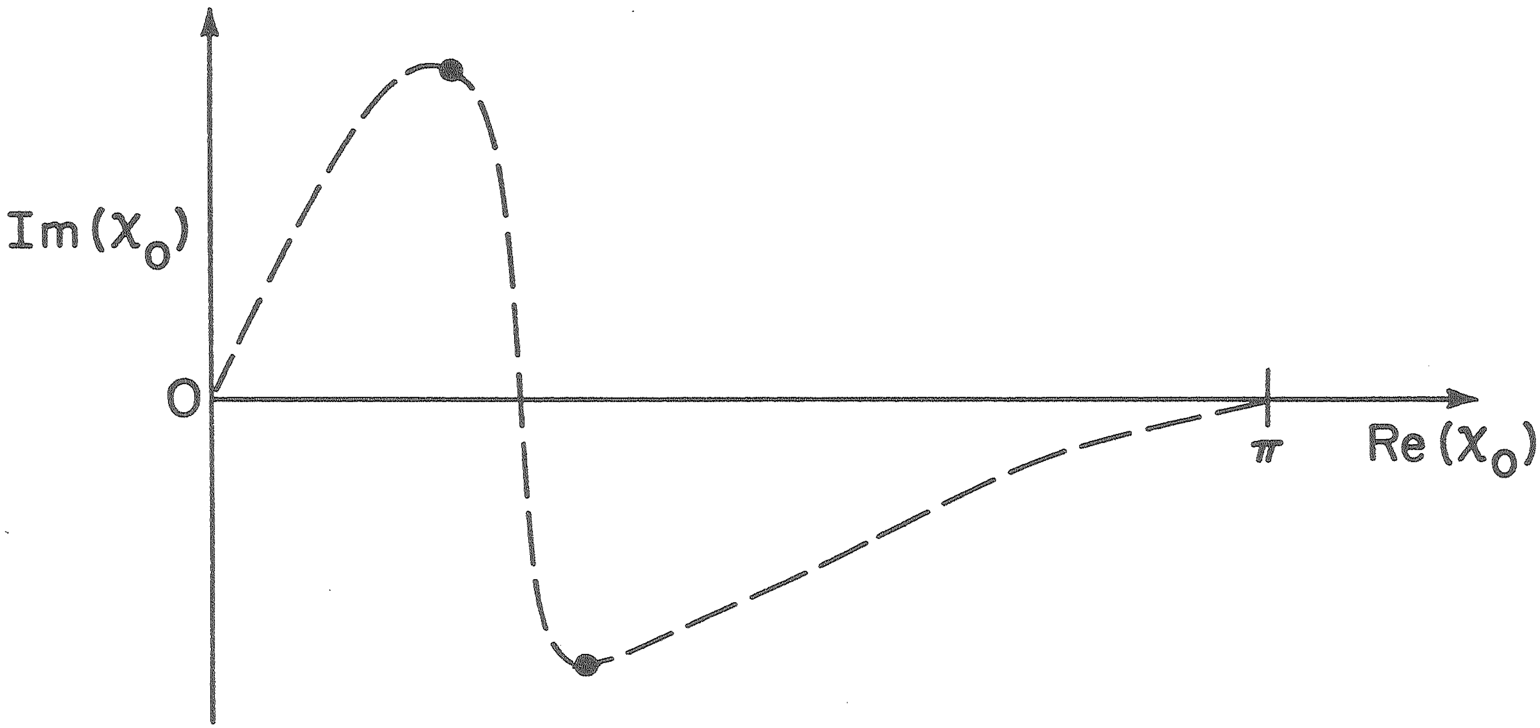

Fig. II-4 Diagram showing how the integration path, which is initially along the real axis can be deformed into a path passing through the stationary phase points of the integrand (represented by the dots)

XBL 774-8298

are considering here) and it is not influenced by the motion of the target nucleus.

The definition of ξ implies that in order for it to become zero the moment of inertia $\mathscr{I}$ has to become infinite, therefore the target does not rotate and in addition the rotational energy levels of the target nucleus become degenerate. The physical situation which is approached by this limit is when the ratio of the collision time to the rotation time becomes very close to zero. This is the so-called "sudden impact" approximation, and besides having theoretical interest for the reasons expressed above, it is close to the actual physical situation since as it was discussed in section 3 and illustrated in Fig. II-2 the transfer of angular momentum for a realistic case takes place in a time interval much smaller than the rotational period.

The equations of motion are now:

$$\frac{d\hat{r}}{d\hat{t}} = \hat{p}_r \; ; \quad \frac{d\hat{p}_r}{d\hat{t}} = \frac{1}{\hat{r}^2} \quad ; \quad \frac{d\chi}{d\hat{t}} = 0 \quad ; \quad \frac{d\hat{I}}{d\hat{t}} = 3q_2 \frac{\sin 2\chi}{\hat{r}^3} \tag{38}$$

From the first two of these equations we obtain the radial momentum as a function of $\hat{r}$

$$\hat{p}_r = \pm \sqrt{1 - 2/\hat{r}} \tag{39}$$

where the - (+) sign applies to the incoming (outgoing) part of the trajectory.

$\hat{\chi}$ is seen to be constant, so it equals its initial value χ_0 ; therefore the equation for $\hat{I}$ can be written as

$$\frac{d\hat{I}}{d\hat{r}} = \pm 3q_2 \frac{\sin 2\chi_0}{\hat{r}^3 \sqrt{1 - 2/\hat{r}}} \tag{40}$$

which can be integrated yielding:

$$\hat{I}\ (\chi_0,\hat{r}) = q_2 \sin 2\chi_0\ [1 \pm (1 + 1/\hat{r})\ \sqrt{1 - 2/\hat{r}}\ ] \tag{41}$$

From (41), the angular momentum of the target after the collision is given by

$$\hat{I}\ (\chi_0) = 2q_2 \sin 2\chi_0 \tag{42}$$

as it was already mentioned in a previous section.

Since $\eta = \infty$, in order to avoid problems with the Coulomb phase shifts we will evaluate the R-matrix, given by

$R_{0\to I} = \exp\{-i[\sigma_0(\eta_0) + \sigma_I(\eta_I)]\}\ S_{0\to I}$ therefore the Coulomb phase shifts appearing in the expression for Δ in Eq. (21) are cancelled. Since χ is constant we can integrate directly

$$\int \chi(t)\ dp_\chi(t) = \chi_0\ p_\chi\ (\chi_0) \tag{43}$$

$\xi = 0$ and $\eta = \infty$ imply that $\bar{\chi} = \chi_0$.

Then,

$$-\int \chi(t)\ dp_\chi(t) + \bar{\chi}\ p_\chi = 0 \quad . \tag{44}$$

$$\eta(\hat{p}_r - \tilde{\hat{p}}_r)\, d\hat{r} = \int \eta\left(\sqrt{1-2/\hat{r}-2q_2\, P_2(\cos\chi_0)/\eta\hat{r}^3} - \sqrt{1-2/\hat{r}}\right) d\hat{r}$$

$$= -\, q_2\, P_2(\cos\chi_0) \int \frac{d\hat{r}}{\hat{r}^3\sqrt{1-2/\hat{r}}} = -\,\frac{4}{3}\, q_2\, P_2(\cos\chi_0) \qquad (45)$$

The R-matrix is then given in this case, by

$$R_{0\to I} = \frac{\sqrt{2I+1}}{2} \int_0^{\pi} \sin\chi_0\, P_I(\cos\chi_0)\, e^{-i\,\frac{4}{3}\, q_2\, P_2(\cos\chi_0)}\, d\chi_0$$

which can be rewritten as

$$R_{0\to I} = \sqrt{2I+1} \int_0^{1} P_I(x)\, e^{-i\,\frac{4}{3}\, q_2\, P_2(x)}\, dx \qquad (46)$$

This integral can be expressed in terms of a confluent hypergeometric function, ${}_1F_1$ as[7] :

$$R_{0\to I} = \frac{\Gamma\left(\frac{I+1}{2}\right)}{2\sqrt{2I+1}\;\Gamma(I+3/2)}\, e^{-i\,\frac{4}{3}\, q_2} (-2iq_2)^{\frac{I}{2}}\, {}_1F_1\left(\frac{I+2}{2}\,,\, \frac{2I+3}{2}\,,\, 2iq_2\right) \qquad (47)$$

This particular confluent hypergeometric function can also be expressed by means of Fresnel integrals, and in the same manner as in Ref. (7) it is possible to obtain a simple recursion relation between

$R_{0\to I-2}$, $R_{0\to I}$ and $R_{0\to I+2}$

$$(I+2)(2I-1)\sqrt{2I+5}\ R_{0\to I+2} = \left[\frac{(2I-1(2I+1)(2I+3)}{4iq_2} + 2I+1\right]\ \sqrt{2I+1}\ R_{0\to I}$$

$$+(I-1)(2I+3)\ \sqrt{2I-3}\ R_{0\to I-2} \tag{48}$$

By giving two consecutive elements of the R-matrix all of them are determined.

In particular we have

$$R_{0\to 0} = \sqrt{\frac{\pi}{4q_2}}\ e^{i\frac{2}{3}q_2}\ \left[C(2q_2) - i\ S(2q_2)\right] \tag{49}$$

where C(x) and S(x) are the Fresnel integrals, and

$$R_{0\to 2} = \frac{1}{2\sqrt{5}}\ \left[\left(\frac{3}{4iq_2} - 1\right)\ R_{0\to 0} - \frac{3}{4iq_2}\ e^{-i\frac{4}{3}q_2}\right] \tag{50}$$

We see that we have succeeded in expressing the R-matrix in terms of analytical functions. This is not very important from a numerical point of view, since the integral appearing in Eq. (46) does not pose any computational difficulties, but it is very significative that the analytical expression found coincides with the quantum mechanical solution for this same case.[7,42]

III. THE CLSM AND ORBITAL DYNAMICS IN SEMICLASSICAL COULOMB EXCITATION THEORY

1. Introduction

The recent availability of very heavy ions has made it possible to populate high spin states ($I \approx 20\ \hbar$) with multiple Coulomb excitation processes. Exact partial-wave, coupled channel calculations are possible for Coulomb excitation with light projectiles,[6] but such calculations are impractical for heavy-ion systems. The most common approach to this problem has used the semiclassical methods developed by Alder and Winther[7] (A-W) and embodied in the widely used Winther-de Boer code[8] to calculate multiple Coulomb excitation probabilities.

In this approach the internal degrees of freedom are treated quantum-mechanically but the projectile dynamics is taken as that of a classical particle on an energy-symmetrized hyperbola.

As Alder et al. have shown[43-44] this accounts quite nicely for the amplitude of the first-order transition matrix elements, but may be in significant error for their phases. Therefore higher order processes such as multiple E2 or E4 excitation which are sensitive to these phases may be affected by corrections to semiclassical calculations. Historically, these corrections have been termed "quantal" or "quantum-mechanical" corrections, since they represent differences between exact (i.e., quantal) calculations and the approximate semiclassical ones. Alder has pointed out[45], however, that a significant part of this "quantal" correction is independent of $\hbar$ and therefore is not a true quantum-mechanical effect at all, but rather is due to the neglect of the electric quadrupole potential in calculating the energy symmetrized

semiclassical trajectories. The weight of the evidence presented in this chapter supports this point of view and we shall refer to these effects as orbital dynamics effects. Any effects that are of a specifically quantum dynamical origin (in a sense to be specified later) are probably beyond the range of this method.

Initial attempts to account for the "quantal" corrections arising from the use of approximate orbital dynamics have involved extrapolations from exact light-ion calculations[43-45] and sophisticated energy and angular momentum symmetrizations in the semiclassical limit[46].

Here we will employ the method discussed in Ch. II and compare it with A-W and quantum-mechanical calculations. From this comparison we expect to understand better the orbital effects in the semiclassical theory and even provide an estimate of the corrections to be made to calculations based on this theory for the case of heavy ions where the quantum mechanical codes available are now impractical.

A short review of the semiclassical theory is presented in Appendix B. We refer to (47) for a more thorough discussion of this theory and also of the quantum mechanical treatment of the Coulomb excitation process.

2. Comparison of CLSM, A-W and quantum mechanical results

In order to evaluate the expression for the classical limit S-matrix given in Eq. (II-23) we wrote a computer code in which first trajectories were run corresponding to the initial conditions:

$$\hat{r}_0 \quad \text{large } (\geq 50)$$

$$\hat{p}_{r_0} = -\sqrt{1 - 2/r_0} \tag{1}$$

$$\chi_0 = \text{uniformly spaced values in the interval } [0\ ,\ \tfrac{\pi}{2}]$$

$$\hat{I}_0 = 0$$

Due to symmetry reasons, the trajectories for χ_0 in the interval $[\frac{\pi}{2}, \pi]$ correspond to those in the interval, $[0, \frac{\pi}{2}]$ by the transformation

$$\begin{aligned} \chi &\to \pi - \chi \\ \hat{I} &\to -\hat{I} \\ \hat{r} &\to \hat{r} \\ \hat{p}_r &\to \hat{p}_r \end{aligned} \tag{2}$$

valid at all times during the trajectory. This fact allows us to run only half of the trajectories needed to evaluate Eq. (II-23), and therefore reduces by a factor of two or so the computer time required by the program.

The integration of the equations of motion, Eq. (II-33) is done by means of a standard Zonneveld-Adams Moulton integration routine.

The quantity

$$-\int [r(t)\ dp_r(t) + \chi(t)\ dp_\chi(t)]$$

that appears in Eq. (II-23) is evaluated by adding the differential Eq. (II-33') to the equations of motion. The integration is concluded when the distance $\hat{r}$ is sufficiently large (we chose the value 50 again).

We should remark here that the values for the S-matrix elements were numerically shown to be independent of the initial and final distances taken for the integration as long as these values lay well out of the region where the interaction takes place. This region can be operationally defined by considering whether the value of the angular momentum is changing or not.

From the values of the dynamical variables at the end of each trajectory the quantities $\bar{\chi}$ and Δ are evaluated and stored.

In order to calculate $\bar{\chi}$, defined in Eq. (II-13') we must perform the integral

$$\int_{\bar{r}_T}^{r} \frac{mp\chi}{\tilde{p}_r} \left(\frac{1}{m\tilde{r}^2} + \frac{1}{\mathscr{I}}\right) d\tilde{r}$$

which in dimensionless variables is written

$$\int_{\hat{\tilde{r}}_T}^{r} \frac{I}{\hat{\tilde{p}}_r} \left(\frac{1}{\eta_0 \hat{\tilde{r}}^2} + \frac{\xi}{3}\right) d\hat{\tilde{r}} \qquad (2)$$

In Eq. (2) $\hat{\tilde{r}}_T$ satisfies $\hat{\tilde{p}}_r(\hat{\tilde{r}}_T) = 0$. This expression can be evaluated analytically, since

$$\hat{\tilde{p}}_r = \sqrt{1 - \frac{\xi}{3} \hat{I}^2 - \frac{2}{\hat{\tilde{r}}} - \frac{\hat{I}^2}{\eta_0 \hat{\tilde{r}}^2}} \qquad (3)$$

In both Eqs. (2) and (3) $\hat{I}$ and $\hat{r}$ represent the final value of these variables for the trajectory considered.

The evaluation of Δ (Eq. II-21) requires as well the evaluation of one integral

$$\int_0^{p_r} \tilde{r}\, d\tilde{p}_r$$

which is expressed in dimensionless variables, previous an integration by parts, as

$$\eta_o[\hat{r}\,\hat{p}_r - \int_{\hat{\tilde{r}}_T}^{\hat{r}} \hat{\tilde{p}}_r\, d\hat{\tilde{r}}] \qquad (4)$$

where $\hat{\tilde{p}}_r$ is given by Eq. (3) and $\hat{r}$ and $\hat{p}_r$ are final values for the trajectory.

After all the trajectories are run, the integration appearing in Eq. (II-23) is done by using a 5 points Newton-Cotes integration subroutine.

This integration is repeated for all the final spins I we are interested in. Note, however, that the equations of motion do not have to be integrated every time, so that the time required for the computation is practically independent of the number of excited final states considered. This is a very convenient feature and the situation is quite different for the other methods to be discussed here.

The calculations for the A-W and quantum mechanical theories were done by using the standard Winther-deBoer[8] and AROSA[6] computer codes. Since these codes give the results in terms of the R-matrix instead of the S-matrix, we have omitted in our code the Coulomb phases appearing in the expression of Δ (Eq. II-21), so as to obtain the R-matrix and thus facilitate the comparison.

From a numerical study we have found that 50 trajectories in the interval $[0,\frac{\pi}{2}]$ are enough to give the CLSM results with good accuracy. The computing time required for our code is less or equal to that required for the Winther-deBoer code and much less than the one consumed by AROSA.

One expects that the CLSM method will be the more valid the more "classical" the system is, i.e., for heavy projectiles and the excitation of large numbers of rotational states. Since this is exactly the situation for which quantum-mechanical calculations are not yet practical this represents one of the attractive features of the method. On the other hand this means that comparisons to quantum-mechanical calculations can only be done exactly for light systems, for which the CLSM method might not be expected to work very well. In fact, we have found that the CLSM gives a highly accurate description of the Coulomb excitation process even for the lightest ions.

The results of these calculations are shown in Figs. III-1-4 for the projectiles ^{1}H, ^{2}H, ^{4}He and ^{10}Be on ^{168}Er, and are tabulated for a closer inspection in Table 1. In the upper part of each figure we have plotted the amplitude and phase of the R-matrix elements for the $\ell = 0$ incident partial wave as a function of angular momentum both for a quantum mechanical calculation and for the CLSM calculation (note that the radial scale is logarithmic). In the lower part of each figure we show the relative deviation of the amplitude and the deviation of the phase of the R-matrix from the quantum mechanical calculation, both for the CLSM method and for the A-W method.

The agreement between the CLSM method and the quantum-mechanical calculation for the amplitude and the phase of the $\ell = 0$ R-matrix, even for protons, is remarkable.

Table III-1. Values of the S-matrix elements $S^{0}_{0\to I}$ calculated by the methods described in the text. The arguments are given in radians. These results are illustrated in Figs. 1-4

SYSTEM	ENERGY (LAB)	SPIN	CLSM		QM (AROSA)[6]		AW(WINTHER - deBOER)[8]	
			MODULUS	ARGUMENT	MODULUS	ARGUMENT	MODULUS	
$^{1}H + ^{168}Er$	7 MeV	0	0.991	0.006	0.994	0.005	0.996	0.001
		2	0.134	4.670	0.113	4.680	0.135	4.670
		4	0.002	3.305	0.003	3.151	0.008	3.142
$^{2}H + ^{168}Er$	7 MeV	0	0.982	0.010	0.986	0.009	0.982	0.003
		2	0.187	4.654	0.167	4.664	0.186	4.653
		4	0.081	3.216	0.082	3.145	0.143	3.140
$^{4}He + ^{168}Er$	14 MeV	0	0.934	0.028	0.940	0.027	0.934	0.014
		2	0.353	4.606	0.339	4.615	0.353	4.599
		4	0.047	3.094	0.044	3.080	0.054	3.067
$^{10}Be + ^{168}Er$	45 MeV	0	0.342	1.027	0.347	0.988	0.330	0.951
		2	0.691	4.517	0.701	4.513	0.661	4.378
		4	0.583	2.736	0.570	2.752	0.595	2.604
		6	0.249	1.153	0.242	1.169	0.298	1.024
		8	0.059	5.960	0.064	5.943	0.101	5.809

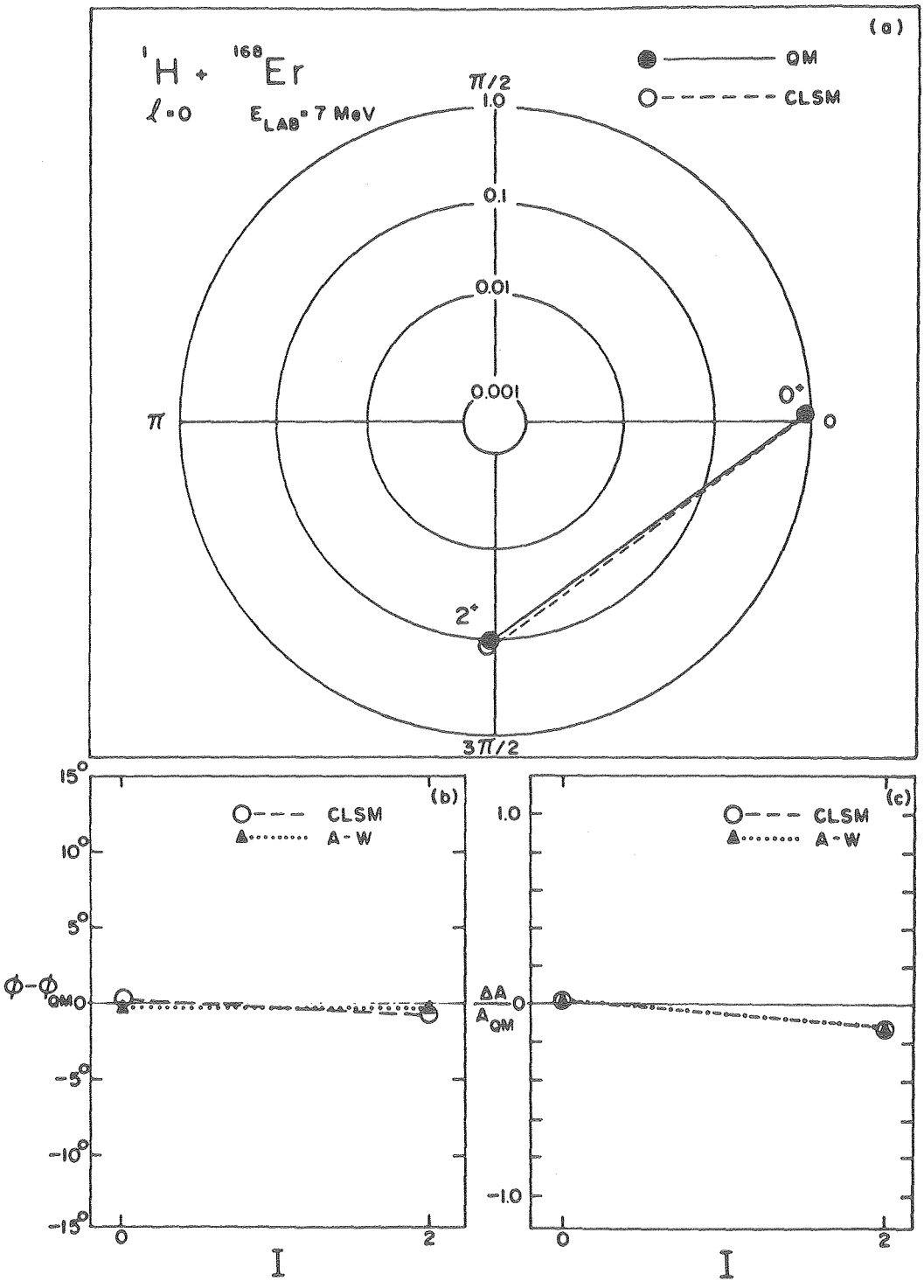

Fig. III-1 XBL 774-8303

Fig. III-1 (a) The $\ell = 0$ R-matrix elements for Coulomb excitation of the ground band of ^{168}Er by 7 MeV ^{1}H projectiles. The radial scale is logarithmic. The quadrupole moment of ^{168}Er is taken to be $Q_0^{(2)} = 7.673$ b and the energy levels are taken from the rotational model with $E_{2+} = 0.0798$ MeV. The Classical Limit S-Matrix (CLSM) calculations are in good agreement with the quantum mechanical calculations done using the computer code AROSA (QM).

(b) The difference in phase between the $\ell = 0$ quantum mechanical R-matrix elements and the CLSM and Alder-Winther (A-W) semiclassical calculations.

(c) The relative difference in amplitudes between the $\ell = 0$ quantum mechanical R-matrix elements and the CLSM and A-W ones.

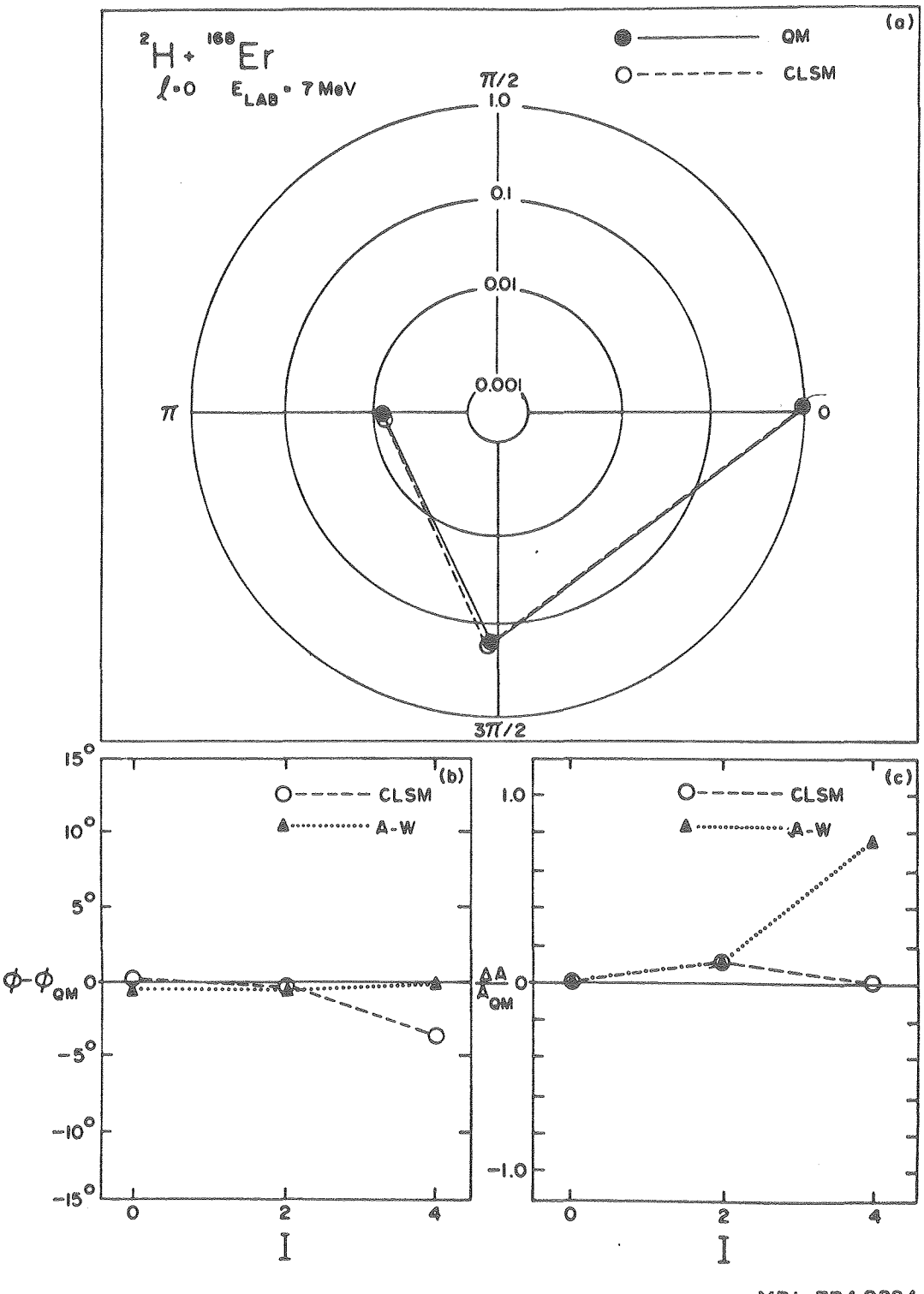

XBL 774-8304

Fig. III-2 Same as Fig. III-1 for the projectile ^2H at 7 MeV laboratory energy.

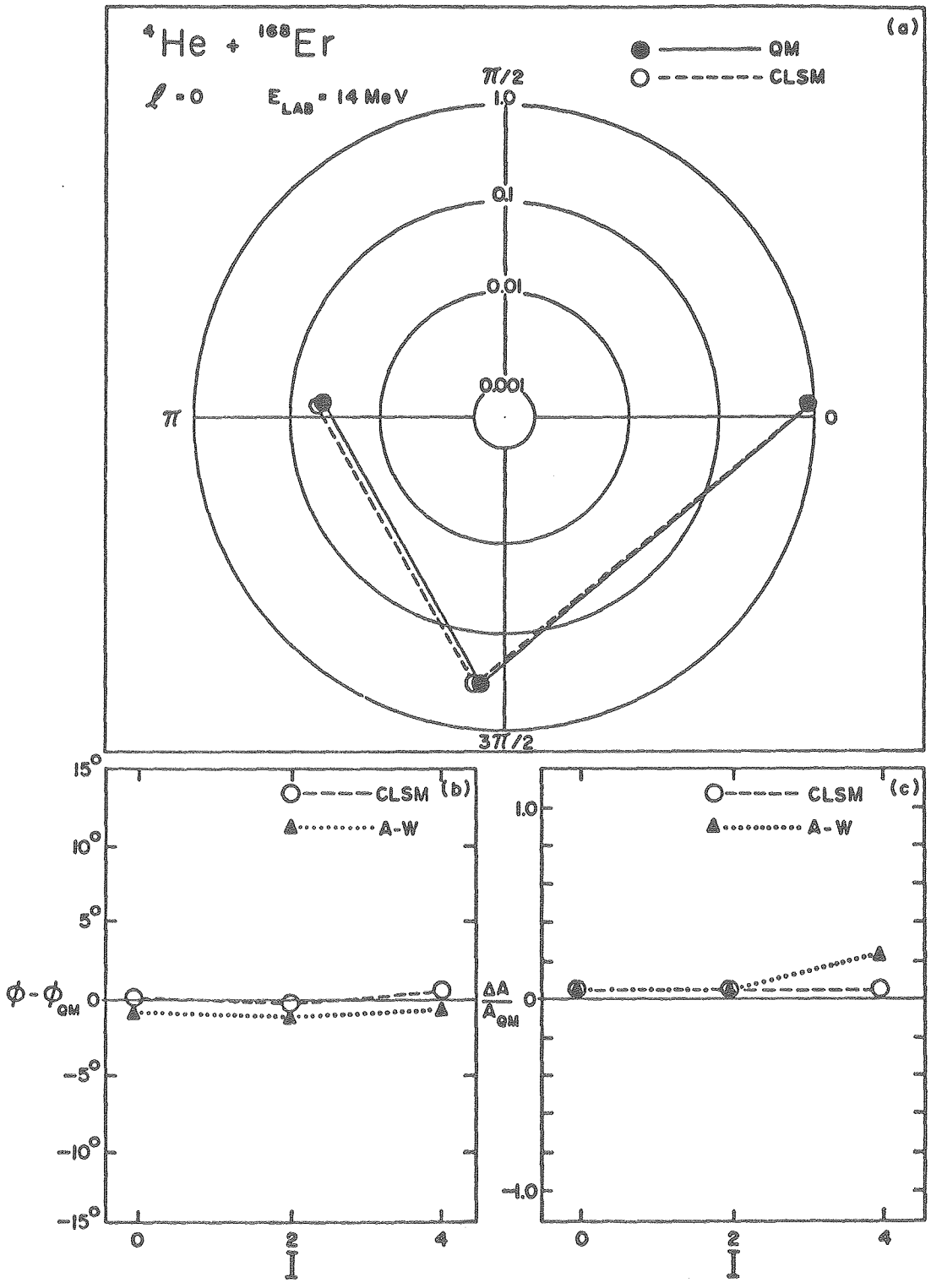

Fig. III-3 Same as Fig. III-1 for the projectile ^{4}He at 14 MeV laboratory energy

XBL 774-8301

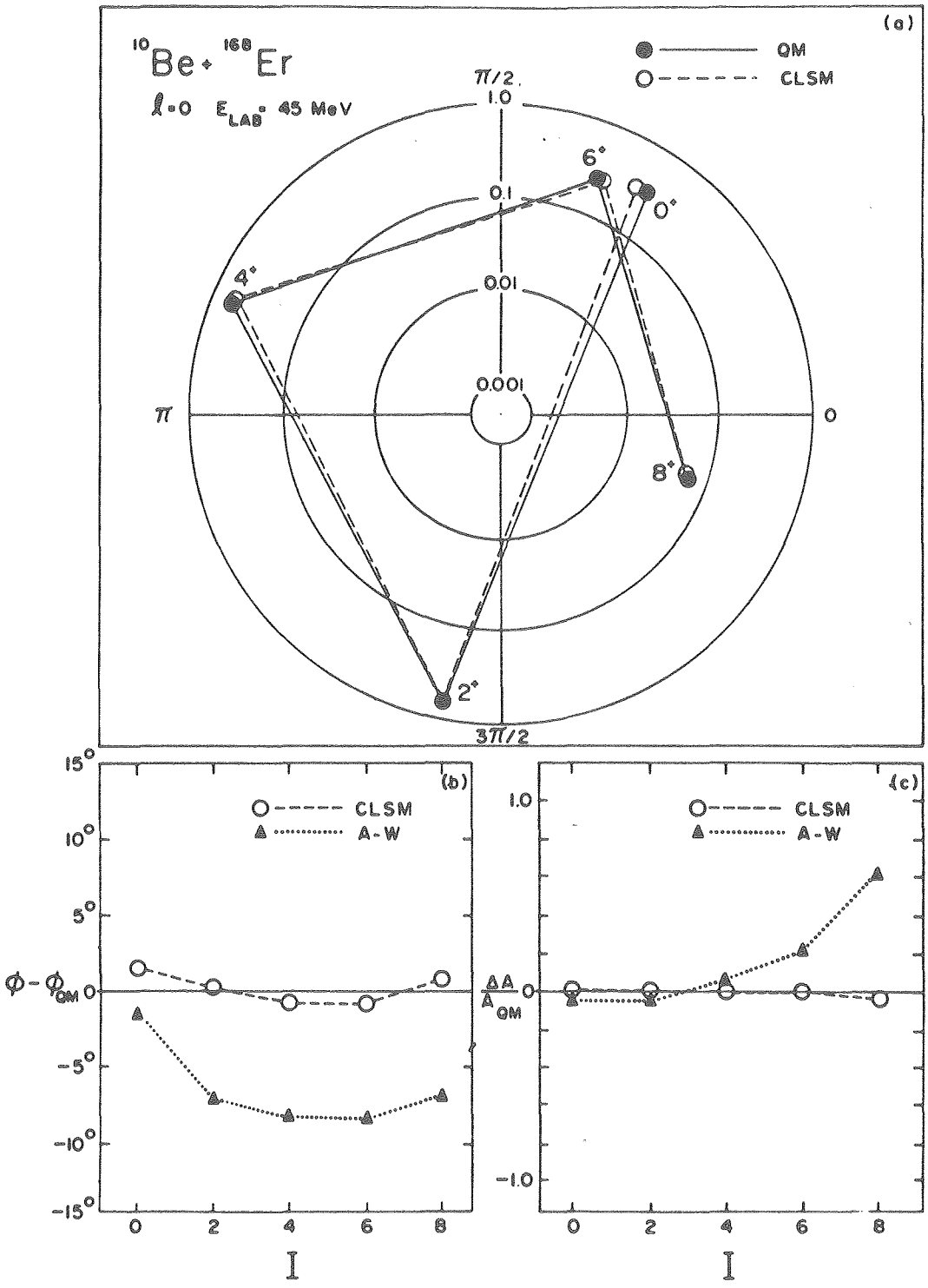

Fig. III-4 Same as Fig. III-1 for the projectile ^{10}Be at 45 MeV laboratory energy

XBL 774-8302

3. The Nature of the A-W and CLSM Approximations

It is important at this point to notice carefully the nature of the approximations implicit in the Alder-Winther semiclassical method and in the classical-limit S-matrix method. In the Alder-Winther[47] approach one solves the time-dependent Schrödinger equation for the deformed target.

$$i\hbar \frac{\partial}{\partial t} |\psi(t)> = [H_0 + H_E(t)]|\psi(t)> \qquad (B\text{-}3)$$

where H_0 is the Hamiltonian of the free nucleus and $H_E(t)$ the electromagnetic interaction with the projectile. In order to obtain $H_E(t)$ the approximation is made that the projectile behaves as a classical particle moving under the influence of the monopole-monopole part of the electromagnetic potential. Therefore the projectile's trajectory is a hyperbola. In order to take into account the fact that the projectile loses energy during the collision, and since it is not possible to determine at which point of the trajectory is this energy transferred to the target, the hyperbola is taken to correspond not to the initial or final energies of the projectile but to the geometric mean of these energies E_I^*.

$$E_I^* = \sqrt{E_0 \cdot E_I} \qquad (5)$$

where E_0 and E_I are the projectile's initial kinetic energy, and the final kinetic energy after leaving the target excited to the rotational spin I, respectively. In terms of the magnitudes defined in Ch. II they are

$$E_0 = \frac{1}{2} m v_o^2 \quad \text{and} \quad E_I = \frac{1}{2} m v_o^2 - \frac{\hbar^2 I(I+1)}{2\mathcal{I}}$$

The resulting trajectory corresponding to E_I^* is often referred to as an energy-symmetrized hyperbola.

In short, we see that the A-W method treats the target internal excitation degrees of freedom quantum-mechanically but treats the projectile degrees of freedom using approximate classical dynamics.

The validity of this approximation rests on whether the wave-packet representing the projectile behaves as a localized particle subject to classical equations of motion and, if so, whether the deviations from a Rutherford trajectory arising from the non-central part of the potential that was completely neglected are sufficient to invalidate the approximate classical dynamics employed.

The first question relates to whether there are explicit quantum dynamical effects operating which cast doubt on the applicability of the concept of a classical trajectory. It is a question about phenomena which vanish in the limit $\hbar \to 0$ and which can only be fully answered in the context of a rigorous quantum mechanical analysis. The second question concerns effects which are due to approximations in the classical dynamics employed and which are independent of $\hbar$. This question might reasonably be answered within a classical or classical-limit framework.

In the CLSM method one forsakes the semiclassical prescription of a quantum-mechanical treatment for the internal degrees of freedom of the target and approximate classical treatment of the projectile motion. Instead, both the internal and projectile degrees of freedom

are described by exact classical dynamics. One retains certain quantum-mechanical features since superposition is implicit in the CLSM formalism, and it is very important to realize that essentially all so-called quantum-mechanical effects result directly from the superposition principle.[48] Therefore it is reasonable to expect that the quantum effects are contained at least qualitatively in the CLSM formalism.

As noted by Marcus[32] the expression we are using for the S-matrix elements does not satisfy the requirement of time reversibility. It is not hard, though, to extend the CLSM formalism to include, at least approximately, this requirement.[32] The numerical results of Miller[11] and Wong and Marcus[30] indicate that we should expect our expression to be quite accurate, except maybe when the excitation probabilities are extremely small.

The results we just showed in Figs. III-1-4 and Table III-1 are in agreement with this conclusion. The use of an expression for the S-matrix satisfying time reversibility is being considered at the present moment.

4. The Parameter η_0

As it has been pointed out many times[7,8,43-45,47] the Sommerfeld parameter η_0 defined in (II-31) plays a most important role in assessing the validity of the semiclassical description. This is to be expected since η_0 equals the ratio of half the distance of closest approach to the projectile de Broglie wavelength

$$\eta_0 = \frac{a}{\lambda_0} \tag{6}$$

Here $\lambda_0 = \hbar/mv_0$ and a is defined as in (II-31). Therefore η_0 measures the spatial confinement of the wave-packet describing the projectile relative to the characteristic interaction distance, and indicates therefore the degree to which the wave-packet will remain intact during the interaction. A classical description of the projectile will be appropriate if $\eta_0 >> 1$ while a full quantum mechanical treatment will be necessary if $\eta_0 << 1$. For reference we give in Table III-2 the values of the Sommerfeld parameter η_0 and also of the other parameters q_2 and ξ appearing in the classical equations of motion written in dimensionless coordinates (Eq. (II-33)), for different systems we are considering in this work. We must keep in mind that these parameters are both system dependent and energy dependent. Their values for other energies can be easily found from their respective energy dependencies:

$$\begin{aligned} \eta_0 &\propto E^{-1/2} \\ q_2 &\propto E^{3/2} \\ \xi &\propto E^{-3/2} \end{aligned} \qquad (7)$$

In these equations E is the total energy of the system taken in either the laboratory or the center of mass reference frames.

From Table III-2 we see that except maybe for the very lightest projectiles the condition $\eta_0 >> 1$ is well satisfied.

Therefore we expect that the errors coming from the assumption that the projectile can be described as a point particle following a classical trajectory instead of a wave-packet obeying the laws of quantum

Table III-2. Values of the dimensionless parameters η_0, q_2, ξ and the auxiliary parameters q_2/η_0 and $q_2\,\xi$ for several physical systems

SYSTEM	LAB ENERGY(MeV)	η_0	q_2	ξ	q_2/η_0	$q_2\,\xi$
$^{1}H + ^{168}Er$	7	4.05	0.231	0.0232	0.057	0.005
$^{2}H + ^{168}Er$	7	5.72	0.322	0.0330	0.056	0.011
$^{4}He + ^{168}Er$	14	11.5	0.630	0.0334	0.055	0.021
$^{10}Be + ^{168}Er$	45	20.2	2.68	0.0190	0.133	0.051
$^{10}BE + ^{154}Sm$	30	22.6	1.54	0.0328	0.068	0.051
$^{40}Ar + ^{178}H_f$	145	107.	4.08	0.0422	0.038	0.172
$^{56}Fe + ^{178}H_f$	240	142.	6.18	0.0363	0.043	0.224
$^{40}Ar + ^{238}U$	170	127.	5.70	0.0196	0.045	0.112
$^{86}Kr + ^{238}U$	400	286.	11.1	0.0185	0.039	0.206
$^{136}Xe + ^{238}U$	600	374	12.9	0.0220	0.034	0.283

mechanics are very small. Then the differences between the quantum mechanical and semiclassical calculations should be due mainly to the approximate orbital dynamics employed in the semiclassical description. The differences between the quantum mechanical and CLSM calculations, on the other hand, should come mostly from the way the target is described, that is, by classical mechanics plus superposition. The results shown before (Figs. III-1-4 and Table III-1) seem to indicate that even for systems for which very little rotational excitation takes place, - those for which the classical description of the rotor is less appropriate -, the CLSM method furnished accurate results. It is to be expected then that for the cases of heavy projectiles where high rotational spins are excited this method should work even better. This conclusion cannot be tested directly, since the now existing computer codes cannot be applied with confidence in this region, but we think the evidence presented here to support it is strong.

Besides the one mentioned before, the parameter η_0 plays another important role. From consideration of the equations of motion (II-33) we see that if we allow η_0 go to infinity in these equations the trajectory of the projectile becomes a hyperbola. Therefore $1/\eta_0$, or rather q_2/η_0 measures the deviation of the projectile orbit from that of a pure Rutherford hyperbola. For this reason Massmann[25] proposed to designate this ratio as a new parameter, which from (7) we see it varies quadriatically with the energy. He also observed that the product $q_2\ \xi$ could be taken as another parameter, with the further advantage of being energy independent, and depending only on the projectile-target

system considered. We have shown the values of q_2/n_0 and $q_2\,\xi$ for several systems in Table III-2.

Since q_2/n_0 measures the deviation of the projectile trajectory from a pure hyperbola, we should find that as q_2/n_0 increases the A-W results become increasingly different from the quantum mechanical ones, while the CLSM results should not suffer in this process.

We have tested this idea for the case shown in Fig. III-5 and in Table III-3, by the simple expedient of raising the energy of the system considered due to the quadratic dependence of q_2/n_0 with the energy. The results verify this prediction. We notice that the percentage error of the Alder-Winther R-matrix increases monotonically with energy as expected from the fact that the quadrupole interaction, which is not considered to affect the orbits in this approach, becomes rapidly more strong as the projectile gets closer to the target due to the larger energy.

Another effect that is apparent from Fig. III-5 is that the relative error increases rapidly with angular momentum. This fits nicely into the idea of an orbital effect, since in the approximate dynamics used in the A-W formalism the angular momentum is not conserved.

By looking now separately at the amplitudes and phases, (see Figs. III-6 and 7) we see that the relative error in the amplitude increases mostly with increasing spin, not showing a clear trend with energy, why the opposite is true with the error in the phase, where the error increases with energy but not with spin.

From Table III-3 we see that the CLSM results do not show much structure with spin or energy, and that the errors are considerably less

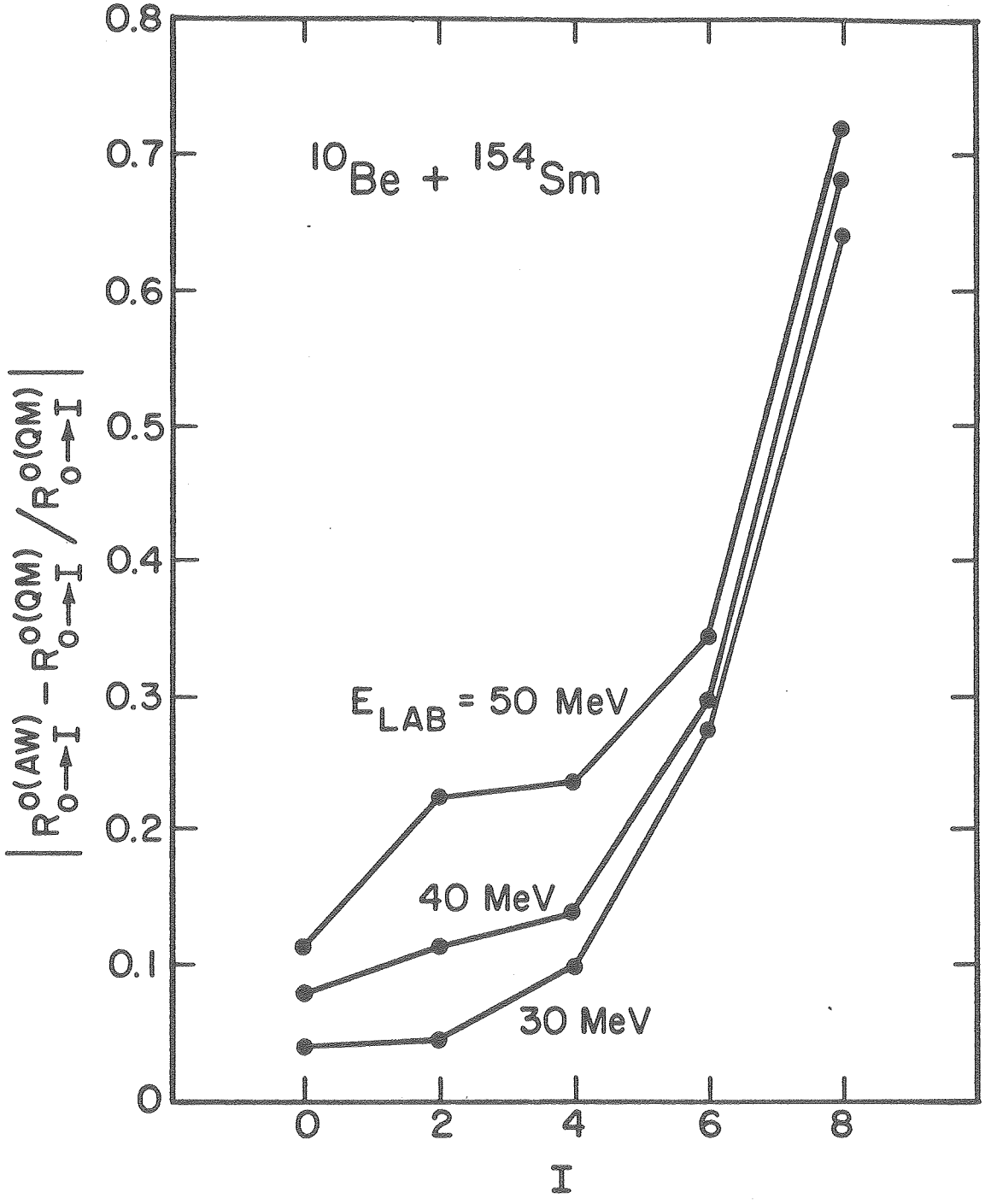

Fig. III-5

XBL 774-8289

Fig. III-5 Relative differences between the quantum mechanical (QM) and semiclassical (A-W) calculations of the complex $\ell = 0$ R-matrix elements for Coulomb excitation of rotational states in ^{154}Sm. The quadrupole moment of ^{154}Sm is taken to be $Q_0^{(2)} = 6.82$ b and the energy levels are taken from the rotational moment with $E_{2+} = 0.082$ MeV. The projectiles are ^{10}Be ions at 30, 40 and 50 MeV laboratory energy. The relative differences are seen to increase both with the projectile energy and with the spin of the excited state.

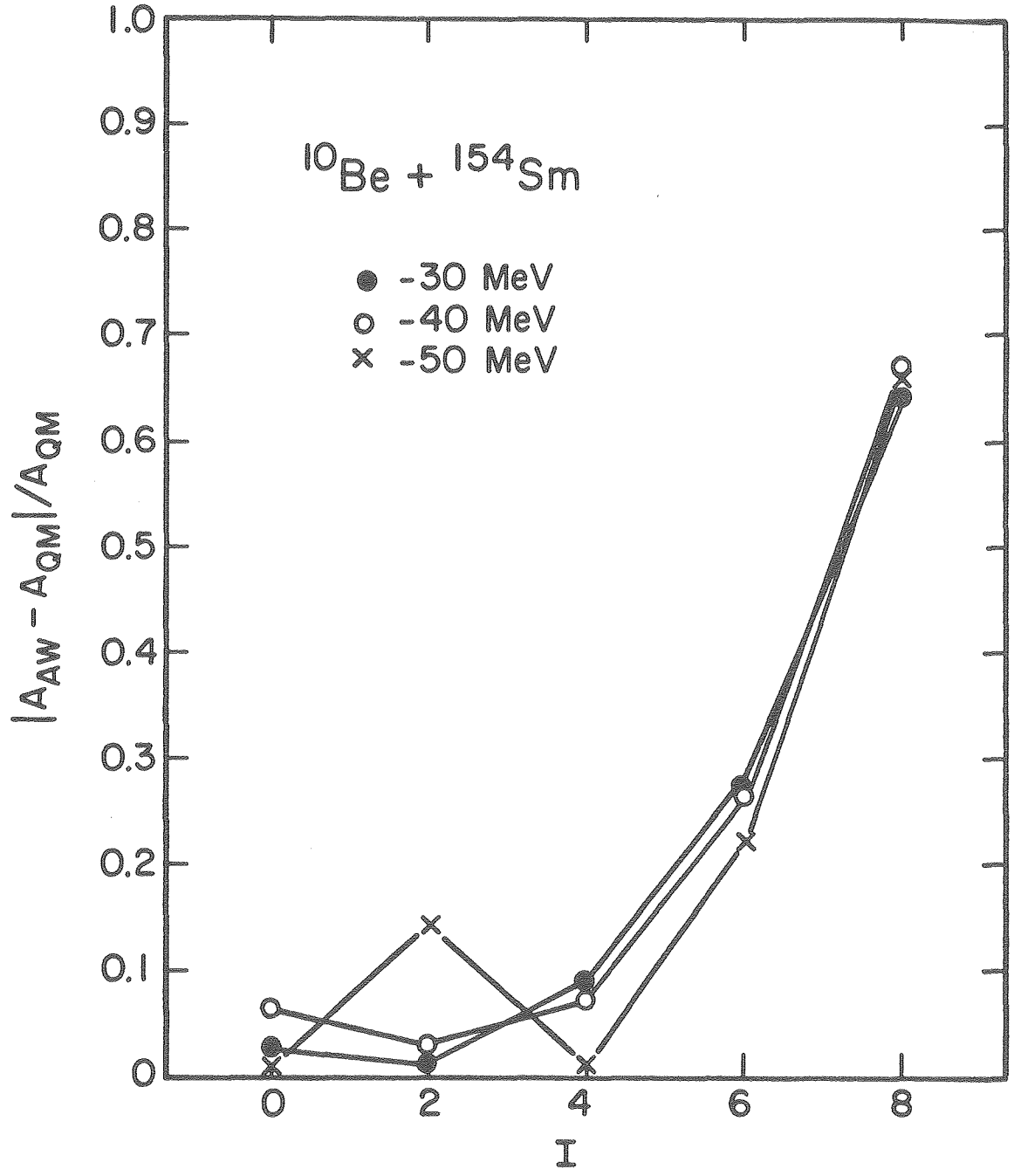

Fig. III-6 Same as Fig. (III-5) except that here the relative differences between the amplitudes of the R-matrix elements are plotted.

XBL 774-8296

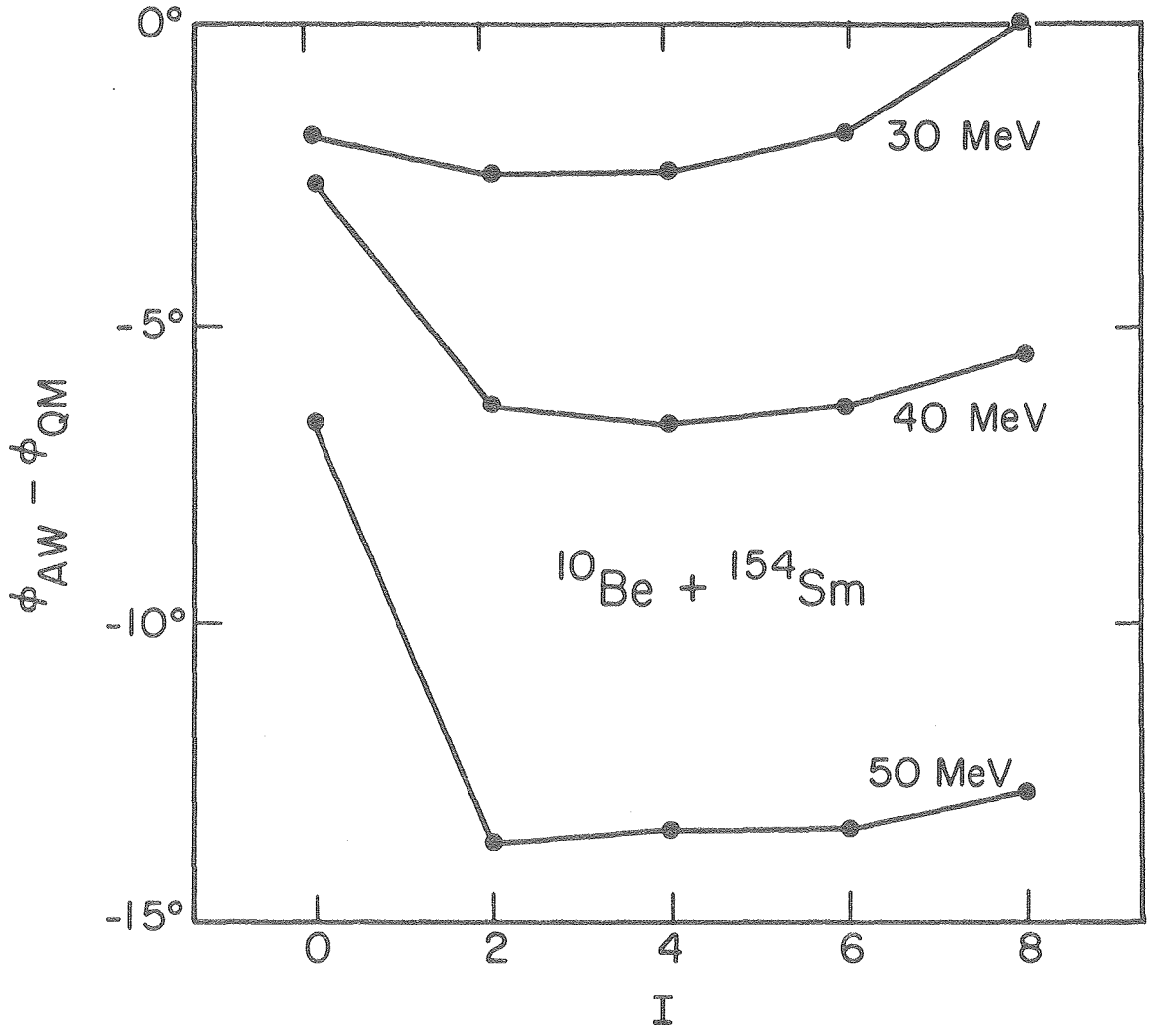

Fig. III-7 Same as Fig. (III-5) except that here the differences between the phases of the R-matrix elements are plotted. XBL 774-8295

Table III-3. Relative errors of the R-matrix elements for $\ell=0$ obtained by the Alder-Winther and CLSM methods. The system considered is $^{10}Be + ^{154}Sm$. The ^{154}Sm was assumed to have a quadrupole moment $Q_2=6.826b$ and the energy levels were taken from the rotational model with $E_{2^+} = 0.082$ MeV.

$$\left| \frac{R^0_{0\to I}(A\text{-}W) - R^0_{0\to I}(QM)}{R^0_{0\to I}(QM)} \right|$$

ENERGY (MeV)	SPIN	ALDER-WINTHER	CLSM
30	0	0.040	0.036
	2	0.045	0.023
	4	0.099	0.076
	6	0.272	0.047
	8	0.642	-
40	0	0.078	0.088
	2	0.113	0.013
	4	0.139	0.057
	6	0.295	0.076
	8	0.683	0.035
50	0	0.116	0.109
	2	0.223	0.085
	4	0.235	0.027
	6	0.341	0.087
	8	0.721	0.008

than the ones of the semiclassical method.

5. The Limit $\eta_0 \to \infty$

It will be instructive to consider a case where the trajectory of the projectile is the same in both the semiclassical and CLSM approaches, since such a case would be a good test of the idea that the approximate orbits used in the semiclassical method are responsible for most of the so-called quantum affects, and it would also be a direct test of how well the CLSM model handles the target rotation.

In order to obtain the same trajectories we must force the CLSM trajectories to be hyperbolas. This is possible by taking the value of the parameter η_0 to be infinity in the equations of motion (II-33). In order that these hyperbolas be the same as in the Winther-deBoer computer code, the simplest procedure is to modify this code so that the energies are not symmetrized. This means that we take all Rutherford orbits corresponding to the different excited rotational states as having the same energy, which is the case in the CLSM code when $\eta_0 \to \infty$. This modified Winther-deBoer computer code will be designated in what follows as the "unsymmetrized" code, while the original one will be referred to as the "standard" or "symmetrized" code.

The orbits in the unsymmetrized Winther-deBoer code and in the CLSM code for $\eta_0 \to \infty$ are exactly the same. We will now proceed to make the comparison of these two methods in this limit.

Since it is very convenient to have quantum mechanical calculations as a reference, our first case to be considered involves the light system $^{10}Be + ^{168}Er$ at 45 MeV laboratory energy.

The results are shown in Table III-4, and plotted in Fig. III-8. Since the quantum mechanical computer code AROSA is restricted to values of η of up to around 30, the limit for $\eta_0 \to \infty$ was obtained from a parabolic interpolation from the calculations done at lower η_0-s.

The analysis of the results shows several interesting features. First of all we see that as $1/\eta_0 \to 0$ both the QM and the CLSM values approach the unsymmetrized Winther-deBoer result. The way this convergence takes place is very similar for the QM and CLSM methods. Finally, it is important to remark that the symmetrization in the Winther-deBoer code always modifies the unsymmetrized results in the direction that approaches them to the QM and CLSM results for the actual value of η_0.

All this is consistent with the point of view expressed before that the main reason for the differences between the semiclassical and the quantum mechanical methods lies in the approximate orbital dynamics considered in the former. A procedure such as the energy symmetrization of the Rutherford orbits which makes the trajectories more realistic should improve the results, and this is actually observed.

The question now is what other steps may be taken in order to approach even more the trajectories employed in the semiclassical method to the ones found classically. Recently[46] attempts have been made to make an additional symmetrization with respect to angular momentum transfer. A marked improvement in the amplitude of the R-matrix was achieved, which is consistent with the previous discussion and the results shown in Fig. III-6.

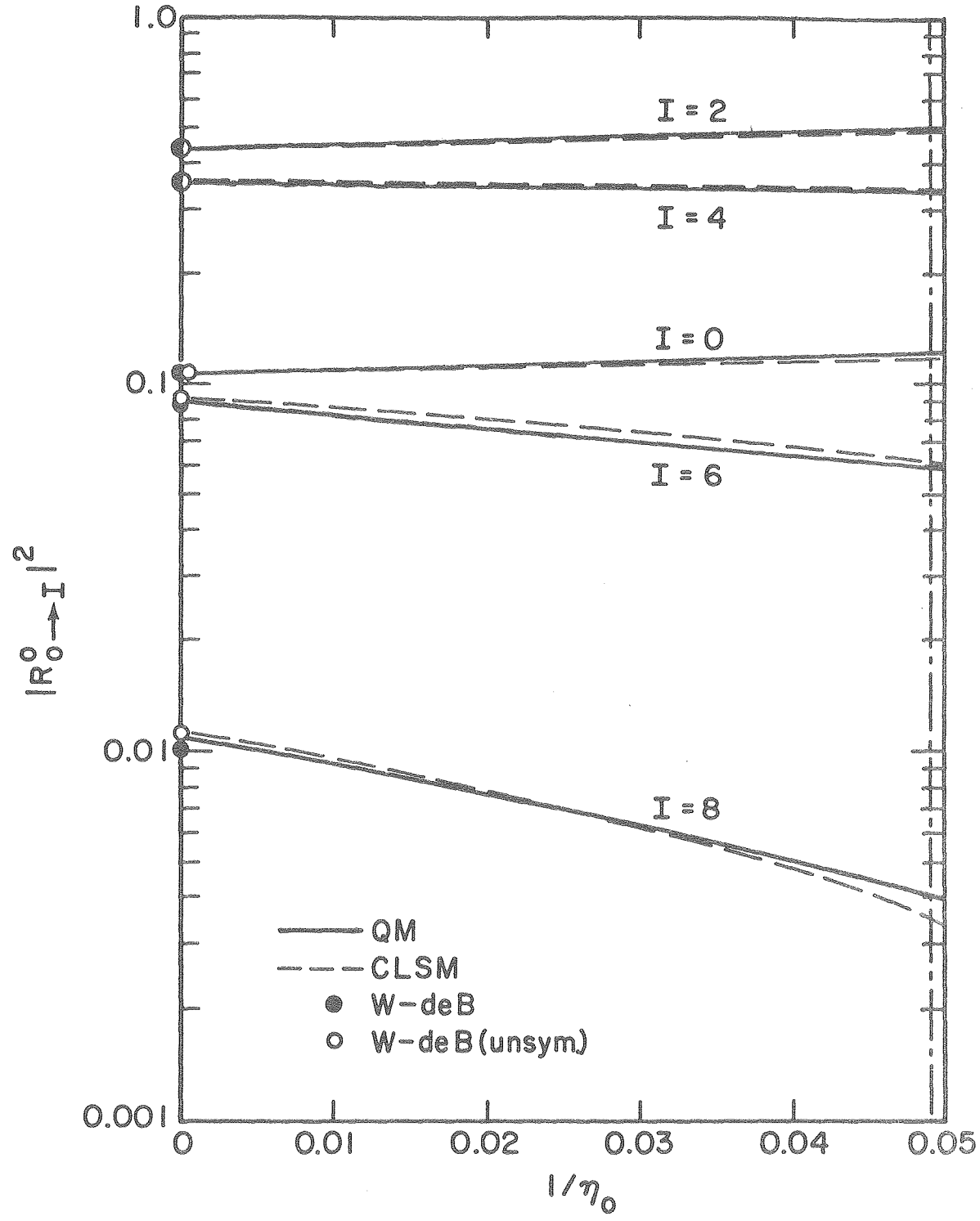

XBL 774-8287

Fig. III-8

Fig. III-8 The $\ell = 0$ R-matrix element amplitudes squared for the same system shown in Fig. (III-4), showing the variation of both the quantum mechanical and CLSM results with $1/\eta_0$. The dashed line at right indicates the actual value of η_0 for the system and energy considered. The dots at left represent the results of the calculations done using the standard Winther-de Boer computer code (full dots) and the one modified as described in the text (open circles). The CLSM and QM calculations are seen to be in good agreement to each other, and to converge to the modified Winther-de Boer results as $1/\eta_0 \to 0$.

Table III-4. The limit $n_0 \to \infty$ for the system $^{10}Be + ^{168}Er$ at ^{45}MeV laboratory energy. Q_2 and E_{2^+} for ^{168}Er were taken the same as in Fig. III-4. The quantities represented are the squares of the amplitudes of the R-matrix elements for $\ell=0$.

$1/n_0$	0.050*		0.040		0.030		0.0 (Extrapolated)		Unsymmetrized	Standard
SPIN	AROSA	CLSM	AROSA	CLSM	AROSA	CLSM	AROSA	CLSM	W-deB	W-deB
0	0.121	0.117	0.117	0.116	0.114	0.114	0.107	0.108	0.109	0.109
2	0.491	0.478	0.480	0.468	0.469	0.459	0.442	0.432	0.434	0.437
4	0.325	0.340	0.332	0.342	0.368	0.346	0.350	0.357	0.355	0.354
6	0.059	0.062	0.065	0.069	0.072	0.075	0.090	0.092	0.091	0.089
8	0.0040	0.0035	0.0051	0.0050	0.0064	0.0065	0.0110	0.0116	0.0111	0.0103

*Actual value of the parameter for this system.

A similar study was done for the heavier system $^{40}Ar + ^{238}U$ at 170 MeV, which lies beyond the range of applicability of the computer code AROSA. The results appear in Table III-5 and the cases for which the deviations are most apparent are illustrated in Fig. III-9. The good agreement found in the previous example plus the consideration that as the system becomes heavier it becomes more amenable to a classical description constitute strong indications that the differences between the CLSM results at the actual value of η_0 and the Winther-deBoer calculations are a measure of the orbit dynamical effects in this last formalism, and since the pure quantum-mechanical effects were seen before to be much smaller than these orbit dynamical effects, they are as well a good estimate of the differences to be expected between a Winther-deBoer calculation and a quantum-mechanical one.

We see that the rise of these effects is considerable specially for the case of high spins.

In Figs. III-10 → 13 we compare our results with those of the Winther-deBoer code for various heavy systems. From the preceding remarks we conclude that the differences between the results of the two methods are fair estimates of the quantum mechanical corrections to the semiclassical theory.

In Figs. III-8 → 13 we have plotted the modulus squared of the R-matrix elements for J = 0 without attaching to them any special physical significance. It should be clear that they represent the probabilities for exciting the different rotational states if we just consider a J = 0 partial wave incident on the target.

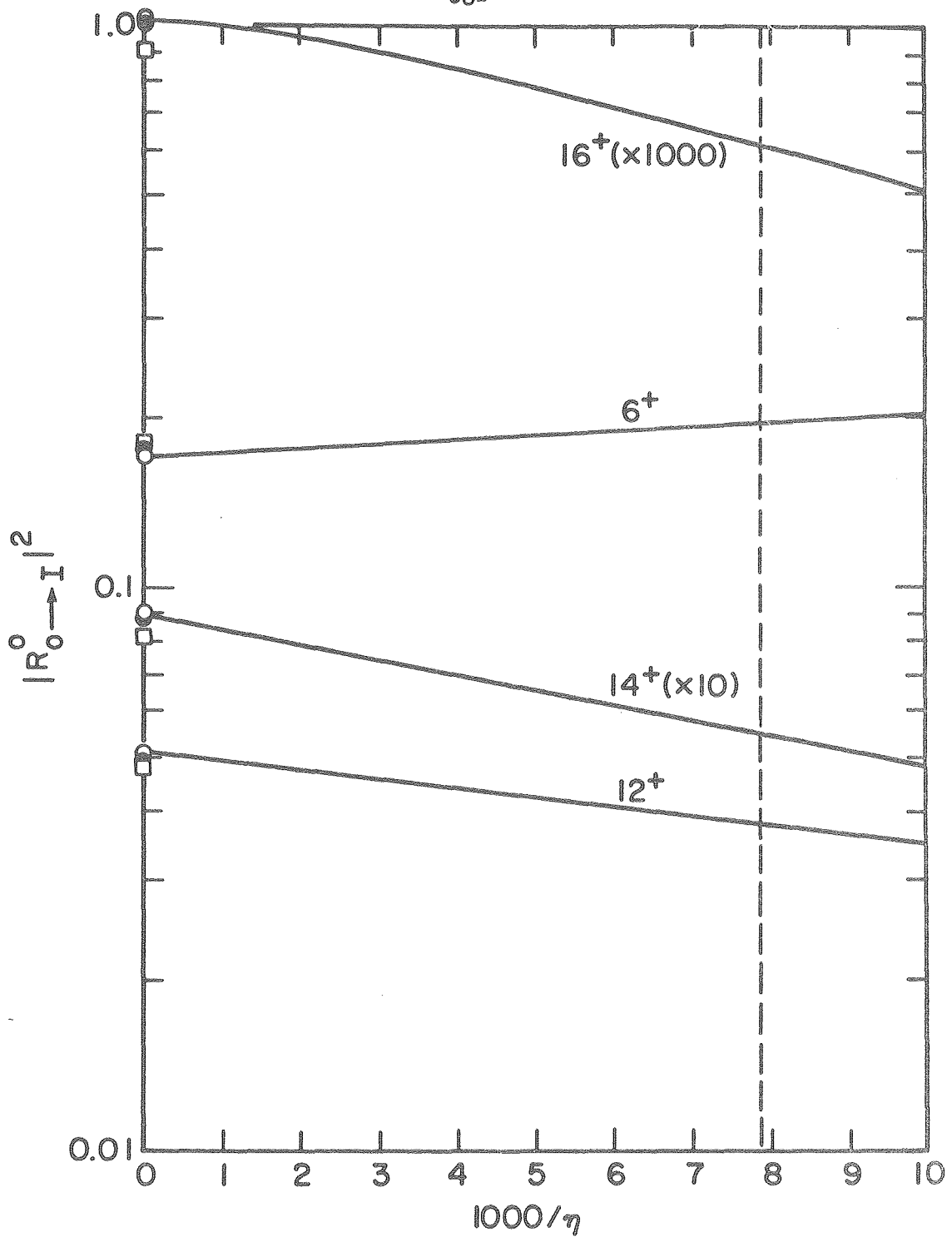

Fig. III-9 Same as Fig. III-8 except that the system is now ^{40}Ar on ^{238}U at 170 MeV laboratory energy. The quadrupole moment of ^{238}U is taken to be 11.12 b and its energy levels are taken from the rotational model with E_{2^+} = 0.0449 MeV. No quantum mechanical calculation is presented in this case. XBL 774-8291

Table III-5. The limit $\eta_0 \to \infty$ for the system $^{40}Ar + ^{238}U$ at 170 MeV laboratory energy. The quadrupole moment of ^{238}U is taken to be 11.12 b and the excitation energies taken from the rotational model for $E_{2+} = 0.0449$ MeV. The quantities represented are the squares of the R-matrix elements for $\ell = 0$.

SPIN \ $1/\eta_0$	CLSM							Winther-deBoer	
	0.0100	0.0079[a]	0.0060	0.0035	0.0025	0.0015	0.0[b]	Unsym.	Standard
0	0.077	0.076	0.075	0.075	0.074	0.074	0.074	0.074	0.074
2	0.171	0.170	0.170	0.169	0.169	0.169	0.169	0.171	0.171
4	0.059	0.059	0.060	0.060	0.061	0.061	0.059	0.058	0.058
6	0.204	0.197	0.191	0.182	0.179	0.175	0.170	0.179	0.181
8	0.300	0.300	0.298	0.297	0.296	0.294	0.291	0.293	0.294
10	0.149	0.154	0.158	0.164	0.167	0.169	0.170	0.167	0.166
12	0.035	0.038	0.041	0.045	0.046	0.048	0.051	0.049	0.048
14	0.0048	0.0055	0.0062	0.0073	0.0077	0.0082	0.0089	0.0087	0.0082
16	0.00051	0.00061	0.00071	0.00086	0.00093	0.00098	0.00103	0.00101	0.00091

(a) actual value of the parameter for this system

(b) parabolically extrapolated

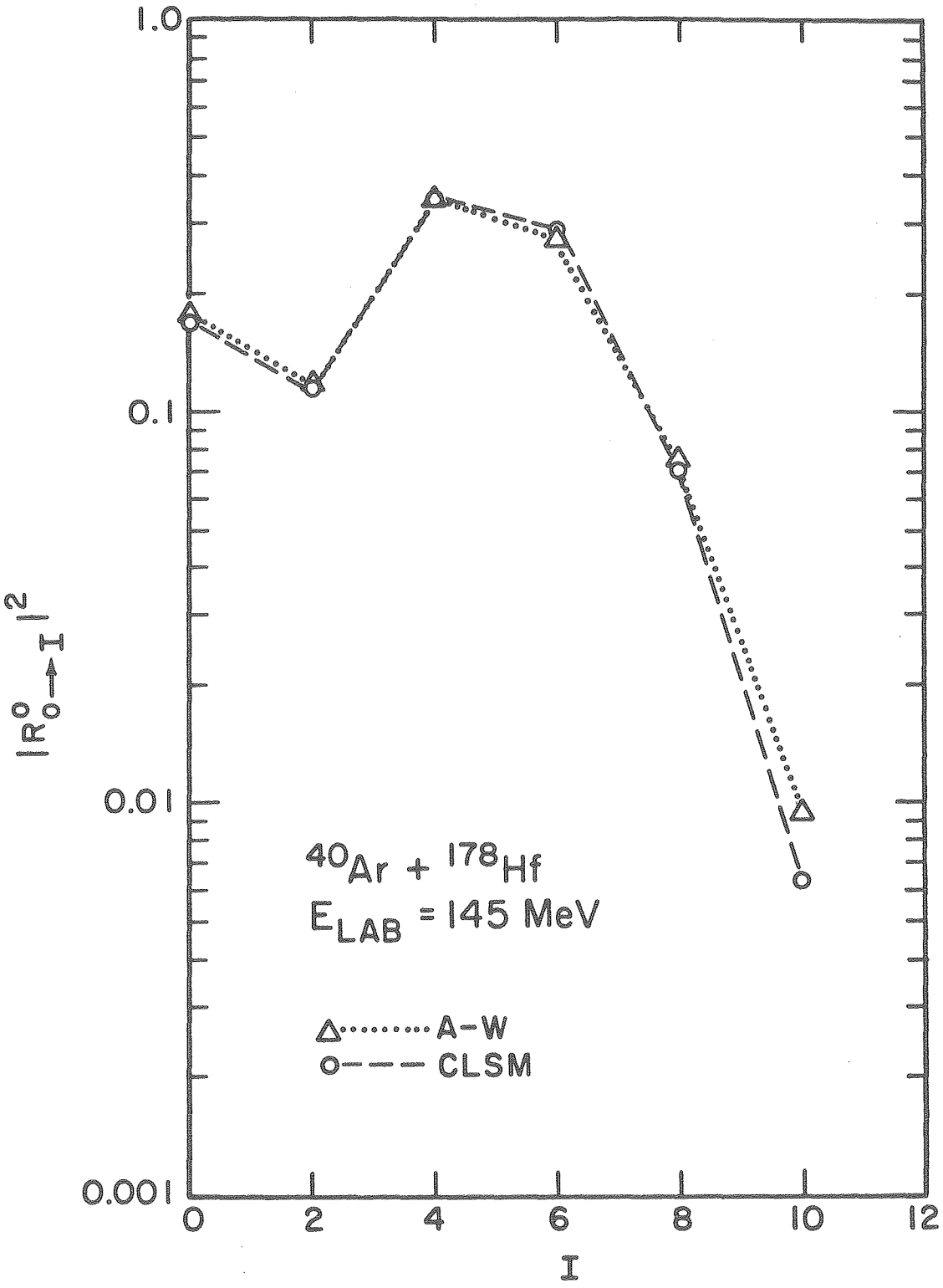

Fig. III-10

XBL 774-8290

Fig. III-10 The $\ell = 0$ R-matrix element amplitudes squared for Coulomb excitation of the ground band in ^{176}Hf by 145 MeV laboratory energy ^{40}Ar projectiles. The quadrupole moment of ^{178}Hf is taken to be 6.81 b and the energy levels are those of the rotational model for $E_{2^+} = 0.0932$ MeV. The comparison between the semiclassical (A-W) and CLSM results shows good agreement, with the same deviation for high spins as observed before (Figs. III 1-4).

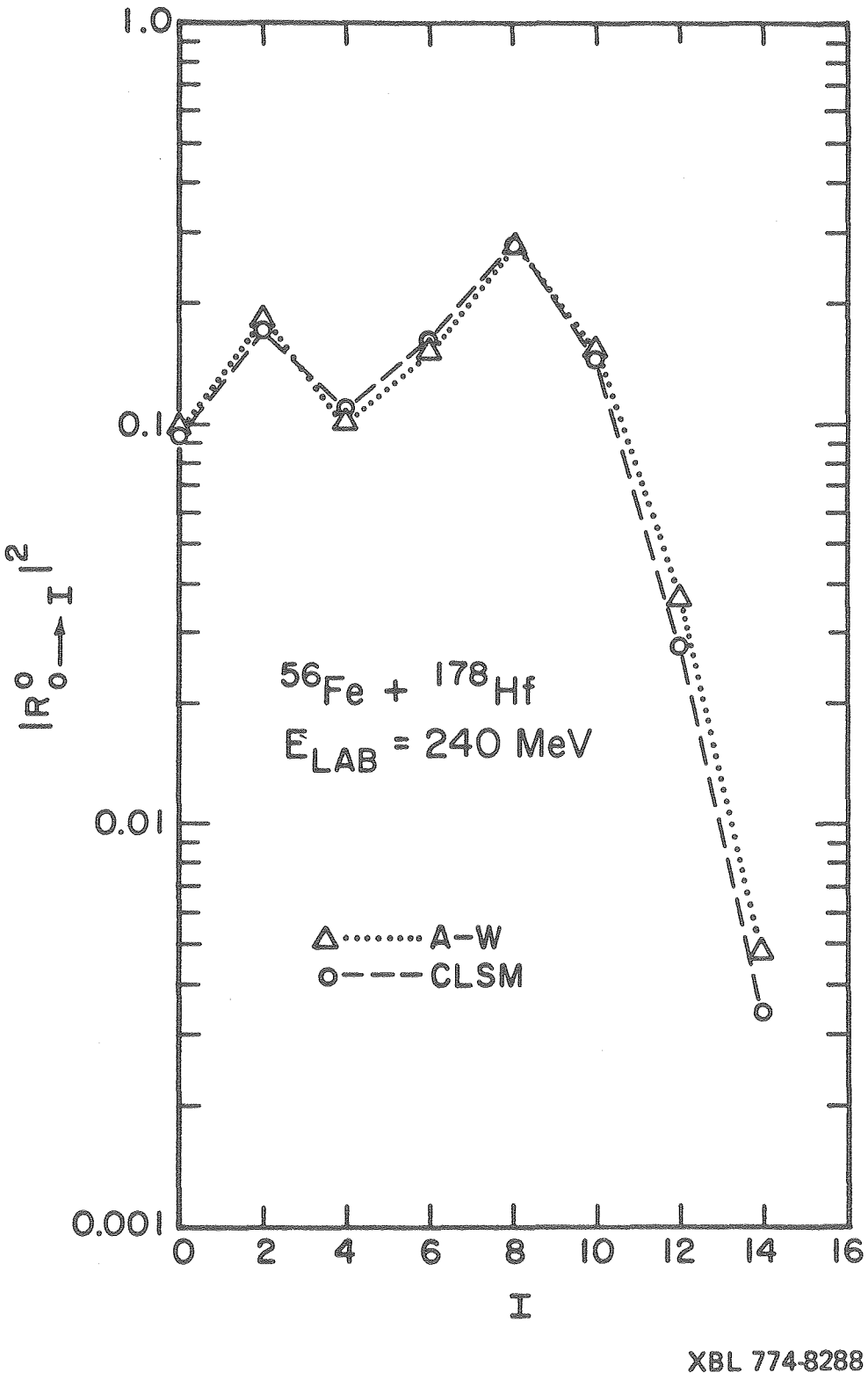

Fig. III-11 Same as (III-10) except that the projectile is ^{56}Fe at 240 MeV laboratory energy.

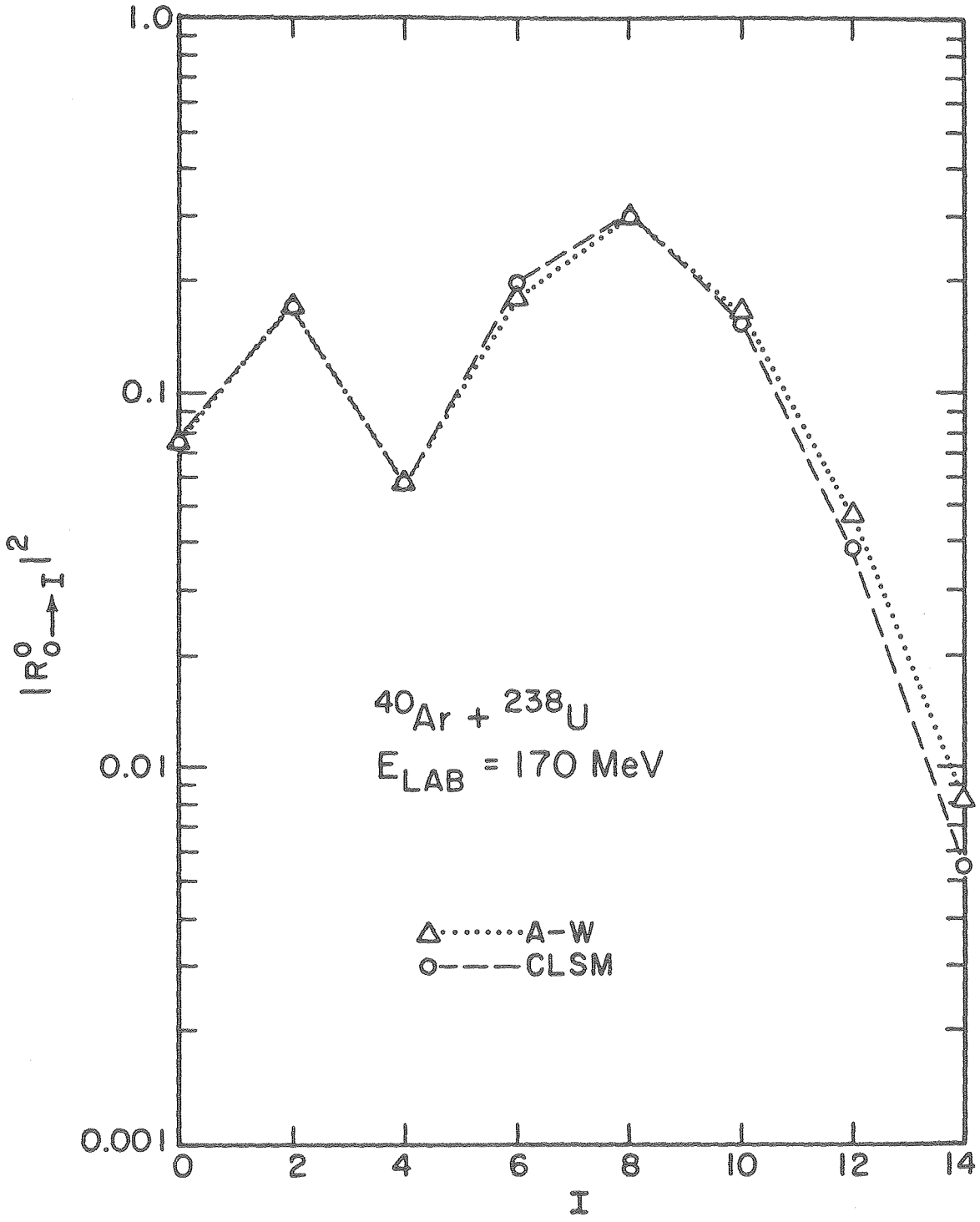

XBL 774-8292

Fig. III-12 Same as III-10 for the same system considered in Fig. III-9.

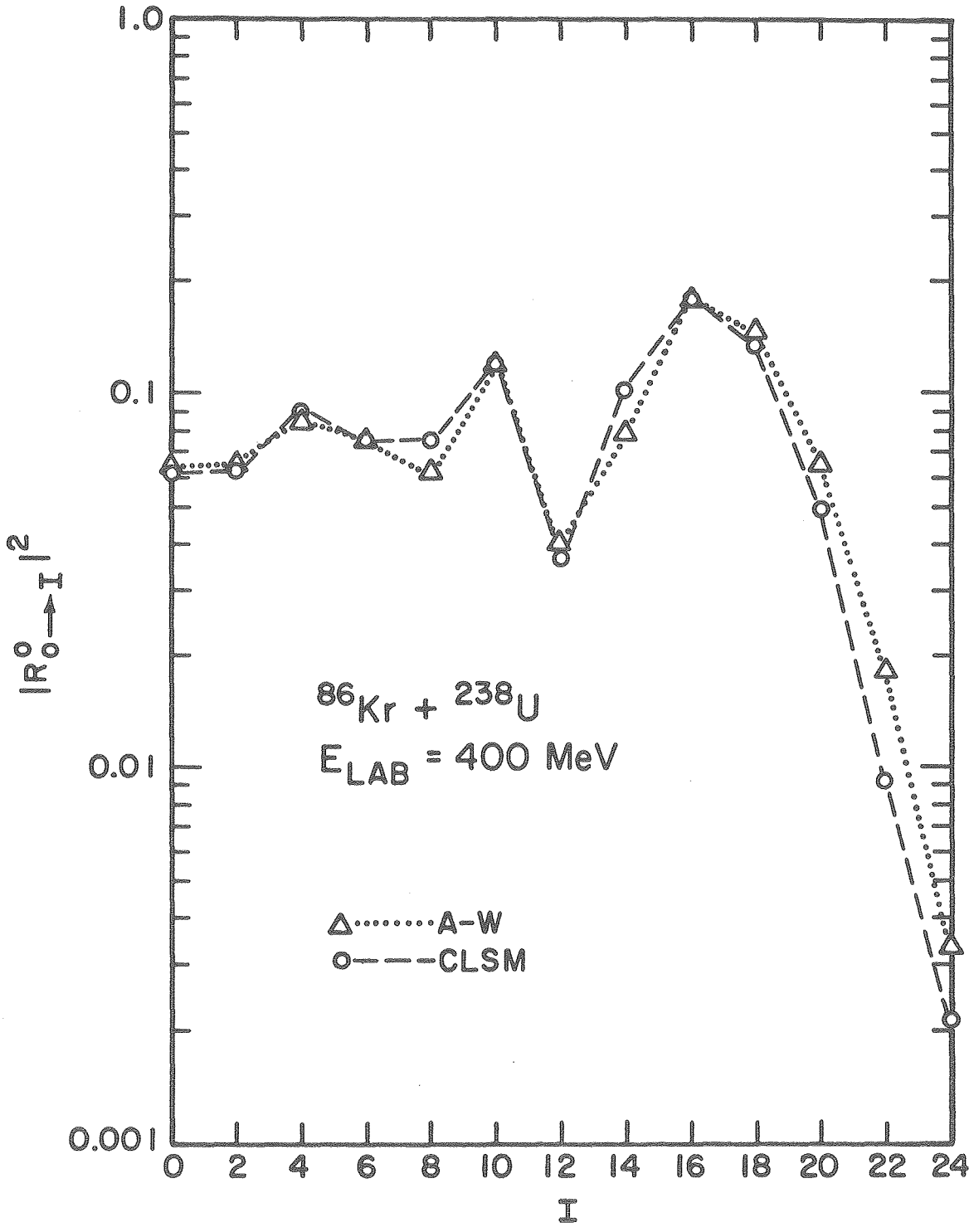

XBL 774-8294

Fig. III-13 Same as III-12 except that here the projectile is ^{86}Kr at 400 MeV laboratory energy.

In Fig. III-14 and Table III-6 we compare these amplitudes squared of the R-matrix elements to the excitation probabilities found by considering the partial wave sum over all J for a deflection angle of 180^{o}. They are actually close in value, and we may regard the quantities $|R^{o}_{0\to I}|^2$ as an approximate measure of $P_{0\to I}(\pi)$.

This could result surprising at first sight, since there are many partial waves contributing to the cross section for any deflection angle. The reason for this may be understood in a model similar to that employed for the Alder-Winther theory. In it we see that the trajectories that contribute most to backward scattering are rather similar, and therefore the time dependent perturbation felt by the target is more or less the same for all these trajectories. The fact that there is a close relation between the excitation probabilities for the $J = 0$ partial wave and those for a deflection angle of 180^{o} when all partial waves are summed appears then because those partial waves that do most of the contribution have similar excitation probabilities patterns.

6. Present limitations of the CLSM theory

The formalism presented in Ch. II requires for its validity that the wavefunction given by Eq. (II-16) be a good approximation to the true wavefunction. This approximation breaks down when the Jacobian $\frac{d\bar{X}}{dX_0}$ goes through zero, because at those points the wave function $\psi^{+}(\bar{X},\tau)$ becomes infinite.

In Fig. III-15 we show the function $\bar{X}(X_o)$ for several systems. We see that for one case shown there, there are points for which $d\bar{X}/dX_0$

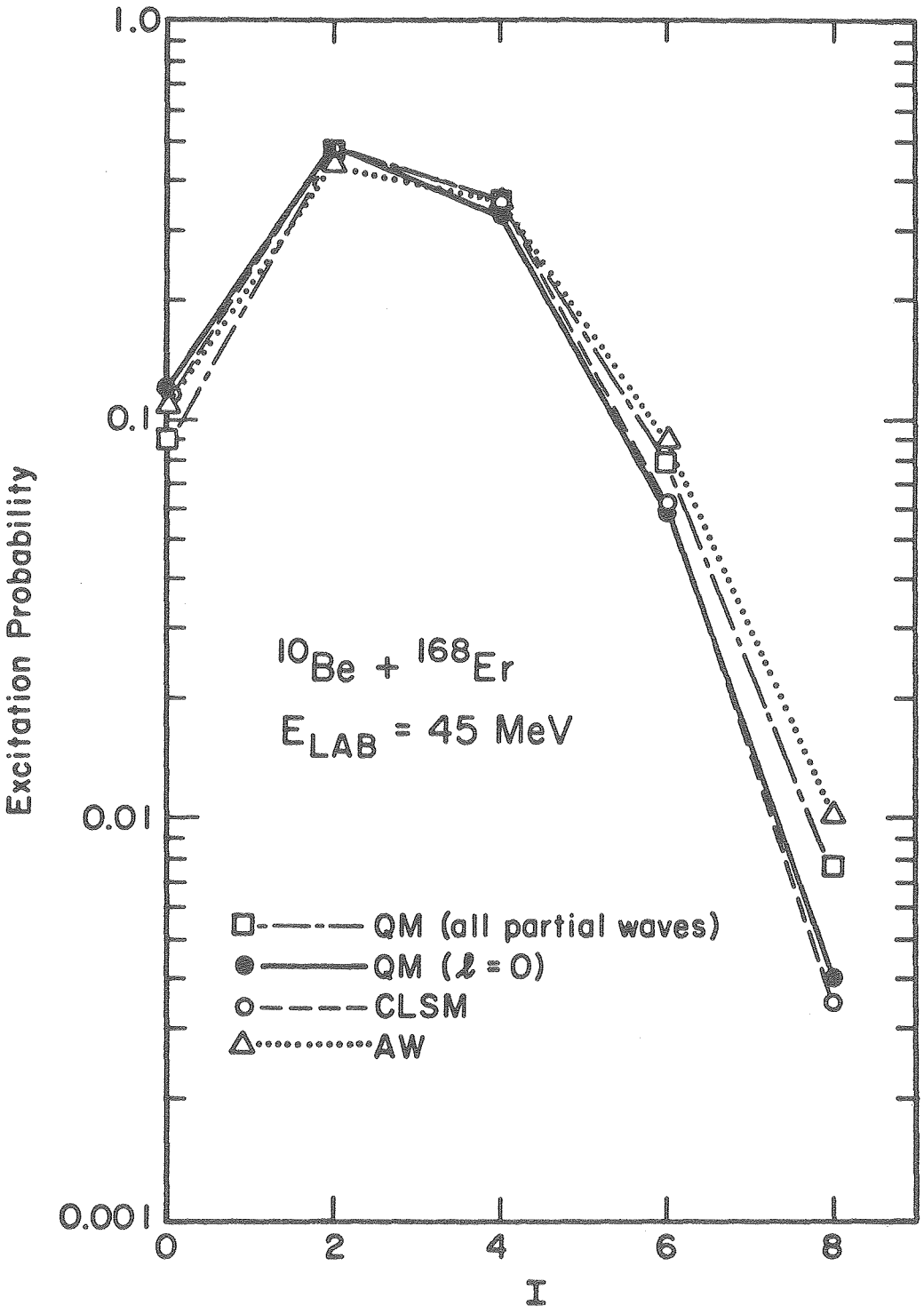

XBL 774-8293

Fig. III-14

Fig. III-14 Comparison of the backward scattering excitation probabilities found by means of the quantum mechanical code AROSA (in which the partial wave sum is evaluated) to the $\ell = 0$ R-matrix amplitudes squared obtained through the same code, through the CLSM method and by the semi-classical formalism (A-W).

Table III-6. Comparison of the excitation probabilities for a deflection angle of 180^{o} found by doing the partial wave sum using the computer code AROSA, to the $\ell = 0$ R-matrix element modulus squared obtained by means of the three other procedures discussed in the text. The system is the same as in Fig. III-4.

SPIN	QM (AROSA, ALL L)	QM (AROSA,L=0)	CLSM	A-W (WINTHER-deBOER)
0	0.089	0.121	0.117	0.109
2	0.475	0.491	0.478	0.434
4	0.352	0.325	0.340	0.354
6	0.078	0.059	0.062	0.089
8	0.0076	0.0040	0.0035	0.0103

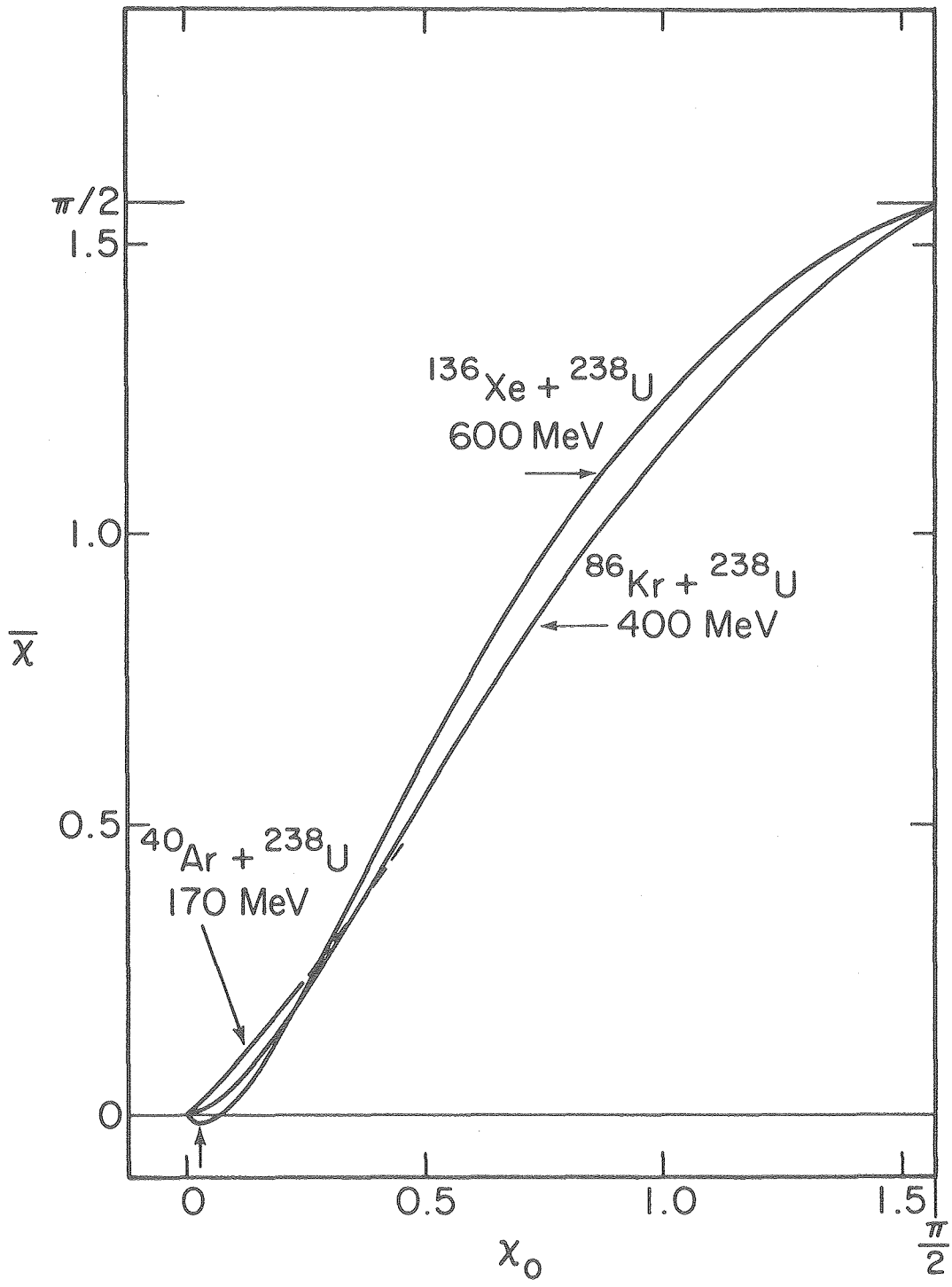

Fig. III-15

XBL 775-8593

Fig. III-15 The function $\bar{\chi}(\chi_0)$ for three different projectiles and energies on ^{238}U. The parameters for ^{238}U are taken to be the same as in Fig. III-9. The behavior of $\bar{\chi}(\chi_0)$ for ^{40}Ar is indicated only for low values of χ_0 in order not to overcrowd the figure. For higher values it is close to and slightly below that of ^{86}Kr. We see that $\bar{\chi}(\chi_0)$ for ^{136}Xe presents a point (marked with an arrow in the figure) at which $\frac{d\bar{\chi}}{d\chi_0} = 0$. Only the interval of χ_0 from 0 to $\frac{\pi}{2}$ was plotted since the curves are symmetrical around the point $(\frac{\pi}{2}, \frac{\pi}{2})$.

becomes zero. This does not mean that the results for cases like this are wrong, but we must accept the fact that some accuracy has been lost, and it is not simple to estimate the error for those cases.

Figure III-16 represents a plot of the region where the CLSM method is fully valid. We see that it is mostly a function of the system considered, in particular of the parameter

$$\frac{Q_0^{(2)}/Z_T}{\mathcal{I}/m} = \frac{4}{3} q_2 \xi \tag{8}$$

where all quantities have been defined in Ch. II Sec. 3.

We point to the fact that this will be also the region of validity of the USCA approximation, since the points where $d\bar{X}/d\chi_0 = 0$ will appear as spurious points of stationary phase.[49] If the true stationary phase points for a transition are not close to these spurious ones, then we expect the USCA to be still applicable, but to be sure one needs to find these spurious points besides the usual roots of $\hat{I}(\chi_0) = I + 1/2$ and this could become a serious problem.

Fortunately the region where the method is valid is quite wide, and one has to be careful only when working with very heavy projectiles.

The alternative of finding an approximate wavefunction of the type of (II-16) that does not have this drawback is presently under study.

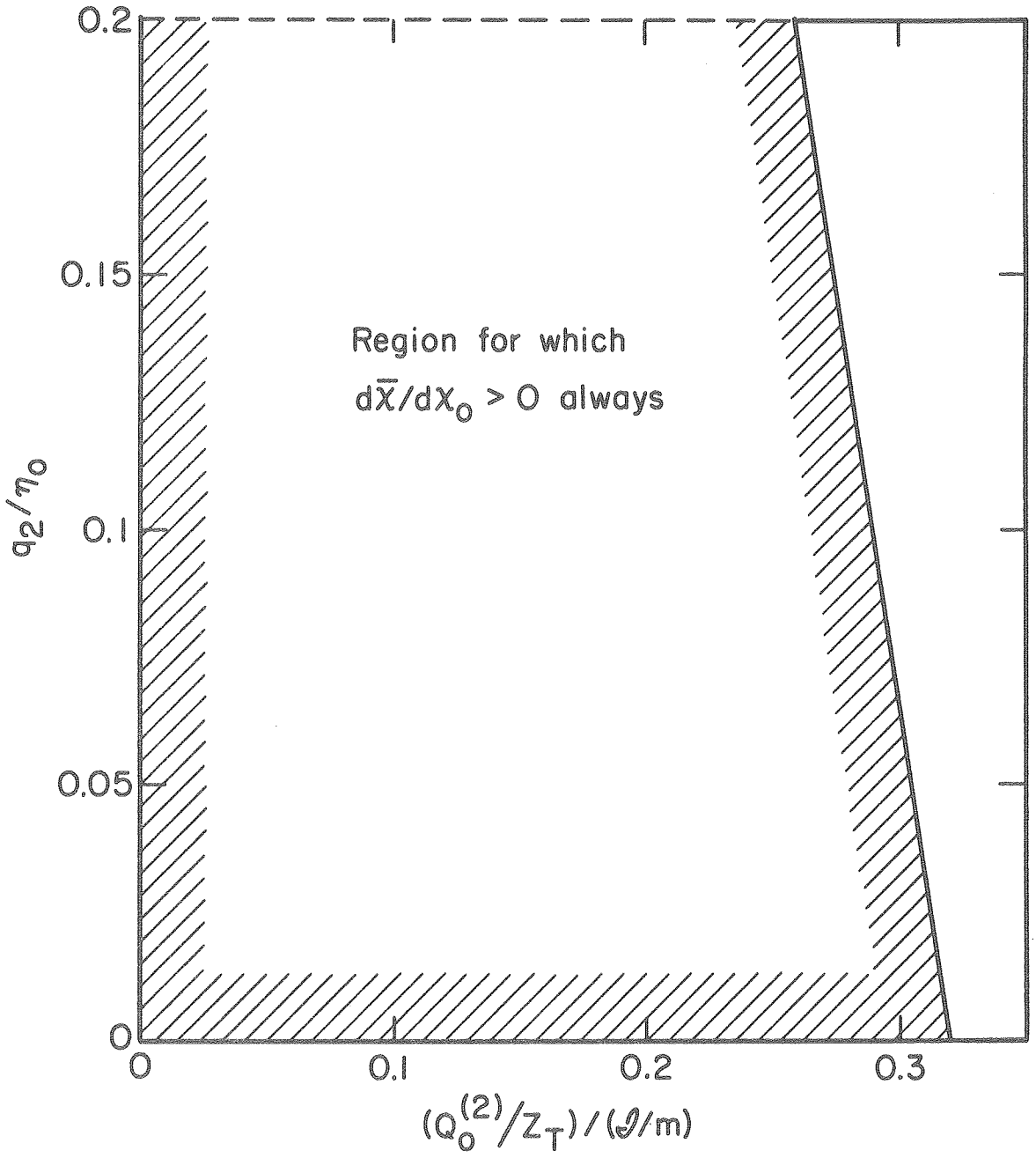

XBL 775-8585

Fig. III-16 Diagram shows the region over which the Jacobian $\frac{d\bar{X}}{dX_0} > 0$ always, and which therefore indicates where the wavefunction given by Eq. (II-16) does not break down.

IV. THEORY OF COULOMB-NUCLEAR INTERFERENCE FOR EXCITATION OF ROTATIONAL STATES

1. Introduction

In the previous chapters we have considered that the incident heavy-ion and the target nucleus interact only through the electromagnetic forces between them. This is valid as long as these two particles do not come into the range of their mutual nuclear interaction. Since the classical limit S-matrix (CLSM) method was seen to work nicely for the pure Coulomb case, the idea of generalizing it to include the nuclear potential follows very naturally. This generalization, however, is not as simple as it might be thought. The nuclear interaction between two heavy ions is usually represented by means of a complex potential; the classical Hamiltonian then becomes complex and therefore we find ourselves dealing with complex equations of motion and complex dynamical variables. The meaning of these complex quantities has to be clarified if we want to extend the CLSM method to the region where the nuclear potential begins to act.

The use of complex trajectories is by no means new in physics, and they were successfully employed in recent years in the study of molecular excitation and reactive collisions[12-18,33,36] in atomic physics while in nuclear physics they were applied to the problem of elastic and inelastic scattering from spherical nuclei.[19-22]

We will consider the case of deformed nuclei. Our concern here will be again to describe the excitation of the rotational states and not to study any other phenomena that appear when two such nuclei touch,

such as excitation of other collective modes, transfer of one or more nucleons, nor of the much more complex processes that appear at higher energies.

We will then assume throughout this chapter that the incoming projectile and the target nucleus are the same before and after the collision takes place, and that the only states excited in the target are those of the ground rotational band, while the projectile is not excited at all. The fact that rotational excitation is not the only process taking place is manifested in the reduction of the outgoing flux due to the imaginary part of the potential. The real part of this nuclear potential will give rise to a torque which is of opposite sense to that due to the electromagnetic forces (Fig. IV-1 illustrates).

We see then that the results should be strongly dependent on the particular nuclear potential that is considered. In fact, we will contend that this method could be a useful tool in finding a good potential for quasi-elastic scattering from deformed nuclei.

Since in the usual Coulomb excitation experiments one carefully limits the beam energy so as to avoid getting into the region where the nuclear interaction becomes effective, there is little experimental data in this region to attempt a determination of the nuclear potential parameters. Experimental work in this area is currently in progress.

2. Hamiltonian and Equations of Motion

The Hamiltonian will be the one given by Eq. (II-29) to which we will add the nuclear potential. We will also include an electric hexadecapole potential because at the higher energies considered in this chapter projectile and target get closer together than in the pure

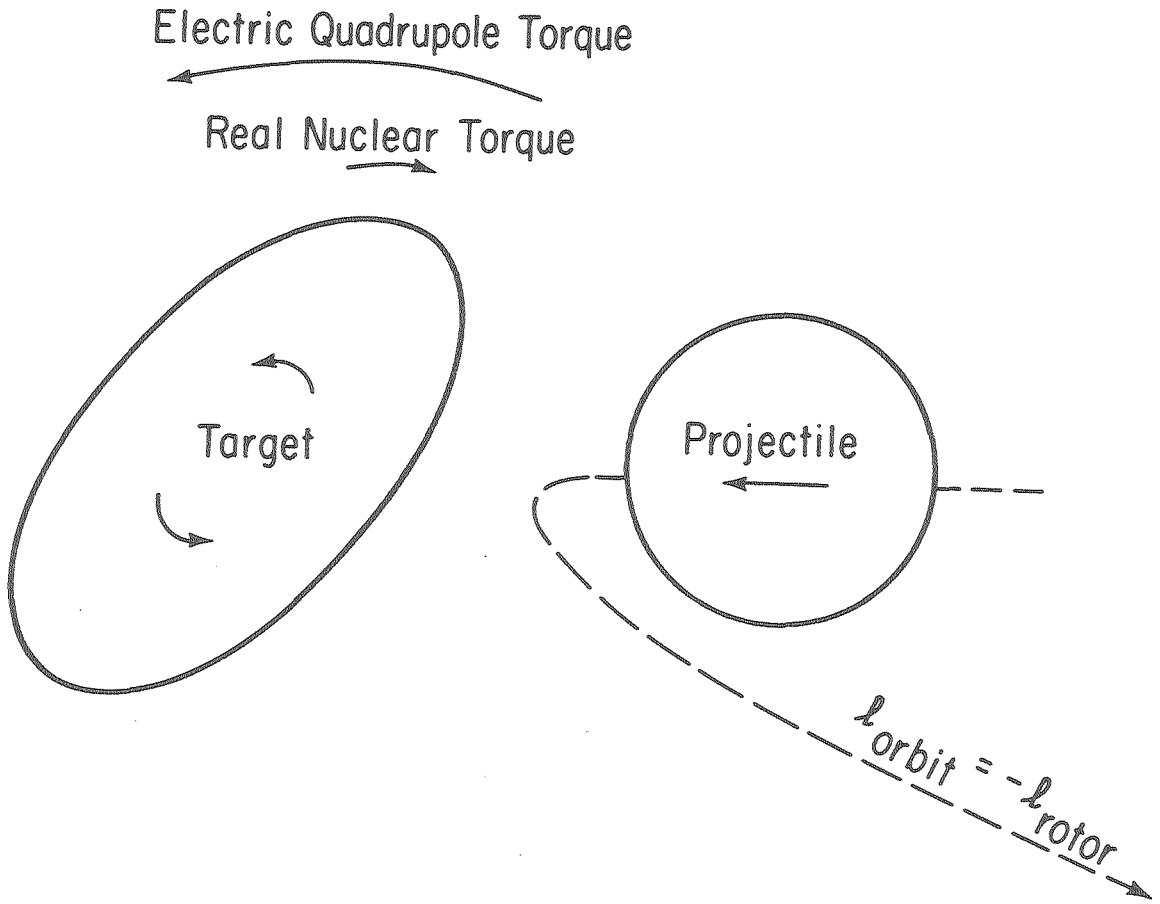

Fig. IV-1 The classical model for competition between the electromagnetic and nuclear forces.

XBL761-12A

Coulomb region and therefore this term becomes more important than before. The Hamiltonian will then be

$$H(r,p_r,\chi,p_\chi) = \frac{p_r^2}{2m} + \left(\frac{1}{2\mathcal{I}} + \frac{1}{2mr^2}\right)p_\chi^2$$

$$+ \frac{Z_p Z_T e^2}{r} + \frac{Z_p Q_0^{(2)} e^2}{2r^3} P_2(\cos\chi) \qquad (1)$$

$$+ \frac{Z_p Q_0^{(4)} e^2}{2r^5} P_4(\cos\chi) - V_R(r,\chi) - i\,V_I(r,\chi)$$

Here $Q_0^{(4)}$ is the hexadecapole electric moment, P_4 the usual Legendre polinomial of order four, V_R and V_I the real and imaginary part of the nuclear potential which precise functional form we will give below, and all other quantities have been defined in Chapter II using the same nomenclature as here. We will take V_R and V_I to have a Saxon-Wood dependence on the radial distance r, since this is the way in which it is most frequently expressed in the current literature. It will be very simple to adopt other parametrizations in this formalism, when enough data is available to make feasible a search for the most appropriate nuclear potential it will be interesting to consider other functional forms, such as the recently presented expressions in terms of proximity forces[50-52].

We take then

$$V_R = \frac{V}{1 + e^{\frac{r-R_R(\chi)}{a_R}}}$$

$$V_I = \frac{W}{1 + e^{\frac{r-R_I(\chi)}{a_I}}} \qquad (2)$$

V and W are the strength parameters of the real and imaginary parts of the potential, respectively, while a_R and a_I are their respective diffuseness parameters. $R_R(\chi)$ is given by

$$R_R(\chi) = R_0^R \left[A_p^{1/3} + A_T^{1/3} \left(1 + \beta_2 Y_{20}(\chi) + \beta_4 Y_{40}(\chi) - \frac{\beta_2^2 + \beta_4^2}{4\pi} \right) \right] \qquad (3)$$

and represents the sum of the radii for a relative orientation χ. Here R_0^R is the real radial parameter, A_p and A_T are the projectile and target mass numbers, respectively, the β_λ are the nuclear deformation parameters, the Y_{20} the spherical harmonic functions and the last term is included to take into consideration volume conservation. We will assume that the real and imaginary parts of the nuclear potential have the same angular dependence, so that $R_I(\chi)$ is obtained by replacing R_0^R in Eq. (3) with R_0^I. This is obviously a non-essential assumption, and it can be lifted very easily. It serves the purpose of limiting the number of parameters that we have to deal with.

We note that we are still taking the form $Z_p Z_T\, e^2/r$ for the monopole-monopole electric interaction. This is not strictly so in the nuclear force region where the charge densities of projectile and target do overlap; a folded potential would be more appropriate. We will nevertheless retain this simpler expression, since we will work at energies where very little interpenetration occurs and where therefore it is not worthwhile evaluating a folded potential.

From the Hamiltonian (1) the classical equations of motion are

$$\dot{r} = \frac{p_r}{m} \tag{4a}$$

$$\dot{p}_r = \frac{p_\chi^2}{mr^3} + \frac{Z_p Z_T e^2}{r^2} + \frac{3}{2}\frac{Z_p Q_0^{(2)} e^2}{r^4} P_2(\cos\chi) + \frac{5}{2}\frac{Z_p Q_0^{(4)} e^2}{r^6} P_4(\cos\chi) + \frac{\partial V_R(r,\chi)}{\partial r} + i\,\frac{\partial V_I(r,\chi)}{\partial r} \tag{4b}$$

$$\dot{\chi} = \left(\frac{1}{\mathscr{I}} + \frac{1}{mr^2}\right) p_\chi \tag{4c}$$

$$\dot{p}_\chi = -\frac{Z_p Q_0^{(2)} e^2}{2r^3}\,\frac{\partial}{\partial\chi} P_2(\cos\chi) - \frac{Z_p Q_0^{(4)} e^2}{2r^5}\,\frac{\partial}{\partial\chi} P_4(\cos\chi) + \frac{\partial V_R(r,\chi)}{\partial\chi} + i\,\frac{\partial V_I(r,\chi)}{\partial\chi} \tag{4d}$$

And as before we add the equation for the phase:

$$\dot{\phi} = -\frac{1}{\hbar}(r\,\dot{p}_r + \chi\,\dot{p}_\chi) \tag{5}$$

We immediately see that due to the imaginary part of the nuclear potential the dynamical variables r, p_r, χ, p_χ and the phase ϕ as well become complex numbers in the general case.

We will start our study by looking at some examples simpler than the general case in order to gain familiarity with the effect of each of the new terms we have incorporated into the Hamiltonian.

3. Purely Real Nuclear Potential

For the case of a purely real nuclear potential the dynamical variables will be real, and therefore there is no problem associated with their physical interpretation. This will allow an unclouded view of the effect that additional terms included in the Hamiltonian have.

The inclusion of the electric hexadecapole moment does not change very much the function $\hat{I}(\chi_0)$ shown in Fig. IV-2, nor the excitation probabilities, shown in Fig. IV-3. The values chosen for the electric multipole moments of ^{238}U are[53] $Q_0^{(2)} = 11.12b$; $Q_0^{(4)} = 1.96b^2$. At the energy chosen for the case shown the addition of a realistic nuclear potential would not appreciably change the results.

If we increase the initial kinetic energy of the projectile the two nuclei begin to interact more and more strongly through their nuclear potential. Figure IV-4 indicates the important changes that take place on the function $\hat{I}(\chi_0)$ as we increase the energy of the projectile. The effect of the nuclear potential is most noticeable

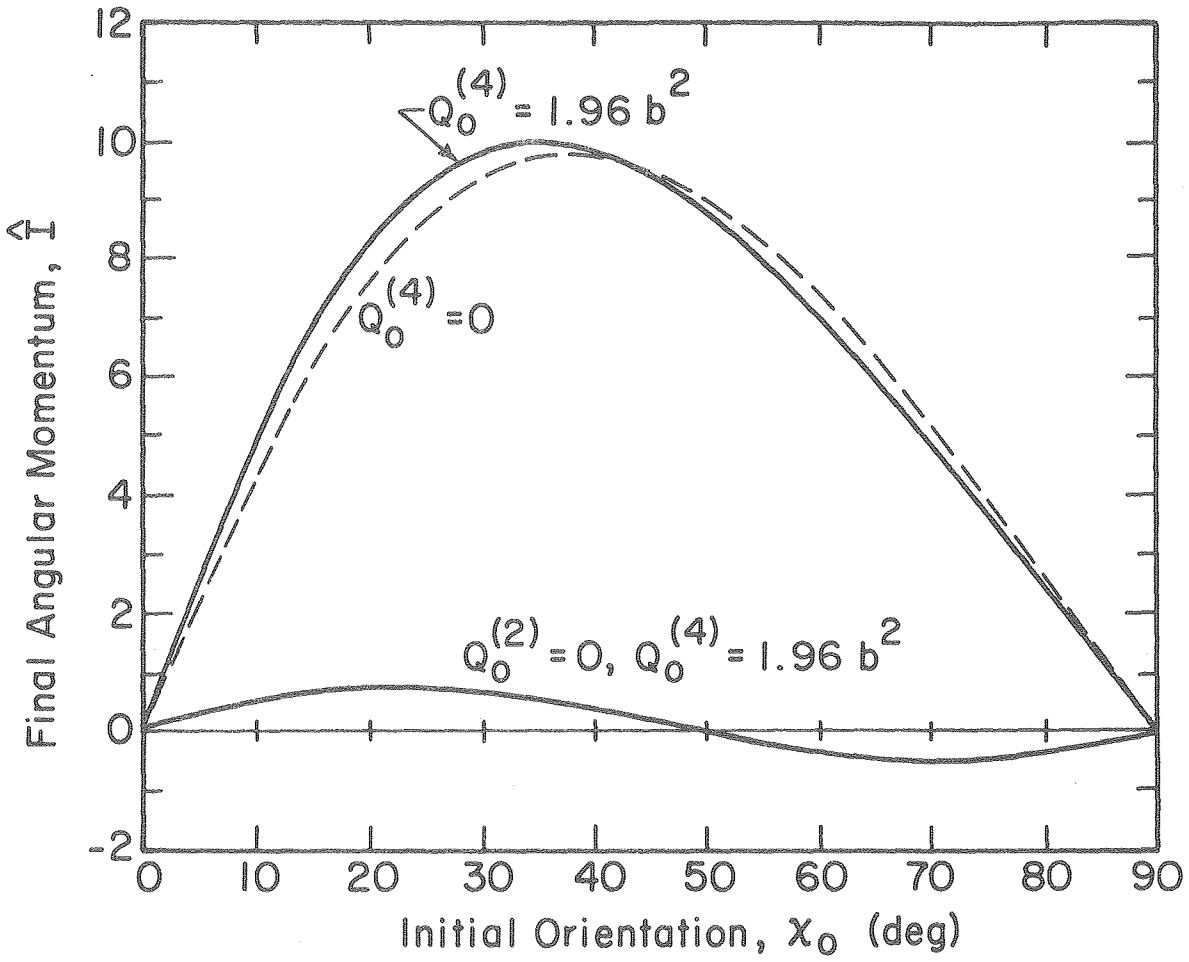

XBL 774-8300

Fig. IV-2 Final spin $\hat{I}$ versus initial orientation angle χ_0 for the system $^{40}Ar + ^{238}U$ at 160 MeV laboratory energy. The quadrupole moment of ^{238}U is assumed to be 11.12b, and the effect of the hexadecupole moment appears as the difference between the functions for $Q_0^{(4)} = 1.96\ b^2$ (experimentally measured value[53]) and $Q_0^{(4)} = 0$. For illustration the situation $Q_0^{(2)} = 0$, $Q_0^{(4)} = 1.96\ b^2$ has also been plotted, and it is clear that the difference between the two previously mentioned curves is qualitatively given by this later function.

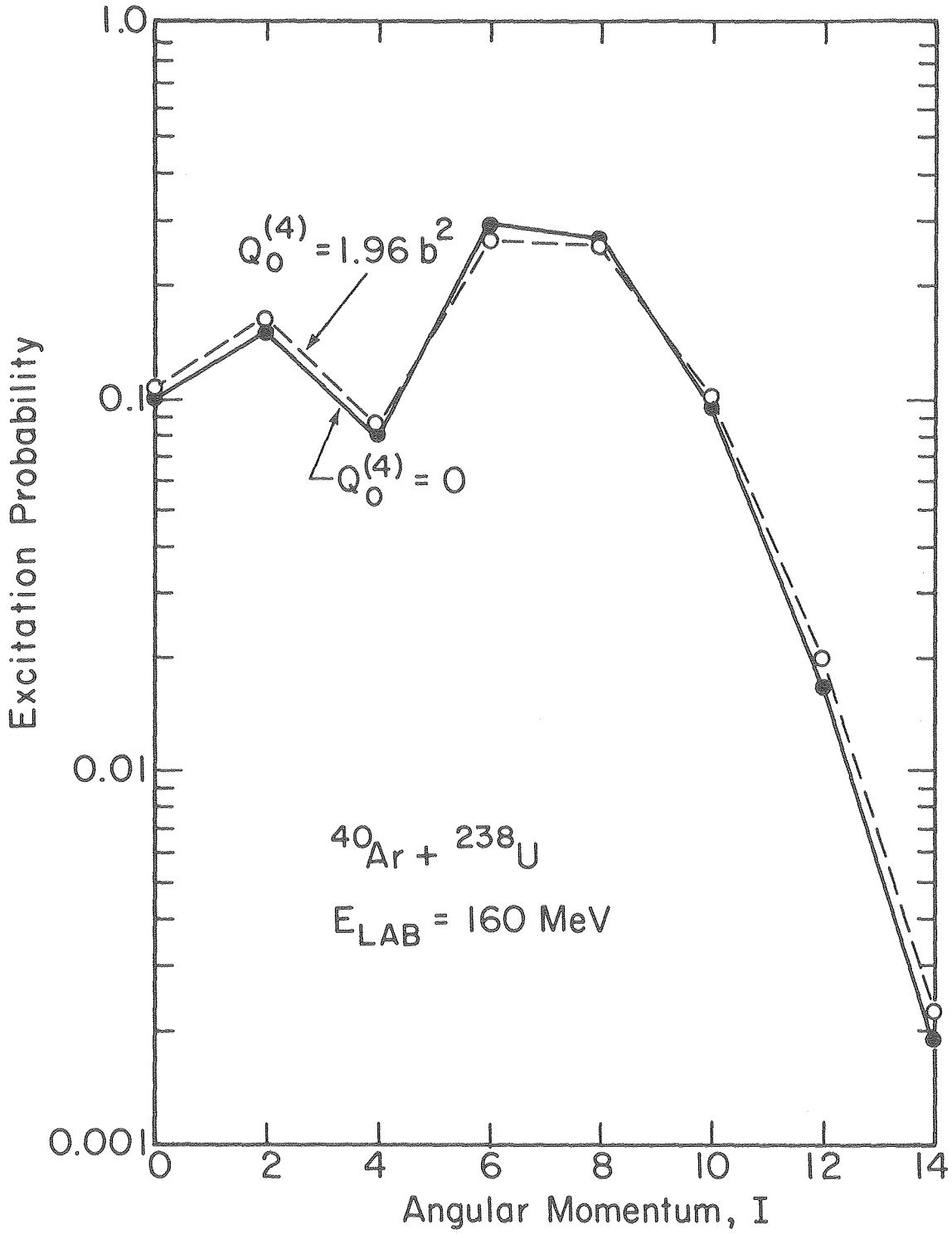

Fig. IV-3 Excitation probabilities, in the sense defined in Chapter III, for the same system considered in Fig. IV-2. XBL 774-8465

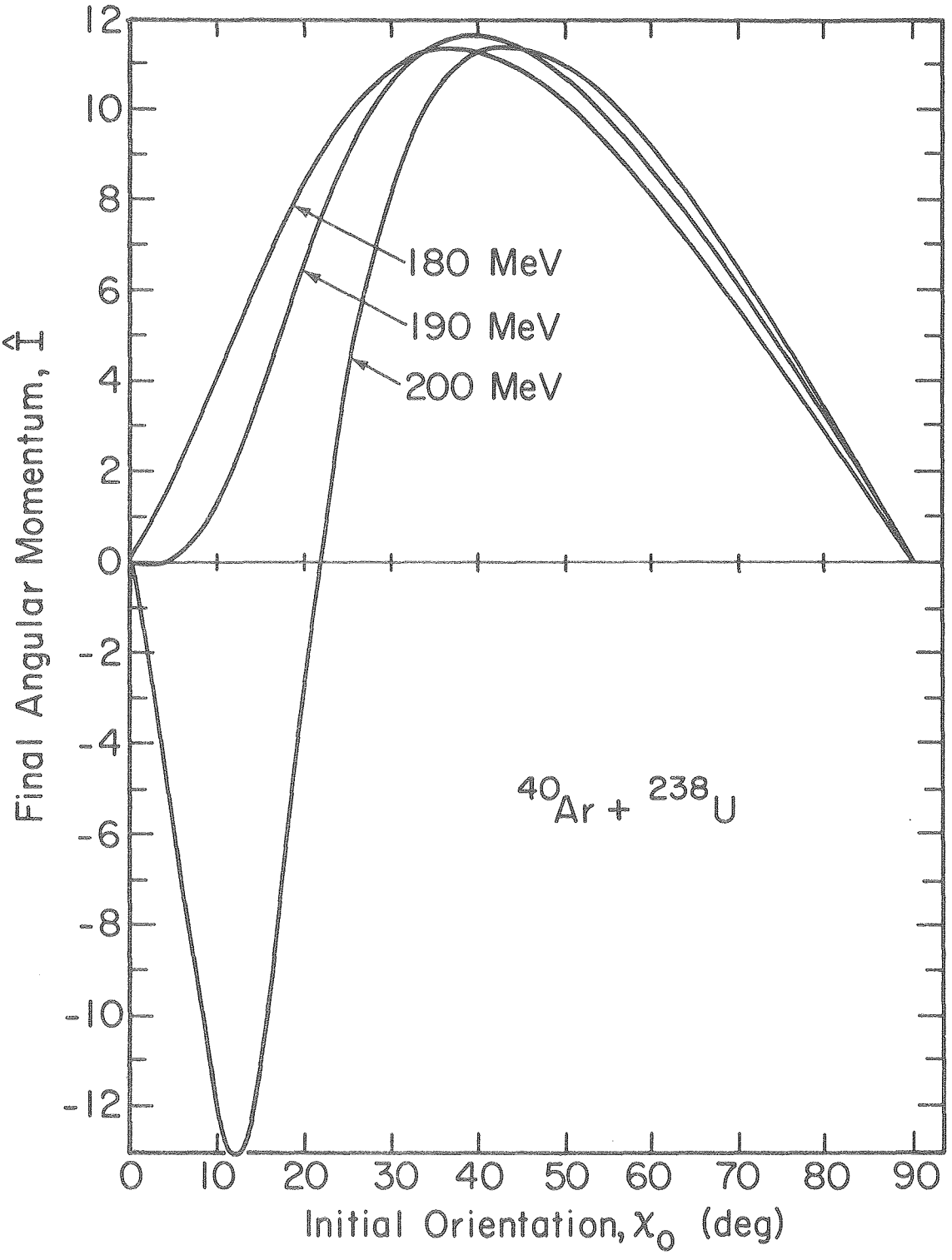

XBL 774-8462

Fig. IV-4

Fig. IV-4 The functions $\hat{I}(\chi_0)$ for the system $^{40}Ar + ^{238}U$ at three different laboratory energies. The multipole moments of ^{238}U were taken to be $Q_0^{(2)} = 11.12$ b, $Q_0^{(4)} = 1.96$ b^2, the energy levels were taken from the rotational model with $E_{2^+} = 0.0449$ MeV and a real nuclear potential was assumed between the collision partners defined by the parameters V = 50 MeV, $R_R^0 = 1.167$F, $a_R = 0.95$ F, $\beta_2 = 0.237$, $\beta_4 = 0.067$.

when the tip of the target is initially oriented close to the beam axis (i.e. χ_0 close to 0^o or 180^o) because in that event the surfaces of the two nuclei get the closest together due to the target deformation. The nuclear interaction produces a torque in the direction opposite to that of the electric quadrupole interaction (see Fig. IV-1). At high enough energies (above $\approx$ 190 MeV lab energy for the system we have been considering here) the nuclear torque dominates in the forward region and we see in Fig. IV-4 how at 200 MeV the behavior of the function $\hat{I}(\chi_0)$ is very different from that at 180 MeV or lower energies. Figure IV-5 shows the results for two of the energies considered in Fig. IV-4.

The procedure for evaluating the CLSM and thus the excitation probabilities is the same at 180 and at 200 MeV, but the different shape of the function $\hat{I}(\chi_0)$ makes a very important difference were we to use the USCA to evaluate the S-matrix. It is evident from Fig. IV-4 and the fact that $\hat{I}(\chi_0)$ is symmetric around 90^o, that there are four real roots of the equation $\hat{I}(\chi_0) = I + 1/2$ for $0 \leqslant I \leqslant 10$ and $E_{lab} = 200$ MeV; at higher spins some or all of those roots become complex. One should consider also the possibility that even for $I \leqslant 10$ there are complex roots to this equation, in addition to the four real ones. This higher number of roots makes the root search longer and more involved but this is indeed a small difficulty as compared to the task of evaluating by the stationary phase approximation the integral expression for the S-matrix in cases like this where the integrand has four or more stationary phase points. The use of simpler expressions such as Eq. A-12 in which the different stationary trajectories are

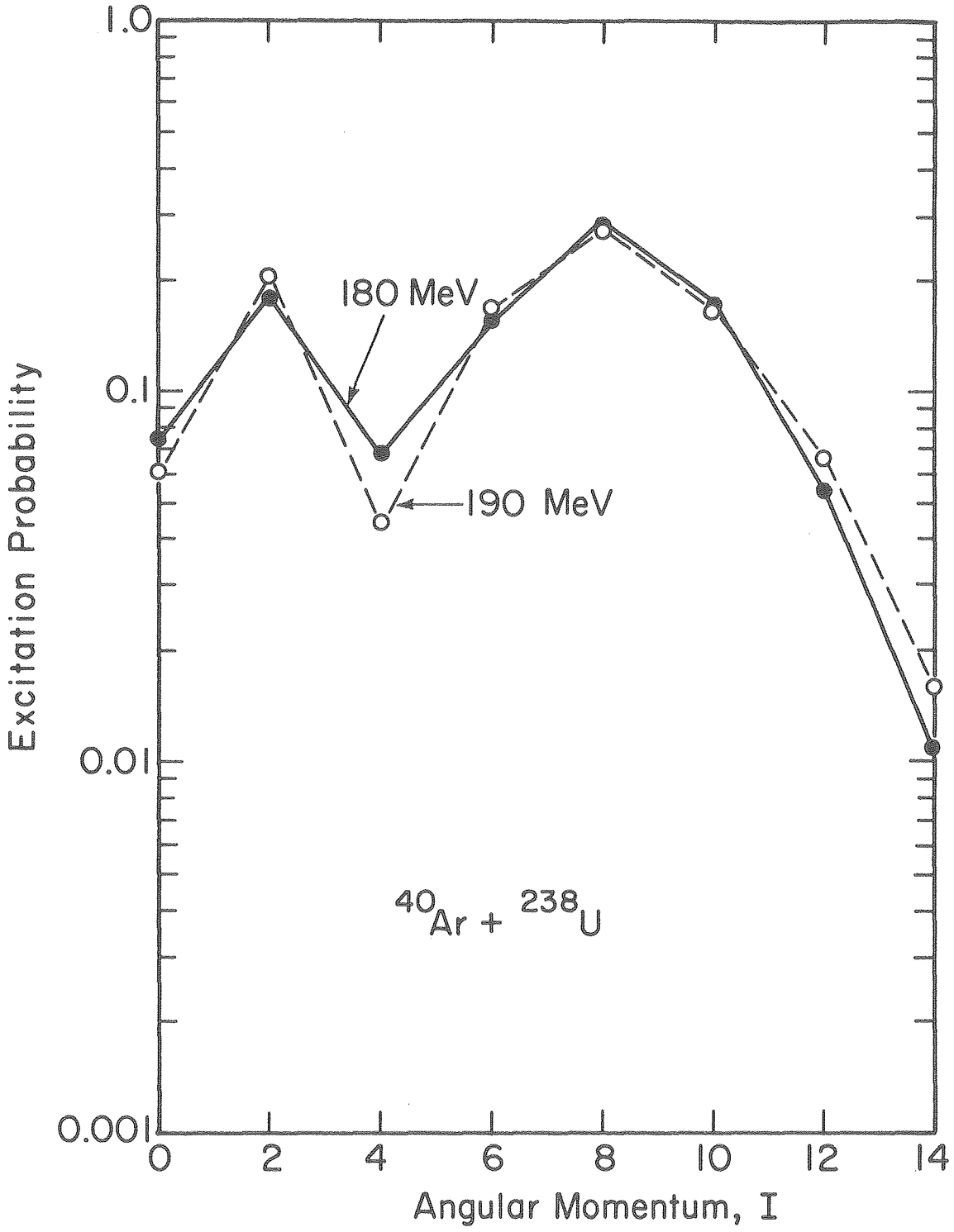

Fig. IV-5 Excitation probabilities calculated for the system shown in Fig. IV-4.

considered isolated of each other is not a good approximation for many cases.[24,25]

We should remark here that the fact that there are more than two trajectories contributing to the excitation of a given final spin in the USCA approach is not a characteristic intrinsic to the nuclear potential. We chose a case where it was present because there it was easy to see why the new roots appear, i.e. because of the strong torque produced by the nuclear potential and since they are real it is easier to understand the process. But it has not been shown that even in the case of a pure quadrupole interaction the number of roots is limited to the two used in the USCA calculations. By the way of an example let us consider the case where only the electric quadrupole and hexadecapole moment terms appear in the Hamiltonian for the case $\xi = 0$ and $\eta = \infty$ discussed in Ch. II in which case we obtain, in the same manner as there, that the expression for the function $\hat{I}(\chi_0)$ is

$$\hat{I}(\chi_0) = 2q_2 \sin 2\chi_0 + \frac{5q_4}{54}(7 \sin 4\chi_0 + 2 \sin 2\chi_0) \tag{6}$$

where

$$q_4 \equiv \frac{Z_p Q_0^{(4)} e^2}{4\hbar v_0 a^4} \tag{7}$$

Equation (6) may be written as a fourth order equation in $\exp(2i\chi_0)$ thereby showing that $\hat{I}(\chi_0) = I + 1/2$ has four (real or complex) roots.

An increasing number of roots does not imply that the USCA gives numerically wrong results when only two of them are considered, since the contribution from all the roots is not the same. This is

illustrated by the fact that the results given in Refs. 23 and 24 are in good agreement with other theoretical calculations.

On the other hand one should be aware of this situation before attempting to extend the USCA method to new cases. The fact that we are performing the integration directly avoids us worries about this type of complications when we introduce the imaginary part of the optical potential, as we will do next.

4. Complex Nuclear Potential

The equations of motion derived from the Hamiltonian given by Eq. (1) are in general complex, and so are the solutions to these equations. The fact that the dynamical variables become complex marks a break from the usual classical mechanics but causes no major difficulties from a quantum mechanical point of view since there the only necessarily real quantities are the physical observables.

As we have seen in the USCA one has to use complex trajectories to study classically forbidden transitions, in the case of a purely real interaction, and for all transitions if the Hamiltonian is complex. The procedure followed there[25,26] is to choose an appropriate complex initial value of χ_0 so that at the end of the trajectory the observable p_χ (or $\hat{I}$, in dimensionless units) be real. By looking at the Hamiltonian (Eq. (1)) in the asymptotic region we see that if p_χ is real then p_r will also be real.

We will choose instead to make the variable r real at the end of the trajectory. In order to do this we take an appropriate complex time path in the asymptotic region of the integration. This complex

time path usually consists of keeping the real part of the time constant while varying its imaginary part. References 13-15, 33 describe how by the introduction of this complex time one is able to solve by means of classical mechanics methods problems that appear to be completely out of its domain of applicability, such as the tunneling through a potential barrier.

Since in our approach we do not need to search for those initial orientations that lead to the final value of p_χ equal to that of the transition being considered, we may as well omit the requirement that p_χ has a real value at the end of each trajectory used in the integration, since it would be very cumbersome to fulfill. This causes no trouble if there are no poles present in the region between the curve over which we do perform the integration (the real axis) and the curve over which the final value of p_χ is real. (The final points of both curves coincide since for $\chi_0 = 0$, the final spin is 0). We have not found problems, but even in the event that they appear it would not be difficult to take the initial values χ_0 along an appropriate curve on the complex plane so as not to leave any poles in the region between the two curves.

The initial conditions for the integration are then the same used for the purely real case, and the equations of motion are solved in the same way as before, with the provision that now all the dynamical variables have complex magnitudes. The only difference is that at the end of each trajectory we allow the time to become complex by keeping its real part constant while changing the imaginary part until r takes a real value. After this the classical limit S-matrix is evaluated in

the way described before in Ch. II with the same observation that quantities such as $\bar{\chi}$, $\frac{d\bar{\chi}}{d\chi_0}$, Δ are now complex numbers.

We have performed some calculations using the system ^{40}Ar on ^{238}U; two different sets of parameters were used for the calculations. They are given in Table IV-1, and their dependence on r is shown in Fig. IV-6. They were obtained by Birkelund et al.[55], from quasi-elastic scattering of ^{40}Ar on ^{238}U at E_{Lab} = 268 MeV.

The calculated excitation probabilities as a function of incident beam energy are shown in Figs. IV 7-14, together with the values obtained when no nuclear potential is included.

We emphasize our reservation about the propriety of these potentials for the application intended here since our calculations are for lower bombarding energies than those at which the nuclear potential parameters were determined; nevertheless they serve as a useful starting point for the investigation of rotational scattering in the barrier region and we can use them to test our method until enough experimental data becomes available so that we can think of doing a search for the best set of nuclear potential parameters to describe the data.

Considering Figs. IV-7-14 we see in all cases that at low energies the results coincide with those of the pure Coulomb excitation, as it might be expected due to the short range of nuclear forces. On the opposite end of the energy scale, at high energies, all excitation probabilities decrease very fast with energy. This is so because the imaginary part of the nuclear potential absorbs an increasingly larger

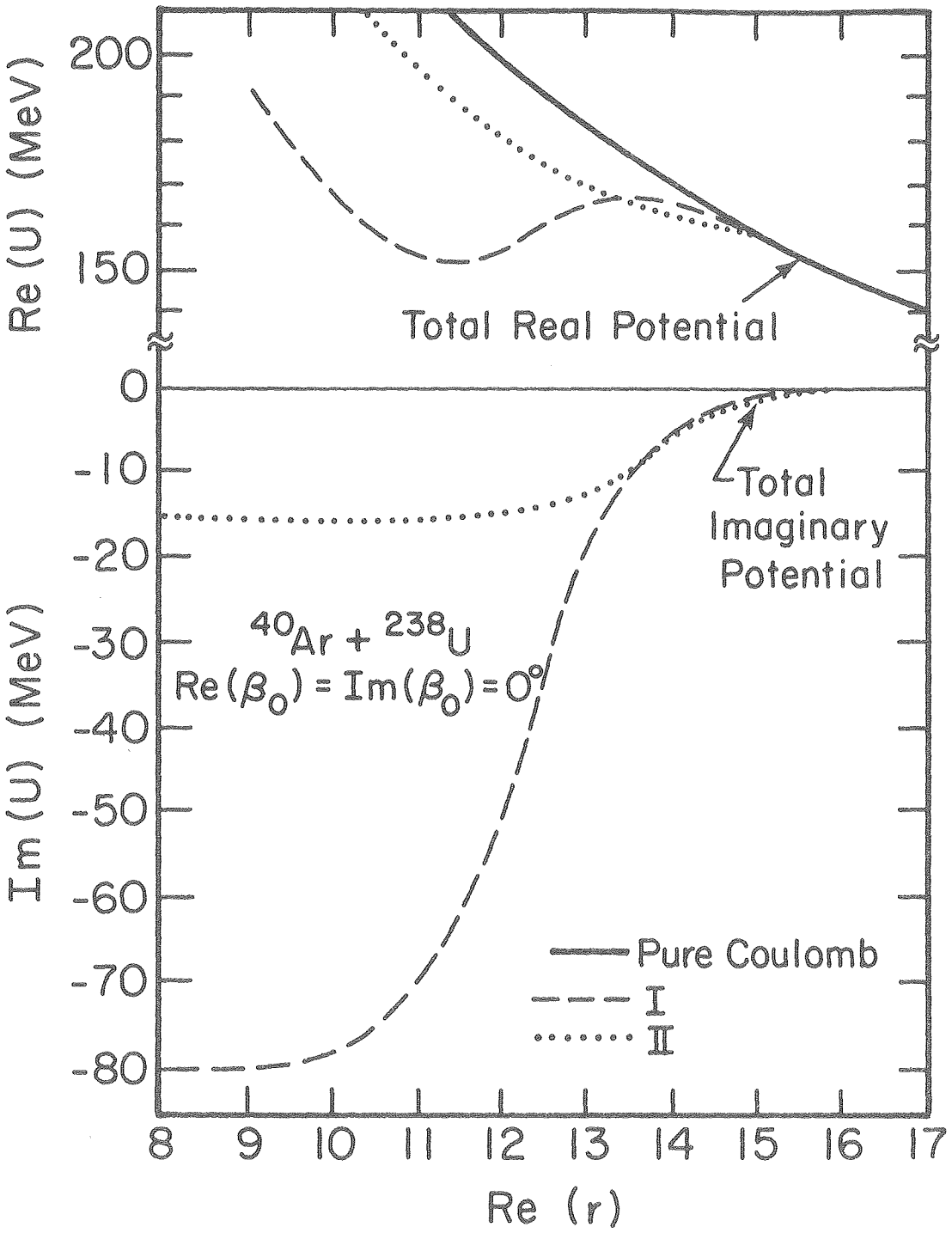

Fig. IV-6 The real and imaginary parts of the potential sets given in Table IV-1 as a function of the real part of the radial coordinate r along the nuclear symmetry axis. XBL 774-8459

Table IV-1

Parameter sets used in the calculation[a)]

	I [d)]	II [d)]
Q_2(b) [b)]	11.12	11.12
Q_4(b^2) [b)]	1.96	1.96
V (MeV)	73.0	17.7
a_R(Fm)	0.62	0.531
R_0^R(Fm)	1.131	1.267
W (MeV)	80.3	15.4
a_I(Fm)	0.624	0.531
R_0^I(Fm)	1.131	1.267
β_2 [c)]	0.237	0.237
β_4 [c)]	0.067	0.067

a) Same notations as in Eq. 1-3

b) From Ref. 55

c) From Ref. 56

d) Nuclear parameters from Ref. 57

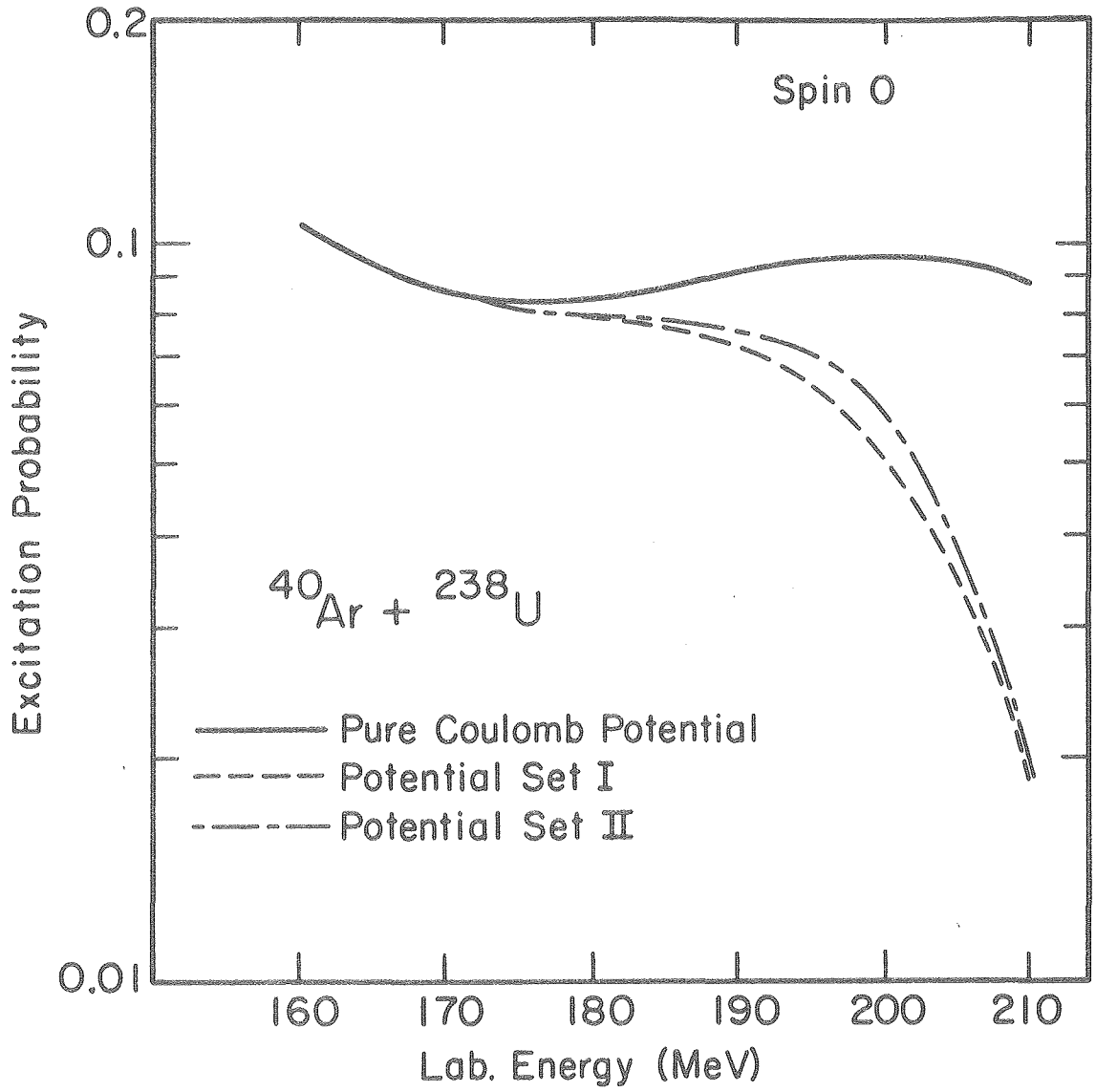

Fig. IV-7 Excitation probability for the 0^+ state in the reaction $^{40}Ar + ^{238}U$ at backscattering angles. The parameter sets used are listed in Table III-1.

XBL 774-8458

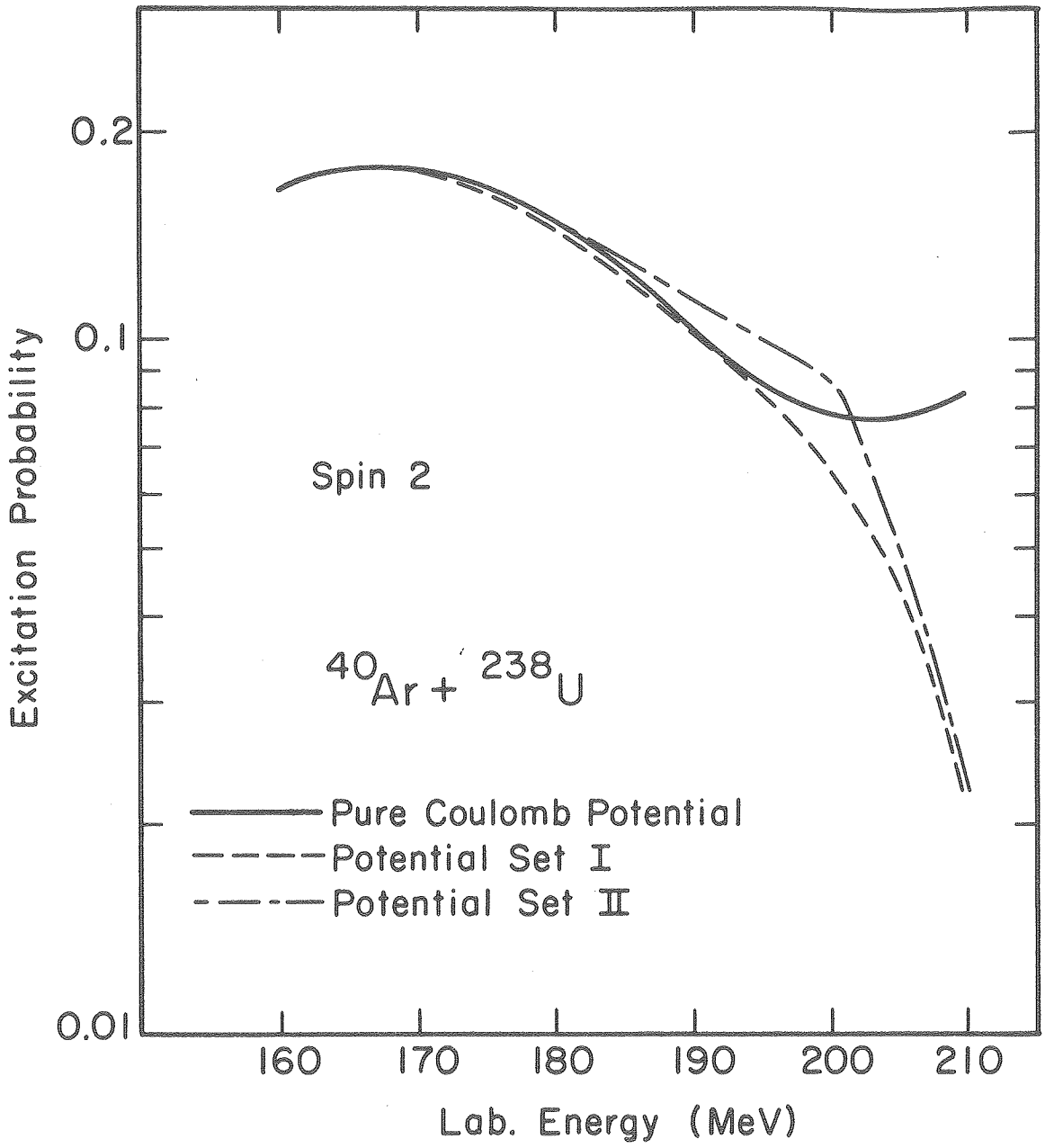

XBL 774-8454

Fig. IV-8 Excitation probability for the 2^+ state in the reaction $^{40}Ar + ^{238}U$ at backscattering angles. The parameter sets used are listed in Table III-1.

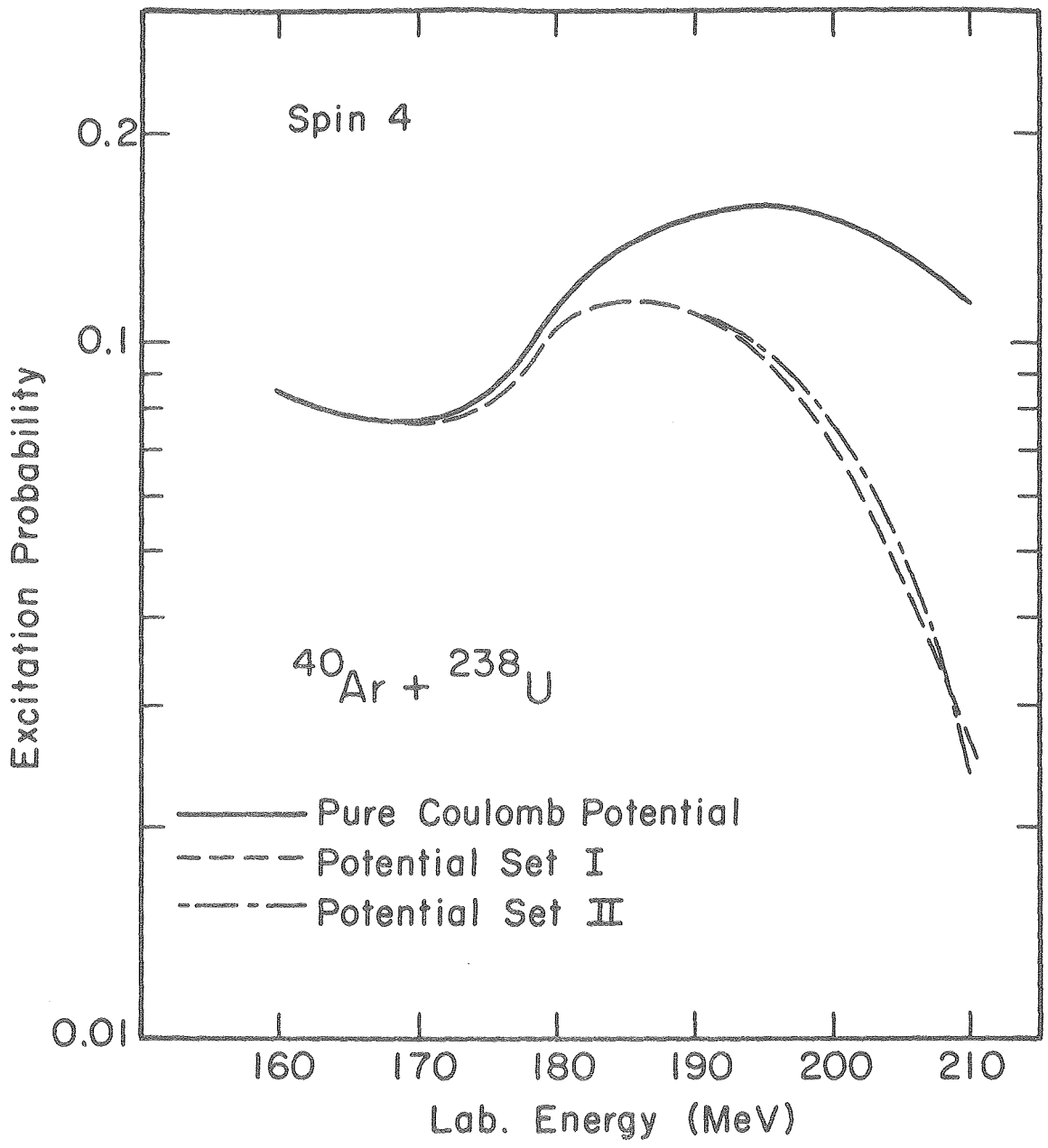

XBL 774-8457

Fig. IV-9 Excitation probability for the 4^+ state in the reaction $^{40}Ar + ^{238}U$ at backscattering angles. The parameter sets used are listed in Table III-1.

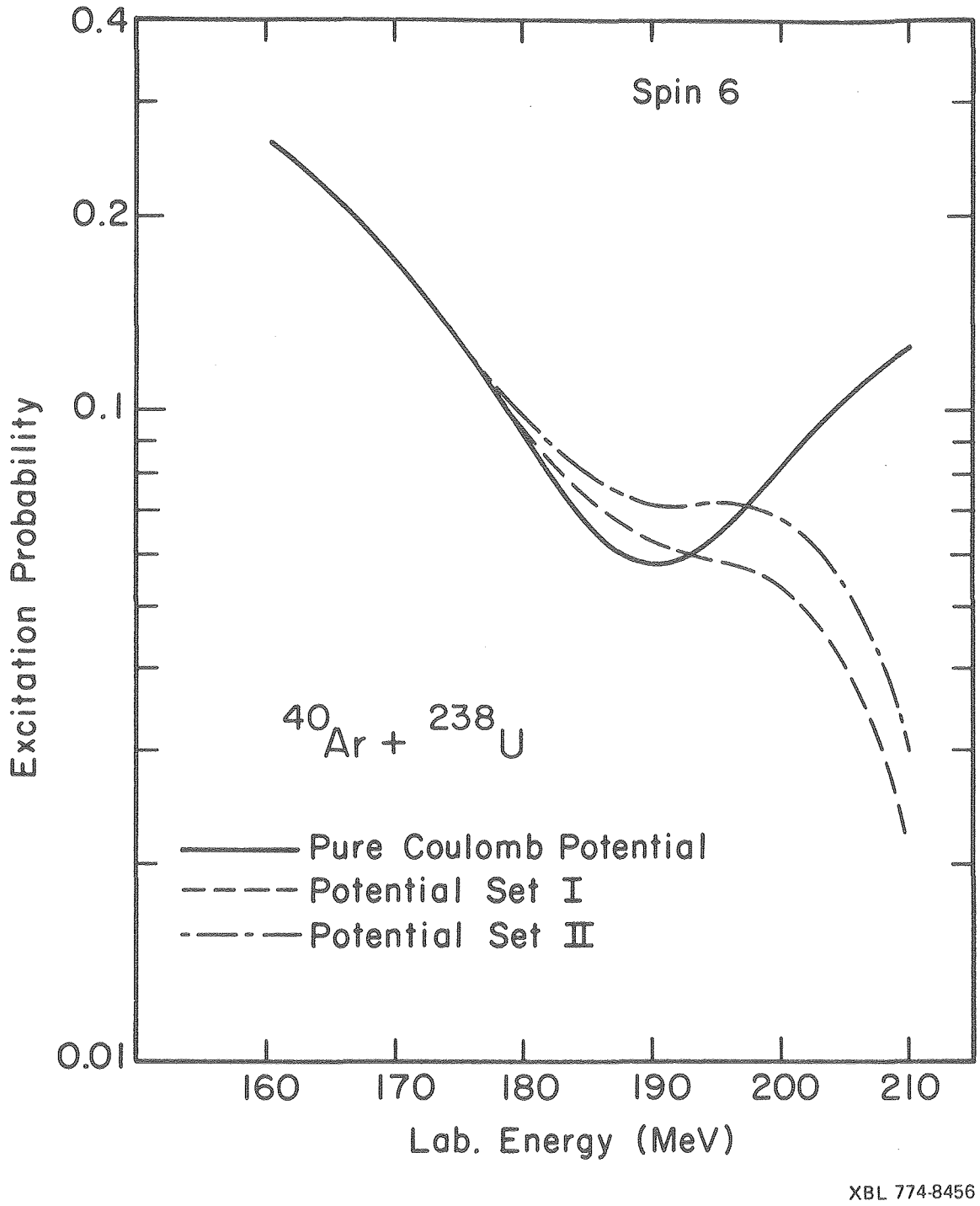

XBL 774-8456

Fig. IV-10 Excitation probability for the 6^+ state in the reaction $^{40}Ar + ^{238}U$ at backscattering angles. The parameter sets used are listed in Table III-1.

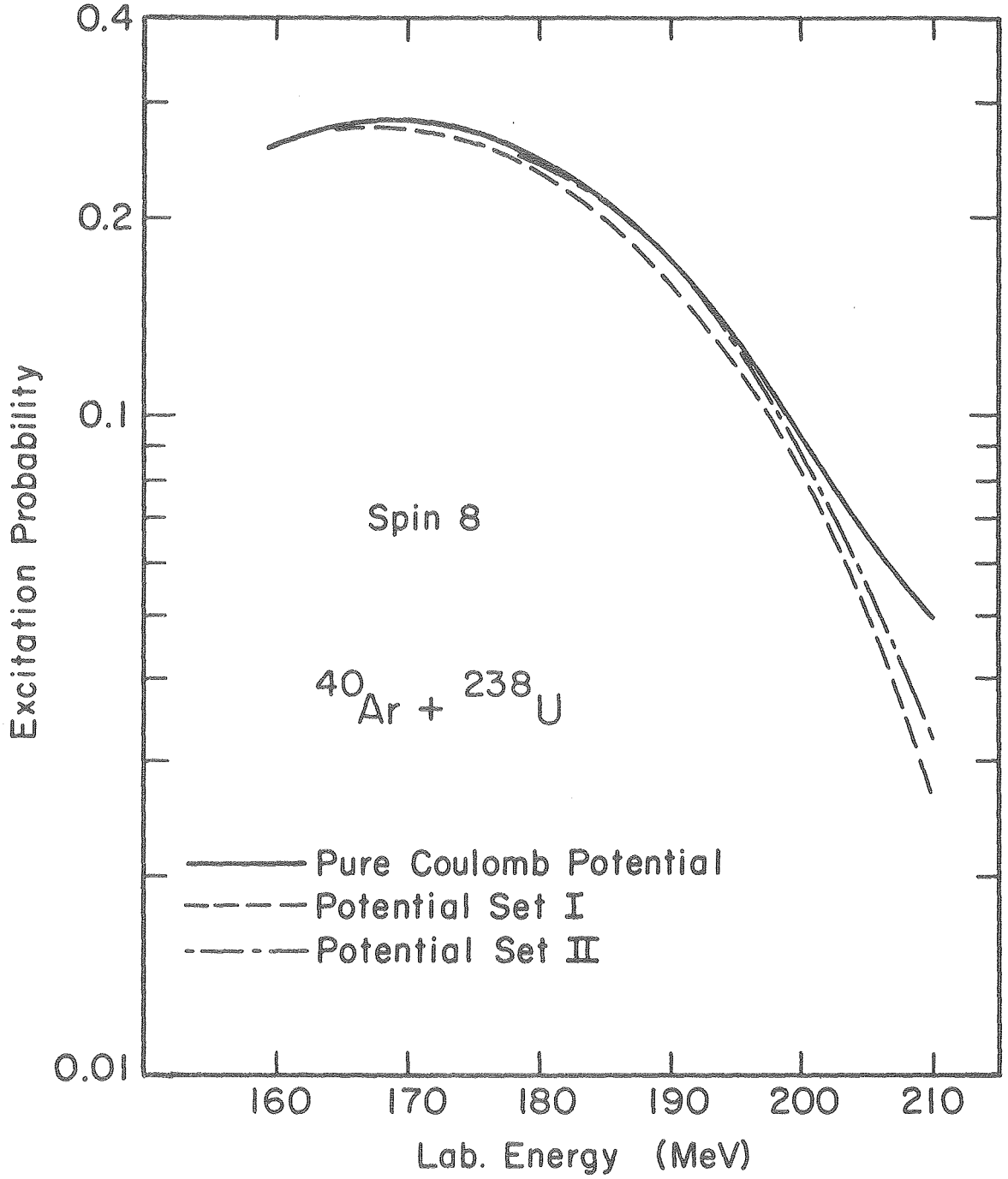

XBL 774-8455

Fig. IV-11 Excitation probability for the 8^+ state in the reaction $^{40}Ar + ^{238}U$ at backscattering angles. The parameter sets used are listed in Table III-1.

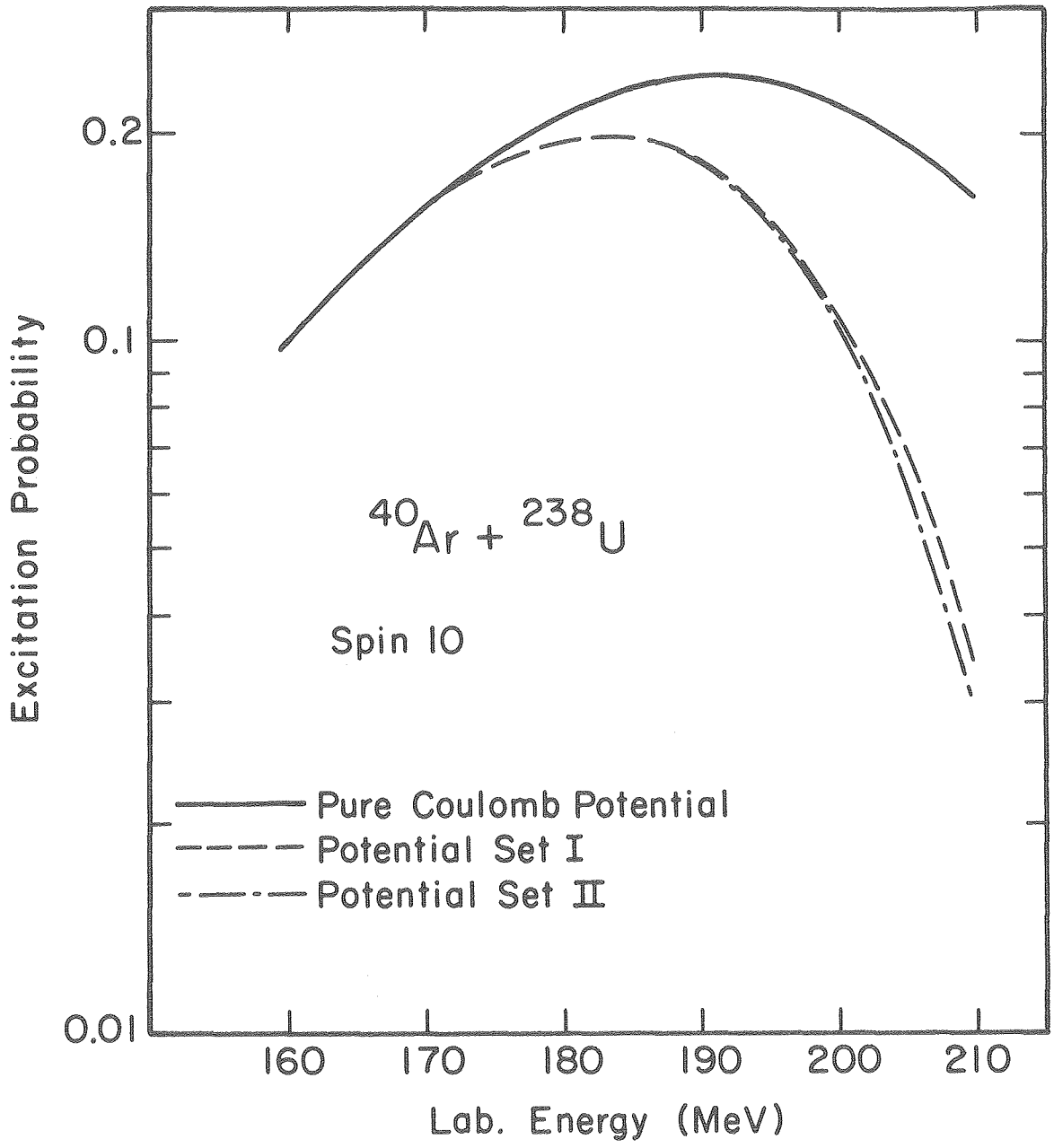

XBL 774-8453

Fig. IV-12 Excitation probability for the 10^+ state in the reaction $^{40}Ar + ^{238}U$ at backscattering angles. The parameter sets used are listed in Table III-1.

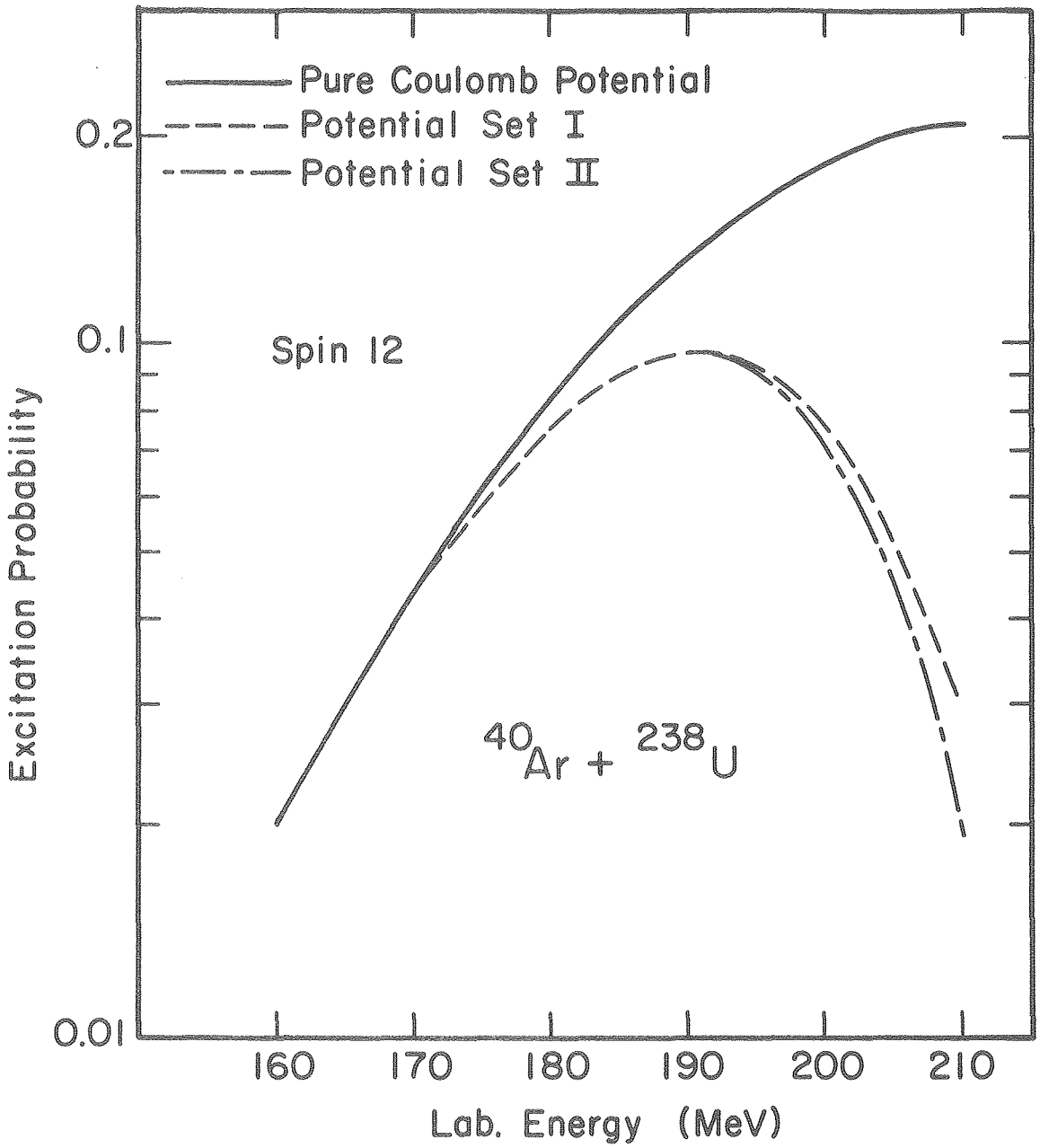

XBL 774-8452

Fig. IV-13 Excitation probability for the 12^+ state in the reaction $^{40}Ar + ^{238}U$ at backscattering angles. The parameter sets used are listed in Table III-1.

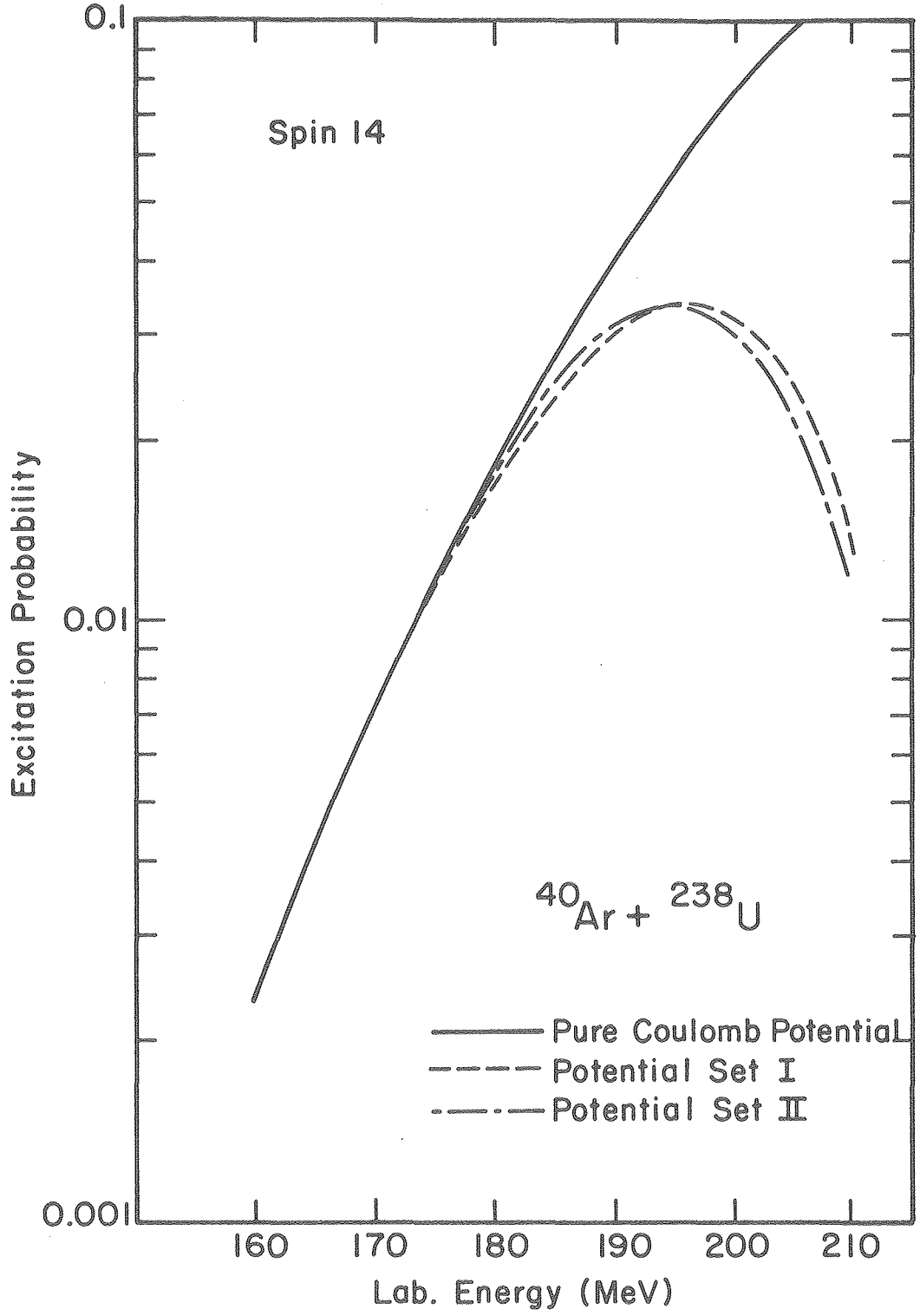

XBL 774-8460

Fig. IV-14 Excitation probability for the 14^+ state in the reaction $^{40}+ ^{238}U$ at backscattering angles. The parameter sets used are listed in Table III-1.

fraction of the incoming flux. This represents mathematically the fact that at these higher energies other channels such as nucleon transfer, fission, and compound nucleus formation are open and complete more and more with the rotational excitation.

In the region between these two extreme cases we notice first a progressive departure from the pure Coulomb values, finding examples of both destructive and constructive interference. These interference effects between the electromagnetic and nuclear potentials are better explained by means of interfering classical trajectories, as it is done in Ref. 26, where only the contribution of two trajectories is considered.

In general the two potential sets predict excitation probabilities that do not differ by more than 25% from each other in the energy range considered here. This is not surprising since as Fig. IV-6 indicates, they are very similar in the critical region $Re(r) \gtrsim 13.5$ F , where most rotational excitation takes place at these projectile energies. But, since many different states are excited, even these small differences might allow for distinction between potentials I and II in a careful experiment.

Because the excitation probabilities are sensitive to Coulomb-nuclear interference effects, we believe that heavy-ion rotational excitation near Coulomb-barrier energies could provide a detailed probe of the potential in the nuclear surface region. (The potential in the nuclear interior is probably inaccessible because of the strong absorption). One may speculate that the potential for a deformed nucleus may exhibit irregular variations with the polar angle β (see Fig. II-1. For example, the imaginary potential may be largely due at

barrier energies to loss of flux into neutron-transfer channels, and hence be strongest in the zones of lightly bound neutron orbitals. If the concept of a classical trajectory has any physical significance in these heavy-ion systems, excitation of different states should probe different angular regions of the nuclear surface. This is clearer in the USCA picture where only a few trajectories are seen to contribute to the Coulomb excitation of a given spin.

Excitation of lower spins should be sensitive, then, to regions closer to the nuclear tips. At sufficiently higher energies the low-angle roots should be damped by the imaginary part of the optical potential, and the larger-angle orientations, which now feel the nuclear force should make the dominant contribution. Therefore one would expect the probabilities in this case to be sensitive to the nuclear potential nearer the equator of the classical nucleus.

As another example, significant attention has recently been directed to the possibility of different charge and matter distributions in the nucleus. Since the calculations discussed here are sensitive to the competition between the nuclear forces (arising from the matter distribution) and electromagnetic forces (arising from the charge distribution), rotational excitation in the surface region could also provide an indication of different charge and mass deformations, if such effects actually occur.

It would be premature to attempt a detailed exploration of potentials with more parameters representing irregular angular dependence, or different charge and matter distributions. There are few data available yet, and only experimental data can ascertain whether the

effects discussed here are measurable. However these considerations indicate that detailed information about the deformed nuclear potential in the surface region may be available in the Coulomb-nuclear interference experiments suggested by these calculations.

We see how a relatively minor modification of the theory presented in Ch. II allows us to treat the problem of Coulomb-nuclear interference for rotational scattering which is very difficult to deal with by other approaches. Quantum mechanical coupled-channel numerical calculations including the nuclear potential are feasible for light ions only[56], since the most applicable computer code available now requires three to four times the computer time needed by the pure Coulomb excitation code AROSA mentioned in Ch. III.

Other semiclassical methods of the Alder-Winther type have been used to describe inelastic scattering from spherical targets in the same energy region.[57] It is hard to imagine how they could be applied to scattering from deformed nuclei, since in this type of methods the trajectory followed by the particle does not depend on the values of the internal coordinates of the target. This is not very bad in the case of pure Coulomb excitation where the trajectory chosen does not deviate so much from the actual trajectories where the classical equations of motion are solved for both projectile and target, as it was discussed in Ch. III. In the case we are treating now, on the other hand, the short range and strength of the nuclear forces make the trajectories to be very strongly dependent on the orientation of the target, so that we do not think that a method based on an assumption that is in direct conflict with this fact can be formulated.

There is another comment to be made on the way the imaginary part of the nuclear potential is considered in our approach and in that of Ref. 57. In this one the real part of the nuclear potential is the only part of it affecting the trajectory, so that all dynamical variables are real, while the imaginary part of it has mainly the effect of giving rise to absorption along this classical trajectory; reflection phenomena associated with the imaginary part of the nuclear potential are not included in this theory, since they correspond, in a classical picture to a modification of the trajectory, and in this formalism it is not possible to modify the projectile motion according to the orientation of the target since the later is described in quantum mechanical terms. As mentioned in this reference this omission may give rise to serious discrepancies with a quantum mechanical description.

Our approaches include the full description of the classical motion, and in particular the imaginary part of the optical potential affects the actual trajectory of the projectile. In this sense we think the CLSM method could improve these results even for the case of spherical targets.

To illustrate the effect of the imaginary part of the nuclear potential on the classical trajectories we show in Fig. IV-15 the behavior of the real part of the function $\hat{I}(X_0)$ for the nuclear potential given by the set of parameters I in Table IV-1. By comparing it with the corresponding functions obtained for the same set of parameters but with the strength W of the imaginary part of the nuclear potential set equal to zero and for the case of no nuclear

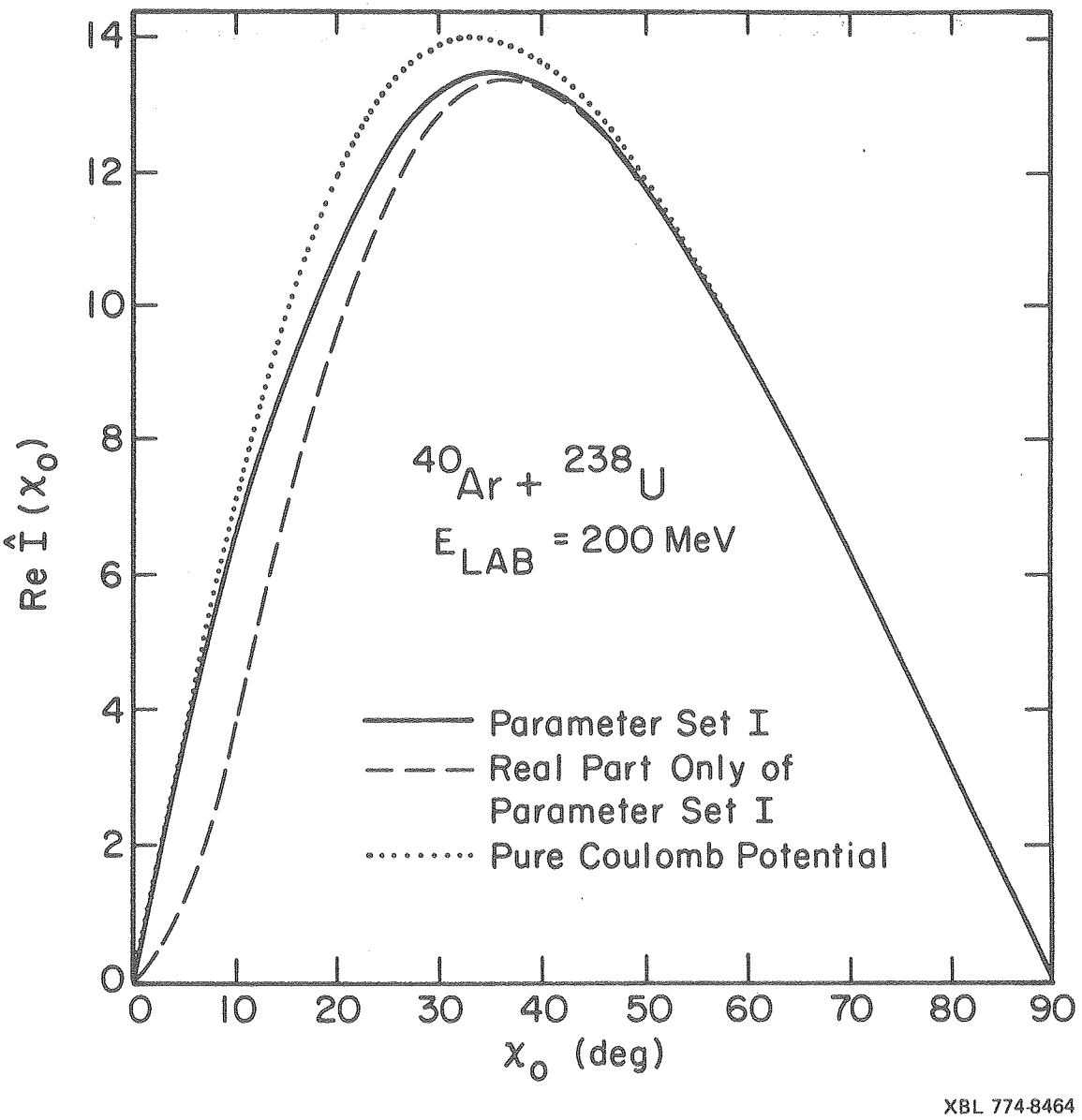

Fig. IV-15 Repulsive effect of the imaginary potential as observed in the real part of the function $\hat{I}(\chi_0)$.

potential, we see that the effect of the imaginary potential is not negligible at all, since it increases the angular momentum, cancelling in part the effect of the real part of the optical potential.

V. FURTHER EXTENSIONS AND OTHER APPLICATIONS OF THE CLASSICAL-LIMIT S-MATRIX THEORY

1. Introduction

In the previous chapters we have considered the application of the CLSM to the case of excitation of the rotational states of a deformed even-even nucleus. The theory is certainly not limited to this problem, as it is already suggested by the fact that the USCA has been successfully applied to study vibrational excitation of molecules,[11,30] reactive molecular collisions,[14,15,28-33] and in nuclear physics, to the two dimensional tunneling of a fission barrier model.[58]

Here we will describe the present status of our study of other problems in nuclear physics in which we are using the CLSM. Since other research groups in the world are involved in similar studies, we find it appropriate to discuss their work in this chapter in order to give a more adequate view of how much has been done and the difficulties to be solved in the problems that we are considering now.

2. Multiple Coulomb excitation for all scattering angles

We would like to generalize our treatment of the backward-scattering Coulomb excitation process described in previous chapters to all scattering angles. This extension is far from being trivial, as we will see. The main reason making the backward scattering case especially simple is that the total angular momentum of the system (J) is zero, and this fact forces the orbital angular momentum of the projectile and the rotational angular momentum of the target to be equal in magnitude and opposite in direction at all times, thus effectively reducing the number

of variables one has to deal with. In the classical trajectories the fact that J = 0 implies that the motion takes place in a plane. This is not going to be true in the general case ($J \neq 0$).

Let us start our study of this case by considering the scattering amplitude f for the Coulomb excitation[4,57] process

$$f_{j_0 m_0 \to j_f m_f}(\theta,\phi) = -\frac{i\sqrt{\pi}}{\sqrt{k_0 k_f}} \sum_{J,\ell_0,\ell} \sqrt{2\ell_0+1}$$

$$\times \langle \ell_0\ 0\ j_0 m_0 | J\ m_0\rangle \langle \ell m\ j_f m_f | J\ m_0\rangle\ i^{\ell_0-\ell} \qquad (1)$$

$$\times Y_{\ell m}(\theta,\phi)\ S_{\ell_0 j_0 \to \ell j_f}$$

Here $j_0 m_0 (j_f m_f)$ are the entrance (exit) total nuclear spin and its corresponding magnetic quantum number, respectively. θ and ϕ are the polar coordinates of the direction of the exit wave vector k_f in a coordinate system in which the incoming wave vector k_0 is along the z-axis and $Y_{\ell m}$ is a spherical harmonics. The variables that appear inside the summation signs can be interpreted as follows. J is the total angular momentum and $\ell_0(\ell)$ the initial (final) orbital angular momentum quantum number, while m is the final orbital magnetic quantum number, being the initial one equal to zero due to the choice of coordinate axis. $S^J_{\ell_0 j_0 \to \ell j_f} \equiv \langle (\ell j_f)\ J | S | (\ell_0 j_0)\ J\rangle$ is the S-matrix element for the transition $\ell_0 j_0 \to \ell j_f$ given a total angular momentum J.

Since we are especially interested in the study of the Coulomb excitation of an even-even nucleus in its ground state, we replace j_0 and m_0 in Eq. (1) by zero, thereby obtaining the simpler expression

$$f_{00\to j_f m_f}(\theta,\phi) = -\frac{i\sqrt{\pi}}{\sqrt{k_0 k_f}} \sum_{J,\ell} \sqrt{2J+1} \times \langle \ell m\ j_f\ m_f | J0\rangle\ i^{J-\ell}\ Y_{\ell m}(\theta,\phi)\ S^{J}_{J0\to \ell j_f} \tag{2}$$

In order to calculate the scattering amplitude $f_{00\to j_f m_f}$ we must evaluate the S-matrix elements $S^{J}_{J0\to \ell j_f}$. We will see how the formalism that we have considered before can be applied to calculate them.

The Hamiltonian for the system can be written,[10] in analogy to the one given by Eq. (II-32)

$$H(q_j,\hat{J},q_\ell,\hat{\ell},\hat{r},\hat{p}_r) = \frac{\hat{p}_r^2}{2} + \frac{\xi}{6\eta_0}\hat{j}^2 + \frac{\hat{\ell}^2}{2\eta_0^2\hat{r}^2} + \frac{1}{\hat{r}} + \frac{2q_2\ P_2(\cos\gamma)}{\eta_0\hat{r}^3} \tag{3}$$

where the angle γ between the rotor axis and the line defined by the centers of target and projectile is given by[10]

$$\cos\gamma = -\cos q_j \cos q_\ell + \frac{\hat{j}^2 + \hat{\ell}^2 - \hat{J}^2}{2\,\hat{\ell}\,\hat{j}} \sin q_j \sin q_\ell \tag{4}$$

In Eqs. (3) and (4) the quantities $\hat{j}$, $\hat{\ell}$, and $\hat{J}$ are the dimensionless variables that represent the measures of the angular momenta of the target, orbital of the projectile and total of the system in units of $\hbar$. The quantities q_j and q_ℓ are the action angle variables canonically conjugate to $\hat{j}$ and $\hat{\ell}$ respectively. The remaining symbols have the same meaning as in Ch. II.

The expression for the S-matrix element in this representation is found in the same way as before (Ch. II). The result is

$$S^J_{J0\to\ell j} = \frac{1}{(2\pi)^2}\int_0^{2\pi} dq_{j_0}\int_0^{2\pi} dq_{\ell_0}\ \sqrt{\frac{\partial(\bar{q}_j,\bar{q}_\ell)}{\partial(q_{j_0},q_{\ell_0})}}\ \exp(i\Delta) \tag{5}$$

where

$$\begin{aligned}\Delta = {} & \bar{q}_j\left[\bar{j}_f - (j+1/2)\right] + \bar{q}_\ell\left[\hat{\ell}_f - (\ell+1/2)\right] \\ & - \int d\hat{t}\ \left(\eta_0 \hat{r}\,\frac{d\hat{p}_r}{d\hat{t}} + q_j\,\frac{d\hat{j}}{d\hat{t}} + q_\ell\,\frac{d\hat{\ell}}{d\hat{t}}\right) \\ & + \sigma_J(\eta_0) + \sigma_\ell(\eta_j)\end{aligned} \tag{6}$$

The quantities $\bar{q}_j$ and $\bar{q}_\ell$ are evaluated in the same way as $\bar{X}$ was in Eq. (II-13), that is

$$\bar{q}_j = q_j + \int_{\tilde{r}_T}^{\hat{r}} \frac{\partial \tilde{p}_r}{\partial \hat{j}}\, d\tilde{r} \tag{7}$$

where $\tilde{p}_r$ satisfies

$$\frac{\tilde{p}_r^2}{2} + \frac{\xi}{6\eta_0}\hat{j}^2 + \frac{\hat{\ell}^2}{2\eta_0^2\hat{r}^2} + \frac{1}{\hat{r}} = \bar{E} \tag{8}$$

Therefore $$\bar{q}_j = q_j - \frac{\xi}{3\eta_0}\hat{j}\int_{\tilde{r}_T}^{\hat{r}} \frac{d\hat{r}}{\tilde{p}_r} \tag{9}$$

and similarly $$\bar{q}_\ell = q_\ell - \frac{\hat{\ell}}{\eta_0^2}\int_{\tilde{r}_T}^{\hat{r}} \frac{d\hat{\tilde{r}}}{\hat{r}^2\tilde{p}_r} \tag{10}$$

q_{j_0} and q_{ℓ_0} are the initial values of the variables q_j and q_ℓ, and $\frac{\partial(\bar{q}_j,\bar{q}_\ell)}{\partial(q_{j_0},q_{\ell_0})}$ is the Jacobian of the variables defined by Eqs. (9) and (10) with respect to the initial values q_{j_0}, q_{ℓ_0}.

$$\frac{\partial(\bar{q}_j,\bar{q}_\ell)}{\partial(q_{j_0},q_{\ell_0})} = \det\begin{Bmatrix} \frac{\partial\bar{q}_j}{\partial q_{j_0}} & \frac{\partial\bar{q}_j}{\partial q_{\ell_0}} \\ \frac{\partial\bar{q}_\ell}{\partial q_{j_0}} & \frac{\partial\bar{q}_\ell}{\partial q_{\ell_0}} \end{Bmatrix} \tag{11}$$

The other quantities appearing in Eqs. (5) and (6) retain the meaning given to them in Ch. II.

In principle one should proceed as before, taking the equations of motion derived from the Hamiltonian (3), from them obtain all quantities appearing in Eqs. (5) and (6) and then perform the double integral appearing in Eq. (5). Unfortunately in this case the problem is not as straightforward as in Ch. II for a variety of reasons.

First of all the equations of motion resulting from Eq. (3) cannot always be integrated directly; whenever $\hat{J}$ approaches zero the variable q_j, which represents the amount of rotation in the plane perpendicular to $\hat{J}$ becomes ill defined, since the plane itself is not well defined. This appears mathematically as a singularity in the expression for $\frac{dq_j}{dt}$. Miller[10] wrote these equations in cartesian coordinates to avoid the problem. This implies to make a transformation from action angle variables to cartesian coordinates at the beginning of each trajectory, to obtain the initial conditions in cartesian coordinates; then run the trajectories in these coordinates and finally transform the final values back into action angle variables.

There are alternative ways to describe the problem, which is appropriate to mention here. Miller[10] proposes the helicity representation (q_j, q_m, r, j, m, p_r) where j is again the rotational angular momentum of the target and m is the helicity, i.e., the projection of the rotational angular momentum of the target onto the relative velocity vector and q_m is its canonically conjugate variable.

The expression for the Hamiltonian in these new variables is

$$\hat{H}(q_j,\hat{j},q_m,\hat{m},\hat{r},\hat{p}_r) = \frac{\hat{p}_r^2}{2} + \frac{\xi}{6n_0}\hat{j}^2$$

$$+ \frac{1}{2n_0^2\hat{r}^2}\left[\hat{j}^2+\hat{j}^2-2\hat{m}^2+2\sqrt{(\hat{j}^2-\hat{m}^2)(\hat{j}^2-\hat{m}^2)}\cos q_m\right] \qquad (12)$$

$$+\frac{1}{\hat{r}} + \frac{2q_2 P_2(\cos\gamma)}{n_0\hat{r}^3}$$

where similarly as before we have taken $\hat{j}$, $\hat{m}$ and $\hat{J}$ to be $j/\hbar$, $m/\hbar$ and $J/\hbar$ respectively. In this set of variables the angle γ, which is defined as before, is given by

$$\cos\gamma = \sqrt{1-\frac{\hat{m}^2}{\hat{j}^2}}\cos q_j \qquad (13)$$

If we consider the case $\hat{J}=0$, from the expression of the Hamiltonian (12) we see that $\hat{m}$ has to be identically zero during the whole motion. Then from (13) we see that $\gamma = q_j$; in this case, and since neither $\hat{m}$ nor q_m will play any role in the Hamiltonian it can finally be written as

$$H^{J=0}(q_j,\hat{J},\hat{r},\hat{p}_r) = \frac{\hat{p}_r^2}{2} + \frac{1}{2}\left(\frac{\xi}{3n_0} + \frac{1}{n_0^2\hat{r}^2}\right)\hat{j}^2$$

$$+\frac{1}{\hat{r}}\frac{2q_2 P_2(\cos q_j)}{n_0\hat{r}^3} \qquad (14)$$

which is identical to the expression we had before for the back-scattering case (Eq. (II-32)). It is now clear that we can regard this helicity representation as a natural extension of the coordinate set used in Ch. II to the three dimensional case. We can obtain an expression for the S-matrix element $S^{J}_{00\to jm}$ in an analogous way as it was done in Ch. II, except that now it will involve a double integral, and quantities such as those just defined in Eqs. (9), (10) and (11).

It is simple to transform the S-matrix from one representation to the other using the relation[10]

$$S^{J}_{00\to jm} = \sum_{\ell} < jm\ J0|\ell{-}m > i^{\ell-J}\ S^{J}_{J0\to \ell j} \qquad (15)$$

or its reciprocal.

Let us begin the study of the S-matrix for the J non-zero case by considering the simplified case analogous to one studied in Ch. II.

3. The limit $\xi = 0$, $\eta = \infty$

The evaluation of the S-matrix elements was carried out in the limit $\xi = 0$, $\eta = \infty$, which was previously considered for the back-scattering case in section 5 of Ch. II. In this limit the orbit of the projectile is a hyperbola. Taking the z axis along the bisector of this hyperbola, and the x axis on the plane defined by it, the position of the projectile is determined by the distance 4 and the azimuthal angle θ, while the axis of the target nucleus is defined by the polar angles, α,β (See Fig. V-1 for illustration).

During the interaction the coordinates α,β remain constant, and this leads to a simplified expression for the S-matrix. Just as

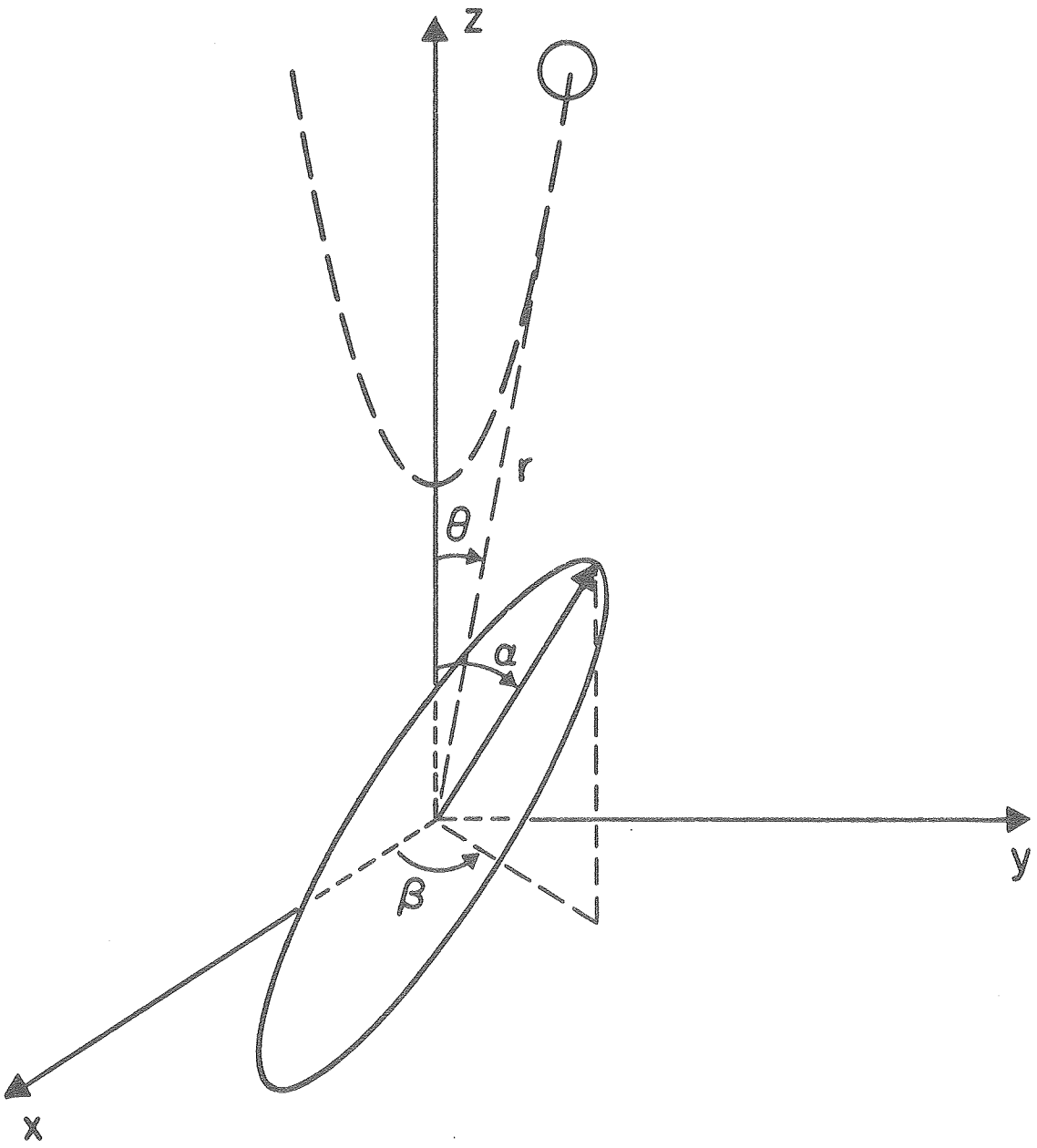

XBL 775-8587

Fig. V-1 Coordinates used to describe the physical system in the general Coulomb excitation process.

we did in section II-5 we may omit the Coulomb phase shifts and give the R-matrix instead by the expression

$$R_{00\to jm}(\lambda) = \frac{1}{\sqrt{4\pi}} \int_0^{2\pi} d\beta \int_0^{\pi} d\alpha \, \sin\alpha \, Y_{jm}(\alpha,\beta) \, e^{i\phi} \tag{16}$$

where λ is the deflection angle of the projectile in the center-of-mass system and the phase ϕ is evaluated following the same procedure of Eq. (II-45), that is

$$\phi = -\eta_0 \int (\hat{p}_r - \tilde{p}_r)\, d\tilde{r} = -\eta_0 \int \left(\sqrt{\tilde{p}_r^{\,2} - \frac{2q_2 \, P_2(\cos\gamma)}{\eta_0 \, \hat{r}^3}} - \tilde{p}_r \right) d\hat{r}$$

$$\eta_0 \to \infty \qquad\qquad \eta_0 \to \infty \tag{17}$$

$$= \int \frac{q_2 \, P_2(\cos\gamma)}{|\tilde{p}_r| \hat{r}^3} \, d\hat{r}$$

where $\cos\gamma$ is expressed in these coordinates as

$$\cos\gamma = \cos\alpha \, \cos\theta + \sin\alpha \sin\theta \cos\beta \tag{18}$$

θ is simply related to $\hat{r}$ by

$$\frac{1}{\hat{r}} = \frac{\dfrac{\cos(\theta - \frac{\lambda}{2})}{\cos(\frac{\lambda}{2})} - 1}{\tan^2 \frac{\lambda}{2}} \tag{19}$$

and $\tilde{p}_r$ is given by

$$p_r = \pm \sqrt{1 - \frac{2}{\hat{r}} - \frac{\tan^2 \frac{\lambda}{2}}{\hat{r}^2}} \qquad (20)$$

Using Eq. (17) ϕ is computed numerically, and then Eq. (16) can be easily evaluated.

In Fig. V-2 we show an example of a calculation done according to this prescription. The numerical results are identical to those obtained with the Winther-deBoer code setting all rotational energies to zero (infinite moment of inertia limit). This agreement was expected from the considerations mentioned in Ch. II.

This $\xi = 0$, $\eta = \infty$ limit could be useful to evaluate, at least in a semi-quantitative way, the excitation probabilities for a given system. In Fig. V-3 we compare this limit with the case where the moment of inertia takes its actual, finite value, for the same system as in Fig. V-2. The agreement is seen to be quite reasonable, and the qualitative trend of the excitation probabilities is well reproduced.

In this computer code we have included an electric hexadecapole potential, plus a complex nuclear potential besides the quadrupole potential indicated in Eq. (17). Therefore it is possible to use it to estimate the effects of these other potentials in the excitation probabilities for partial waves other than $\ell = 0$.

4. Present status of this problem

In order to evaluate the S-matrix element $S^J_{00 \to jm}$ we ran trajectories using the equations of motion derived from the Hamiltonian (14). From the final values of the dynamical variables we found the quantities $\bar{q}_j$, and $\bar{q}_m$, analogous to $\bar{\chi}$ in the $J = 0$

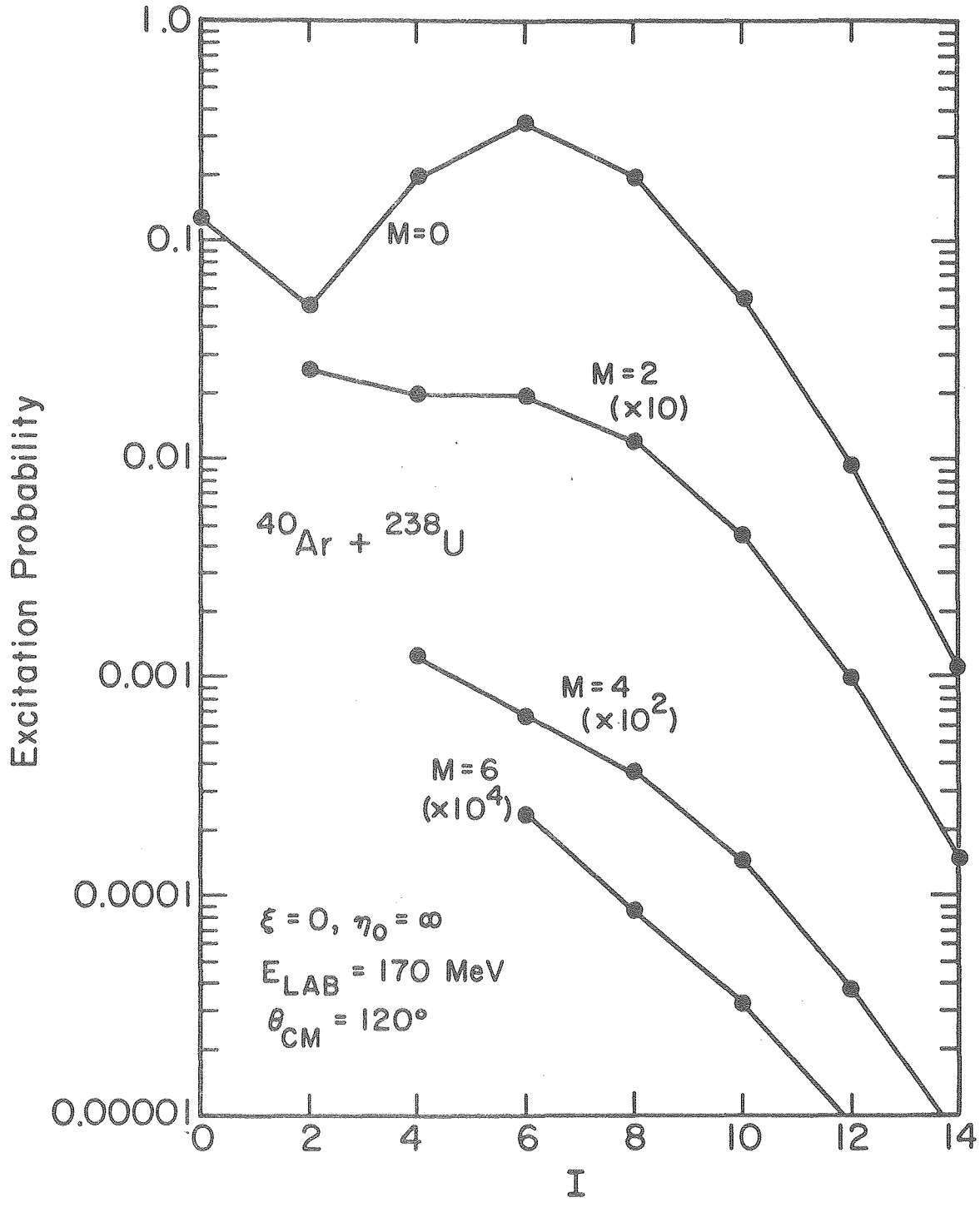

XBL 775-8590

Fig. V-2

Fig. V-2 Probabilities to excite the ground rotational band of ^{238}U by 170 MeV ^{40}Ar ions in the $\xi = 0$, $\eta_0 = \infty$ limit. The deflection angle is 120° in the center of mass system. Excitation probabilities for the same value of M are joined by lines to guide the eye.

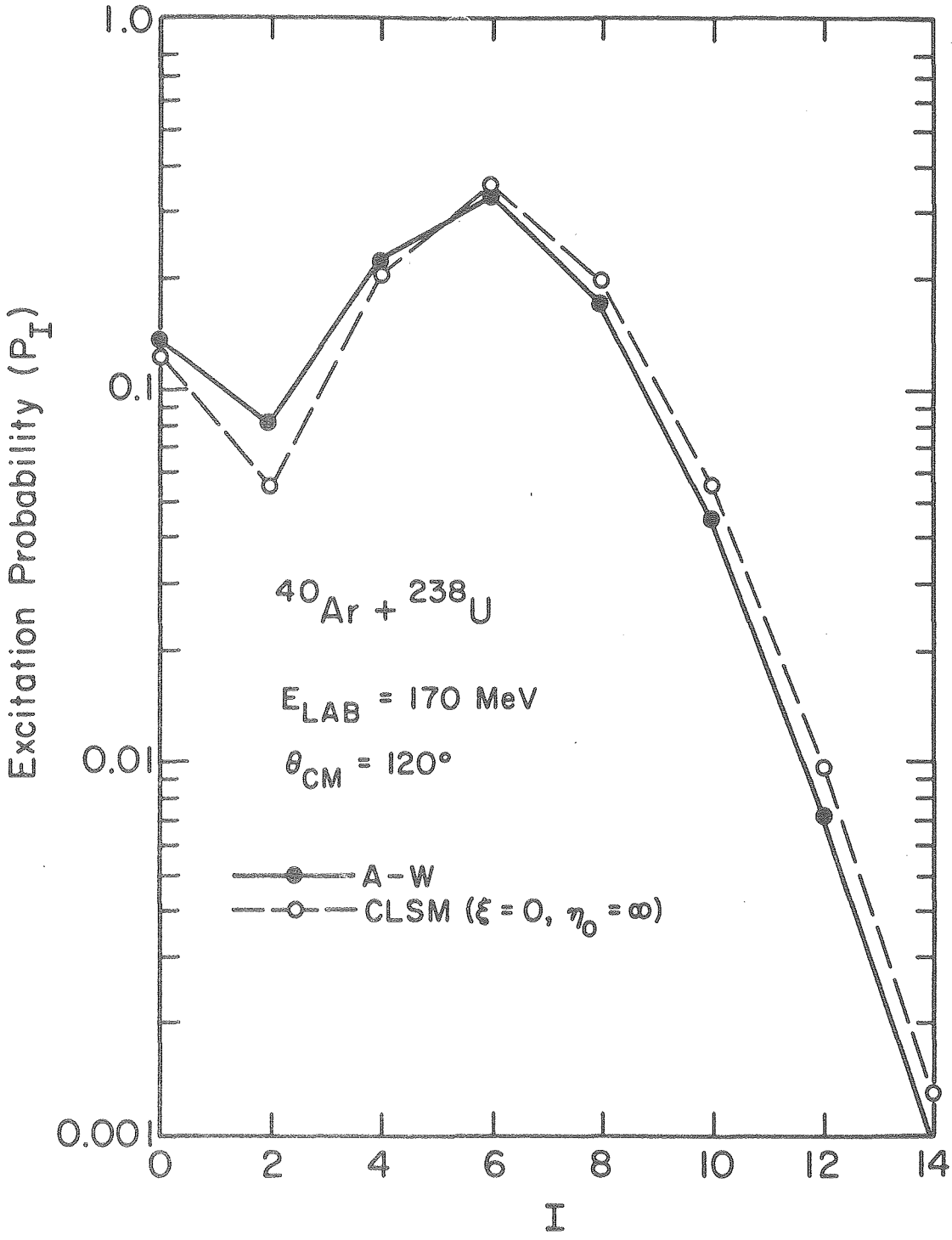
1.0
0.1
0.01
0.001
Excitation Probability (P_I)
$^{40}Ar + ^{238}U$
E_{LAB} = 170 MeV
θ_{CM} = 120°
A-W
CLSM ($\xi = 0$, $\eta_0 = \infty$)
0
2
4
6
8
10
12
14
I
XBL 775-8588

Fig. V-3

Fiv. V-3 Comparison of the excitation probabilities obtained using the CLSM method in the $\xi = 0$, $\eta_0 = \infty$ limit and the Alder-Winther semiclassical theory for the actual values of the physical parameters. The system and deflection angle are the same as in Fig. V-2.

case. Then the Jacobian $\partial(\bar{q}_j,\bar{q}_m)/\partial(q_{j0},q_{m0})$ was evaluated. It was found that this Jacobian became zero along curves in the (q_{j0},q_{m0}) plane. For these curves (caustics) the semiclassical wavefunction breaks down, as discussed in Ch. III; besides it was seen that the range of cases where caustics appear is much wider than for the $\ell = 0$ case, where they appeared only for the heaviest projectiles. Therefore before employing the integral expression for the S-matrix it is necessary to deal with this problem with the caustics. Probably the best way is to go back to the $\ell = 0$ case and treat it there, in a case that is much easier to study and which is more familiar. As was mentioned before, this is being considered at the present time.

In Ref. (49) it is indicated that if the physical stationary points for a certain transition are far from the caustics, which appear as spurious stationary points, then the integral defining the S-matrix element for the transition can be evaluated asymptotically, ignoring completely the spurious stationary phase points.

Fröbrich et al.,[59,60] have used the stationary phase method in the study of rotational excitation. They found that the method gives accurate results for the classically allowed transitions, but that it was much harder to apply than the uniform approximation in one dimension.[23-25] Therefore they consider doubtful whether it can be extended in practice to the study of classically forbidden transitions or to the inclusion of a complex nuclear potential.[61] They have considered the alternative of using the integral representation, but the first indications were that they found the same type of caustic-related problems described before.[61]

As it stands now, this appears to be rather a technical difficulty and not a deep conceptual problem, since it takes place for heavy systems, where the classical model should work best.

5. Octupole vibration-rotation band of a deformed nucleus

Recently Grosse et al[62] have excited the lowest octupole vibrational band of ^{238}U up to spin 19. They found that the one predominantly excited was the $K=0$ band, which corresponds to an oscillating deformation in the nuclear shape proportional to $P_3(\cos\theta)$, where θ is the azimuthal angle and P_3 the standard 3rd order Legendre polynomial.

The interaction term between the projectile and target motions is now given by:

$$V_{(r,\alpha,\chi)} = \frac{Z_p Z_T e^2}{r} + \frac{Z_p Q_0^{(2)} e^2 P_2(\cos\chi)}{2r^3} + \frac{Z_p Q_0^{(3)}(\alpha)\, e^2 P_3(\cos\chi)}{2r^4} \qquad (21)$$

where $Q_0^{(3)}$ is the octupole moment of the target, which is dependent on the amplitude α of the octupole vibration. All other quantities retain the meaning assigned in Ch. II.

The classical Hamiltonian for this system can then be found by adding $V(r,\alpha,\chi)$ to the translation, rotation and vibrational energies. For the backscattering case it is given by

$$H(r,q,\chi,p_r,n,p_\chi) = \frac{p_r^2}{2m} + \frac{p_\chi^2}{2}\left(\frac{1}{\mathcal{I}} + \frac{1}{mr^2}\right) + \hbar\omega_0(n+1/2) + V(r,\alpha,\chi) \qquad (22)$$

where ω_0 is the characteristic frequency of the octupole-vibration, n is the vibrational quantum number and q is the phase of the oscillator. The amplitude α is related to the phase q and n by

$$\alpha = \sqrt{\frac{2\hbar\omega_0(n+1/2)}{C_3}}\cos q \tag{23}$$

where C_3 is the restoring force parameter for the octupole vibration. $Q_0^{(3)}$ can then be written as

$$Q_0^{(3)}(\alpha) = \frac{3Z_T R_0^2 \alpha}{\sqrt{5\pi}} = 3Z_T R_0^2 \left(\frac{2\hbar\omega_0(n+1/2)}{5\pi C_3}\right)^{1/2}\cos q \tag{24}$$

From this expression for the Hamiltonian we can write the equations of motion for the system, and for the final values of the dynamical variables we can evaluate the expression for the S-matrix for the transition from the initial state ($I = 0$, $n = 0$) to the final state I,n.

$$S_{0,0\to I,n} = \frac{\sqrt{2I+1}}{4\pi}\int_0^{\pi} d\chi_0 \int_0^{2\pi} d\bar{q}_0 \sqrt{\sin\chi_0 \sin\bar{\chi}\ \frac{\partial(\bar{q},\bar{\chi})}{\partial(\bar{q}_0,\chi_0)}} \tag{25}$$

$$\times P_I(\cos\bar{\chi})\exp(i\bar{q}n)\exp(i\Delta/\hbar)$$

In this expression $\bar{q}_0$ and $\bar{q}$ are defined in exactly the same way as $\bar{X}$ was in Eq. (II-13') (See also Ref. 11 for additional information). Δ is given now by

$$\Delta = -\int [r(t)dp_{r(t)} + \hbar\, q(t)dn(t) + \chi(t)dp_{\chi(t)}] + \bar{X}\, p_\chi^f + \hbar\bar{q}\, n^f + \int_0^{p_r} \tilde{r}\, d\tilde{p}_r + \hbar\,(\sigma_0(\eta_0) + \sigma_I(\eta_I)) \tag{26}$$

where p_χ^f and n^f are the final values of p_χ and n, respectively, and the other quantities have the same meaning as in Eq. (II-21).

The characteristics of the problem lend themselves to a simplification which reduces the double integral in Eq. (25) to a single integral, and which besides allow for an interpretation in simpler terms of the expression for the S-matrix.

This approximation is based on the fact that the octupole vibration affects very little both the projectile motion and the angular momentum transfer between projectile and target. This is so because the octupole vibration amplitude is small and its frequency high.

We can therefore assume that the octupole moment acts only in the phase Δ, and then as a perturbation. In this way it is possible to factor the expression for the S-matrix, Eq. (25), in the following way:

$$S_{0,0\to I,n} \approx \frac{\sqrt{2I+1}}{2}\int_0^{\pi} d\chi_0 \sqrt{\sin\chi_0 \sin\bar{\chi}\,\frac{\partial\bar{\chi}}{\partial\chi_0}}\, P_I(\cos\bar{\chi})\exp(i\Delta_1/\hbar)$$

$$\times \frac{1}{2\pi}\int_0^{2\pi} d\bar{q}_0 \sqrt{\frac{\partial\bar{q}}{\partial\bar{q}_0}}\exp(i\bar{q}n)\exp(i\Delta_2/\hbar) \tag{27}$$

We have made use of the fact that $\bar{\chi}$ is independent of $\bar{q}_0$, so that $\frac{\partial\bar{\chi}}{\partial\bar{q}_0} = 0$; therefore $\frac{\partial(\bar{q},\bar{\chi})}{\partial(\bar{q}_0,\chi_0)} = \frac{\partial\bar{q}}{\partial\bar{q}_0}\cdot\frac{\partial\bar{\chi}}{\partial\chi_0}$.

The phase Δ_1 is taken to be the same as in Eq. (II-21); that is,

$$\Delta_1 = -\int\left[r(t)\,\frac{dp_{r(t)}}{dt}\bigg|_{Q_0^{(3)}=0} + \chi(t)\,\frac{dp_\chi(t)}{dt}\right]dt + \bar{\chi}\,p_\chi^{\,f}$$

$$+\int_0^{p_r}\tilde{r}\,d\tilde{p}_r + \hbar\left[\sigma_0(n_0) + \sigma_I(n_I)\right] \tag{28}$$

while $\Delta_2 = \Delta - \Delta_1$ can then be written as

$$\Delta_2 = -\int\left[r(t)\left(\frac{dp_{r(t)}}{dt}\bigg|_{Q_0^{(3)}\neq 0} - \frac{dp_{r(t)}}{dt}\bigg|_{Q_0^{(3)}=0}\right)\right. \tag{29}$$

$$\left. + \hbar\, q(t)\,\frac{dn(t)}{dt}\right]dt + \hbar\,\bar{q}n^f$$

in Eqs. (28) and (29) we indicate by $Q_0^{(3)} \neq 0$ ($Q_0^{(3)} = 0$) quantities that are evaluated (not) considering the octupole term in Eq. (21).

We see that the expression for the S-matrix element given by Eq. (27) is identical to the one found in Ch. II, Eq. (II-22), for the Coulomb excitation of the ground band, except that the integrand is multiplied by a factor

$$a(\chi_0) = \frac{1}{2\pi} \int_0^{2\pi} d\bar{q}_0 \sqrt{\frac{d\bar{q}}{d\bar{q}_0}} \exp(i\bar{q}n) \exp(i\Delta_2/\hbar) \tag{30}$$

Let us consider Eq. (29). From Eqs. (21)-(27) we have

$$\left.\frac{dp_{r(t)}}{dt}\right|_{Q_0^{(3)} \neq 0} - \left.\frac{dp_{r(t)}}{dt}\right|_{Q_0^{(3)} = 0} = \frac{2Z_p Q_0^{(3)}(\alpha)\, e^2\, P_3(\cos\chi)}{r(t)^5} \tag{31}$$

$$\frac{dn(t)}{dt} = \frac{Z_p Q_0^{(3)}(\alpha) \tan q\, e^2\, P_3(\cos\chi)}{r(t)^4} \tag{32}$$

The r^{-4} dependence of the integrand in Eq. (29) indicates that most of the contribution to the integral is at the point of closest approach. Due to the low angular velocity of the target as compared to the collision time it is then possible to approximate Eq. (29) by giving to χ its value at the point of closest approach χ_{CA}. This is true in the case of n^f as well, since from Eq. (32)

$$n^f = \int_{t_0}^{t_f} \frac{Z_p Q_0^{(3)}(\alpha) \tan q\, e^2\, P_3(\cos\chi}{r^4}\, dt \tag{33}$$

Therefore the phase Δ_2 can be written in the form

$$\Delta_2 \approx \hbar\, K\, P_3\,(\cos \chi_{CA}(\chi_0)) \tag{34}$$

where K is approximately independent of χ_0.

Therefore in (30) the dependence of $a(\chi_0)$ on χ_0 is essentially through the factor $\exp(i\, K\, P_3(\cos \chi_{CA})$. Since $Q_0^{(3)}$ is very small, then n^f and K will be small numbers. The fact that n^f is small means that only the $n = 1$ state can be appreciably excited. We therefore drop the $n = 1$ subindex of the S-matrix element. Since K is small one may approximate

$$\begin{aligned} a(\chi_0) &\approx \text{const.}\ \exp(i\, K\, P_3(\cos \chi_{CA})) \\ &\approx \text{const.}\ (1 + i\, K\, P_3(\cos \chi_{CA})) \end{aligned} \tag{35}$$

When replaced in Eq. (27) the first term in Eq. (35) does not contribute to the integral. Therefore the S-matrix is given by

$$\begin{aligned} S_{0\to I} \sim i\, \frac{\sqrt{2I+1}}{2}\, K \int_0^{\pi} d\chi_0 \sqrt{\sin\chi_0 \sin\bar{\chi}\, \frac{d\bar{\chi}}{d\chi_0}} \\ \times P_I(\cos\bar{\chi})\, P_3(\cos\chi_{CA})\, \exp(i\Delta_1/\hbar) \end{aligned} \tag{36}$$

$I = 1,3,5,\ldots$

which is similar to Eq. (II-22) except for the form factor $P_3(\cos \chi_{CA})$.

This form factor can be found also in a less rigorous but more illuminating way. The $K = 0$ octupole vibration has a $P_3(\cos\theta)$ dependence. We expect the excitation of this vibration by a charged projectile to be strongly dependent on the particular trajectory

followed by the projectile, specially at the point of closest approach. In particular we expect that trajectories such as that labelled (1) in Fig. V-4 that approach the target along a node of the octupole vibration will excite it little or not at all; while those like (2) will excite it much more, since their point of closest approach is near the region where the vibration amplitude is maximum. In general the excitation will go as $P_3(\cos\chi_{CA})$, if we neglect the fact that the quadrupole moment of the target changes slightly the point of closest approach and therefore the intensity of the exciting force. Figure V-5 shows that $P_3(\cos\chi_{CA})$ is a good approximation to the expression

$$a(\chi_0) = C \int \frac{P_3(\cos\chi(t))}{r(t)^4}\, dt \qquad (37)$$

where the constant C is chosen so that $a(0) = 1$. This is an indication that these other dynamical effects discussed here are small.

In Figs. V-6,7 we show the results obtained from Eq. (33), normalizing them, and comparing with those obtained through the Winther-de Boer program. The agreement is good, which indicates that the classical picture on which Eq. (33) was based is indeed correct and that the approximations involved are not excessive. This is also confirmed by the case shown in Fig. V-8 where by taking the $\xi = 0$, $\eta = \infty$ limit we have that the point of closest approach lies at a distance independent of the target orientation. In this case the agreement is much better.

Table V-1 summarizes all the results for one of the cases depicted in the previous figures.

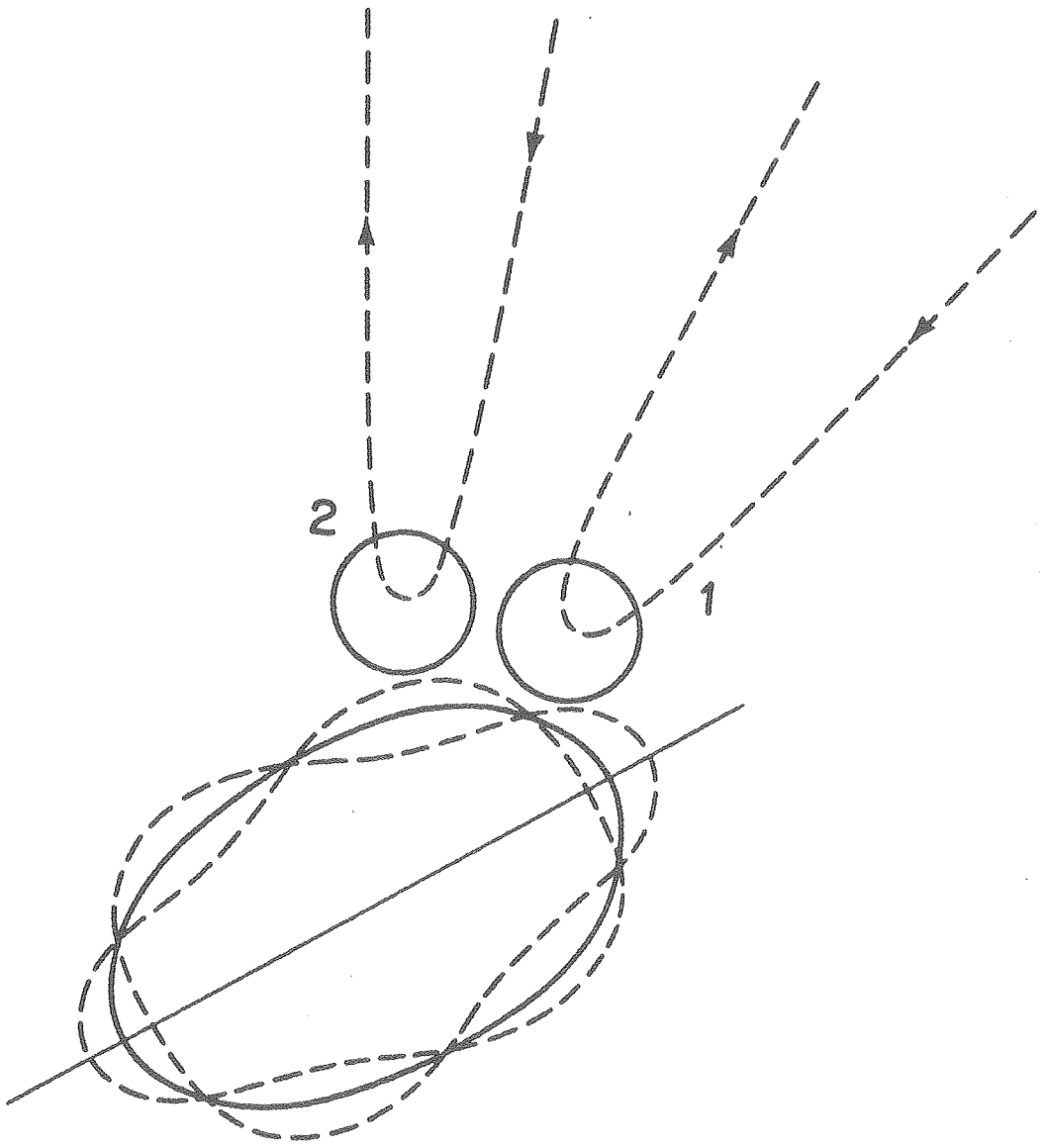

XBL 775-8586

Fig. V-4

Fig. V-4 The K = 0 octupole vibration is represented as a standing wave on the nuclear surface. Trajectory labeled (2), which has its point of closest approach near a maximum in the vibration amplitude, excites the octupole vibration much more than trajectory (1), which has it close to a node in the vibration.

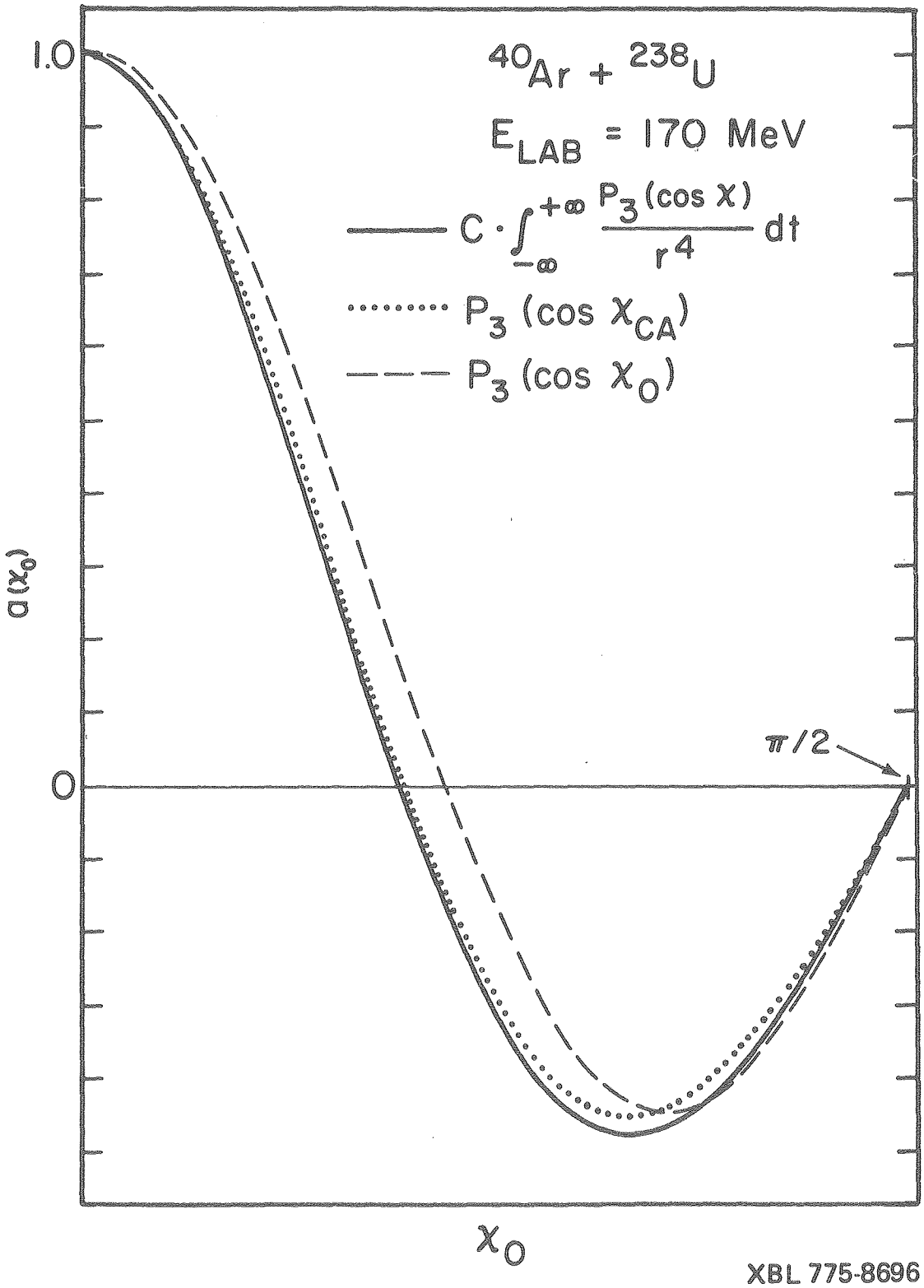
1.0
0
$\sigma(\chi_0)$
$^{40}Ar + ^{238}U$
E_{LAB} = 170 MeV
$C \cdot \int_{-\infty}^{+\infty} \frac{P_3(\cos\chi)}{r^4} dt$
$P_3(\cos\chi_{CA})$
$P_3(\cos\chi_0)$
$\pi/2$
χ_0
XBL 775-8696

Fig. V-5

Fig. V-5 Comparison of $P_3(\cos x_{CA})$ to $\int_{-\infty}^{+\infty} \frac{P_3(\cos \chi(t))}{r(t)^4}\, dt$, where the value of the constant C is chosen so that this last expression equals 1 when $\chi_0 = 0$. $P_3(\cos \chi_0)$ is also plotted as a reference.

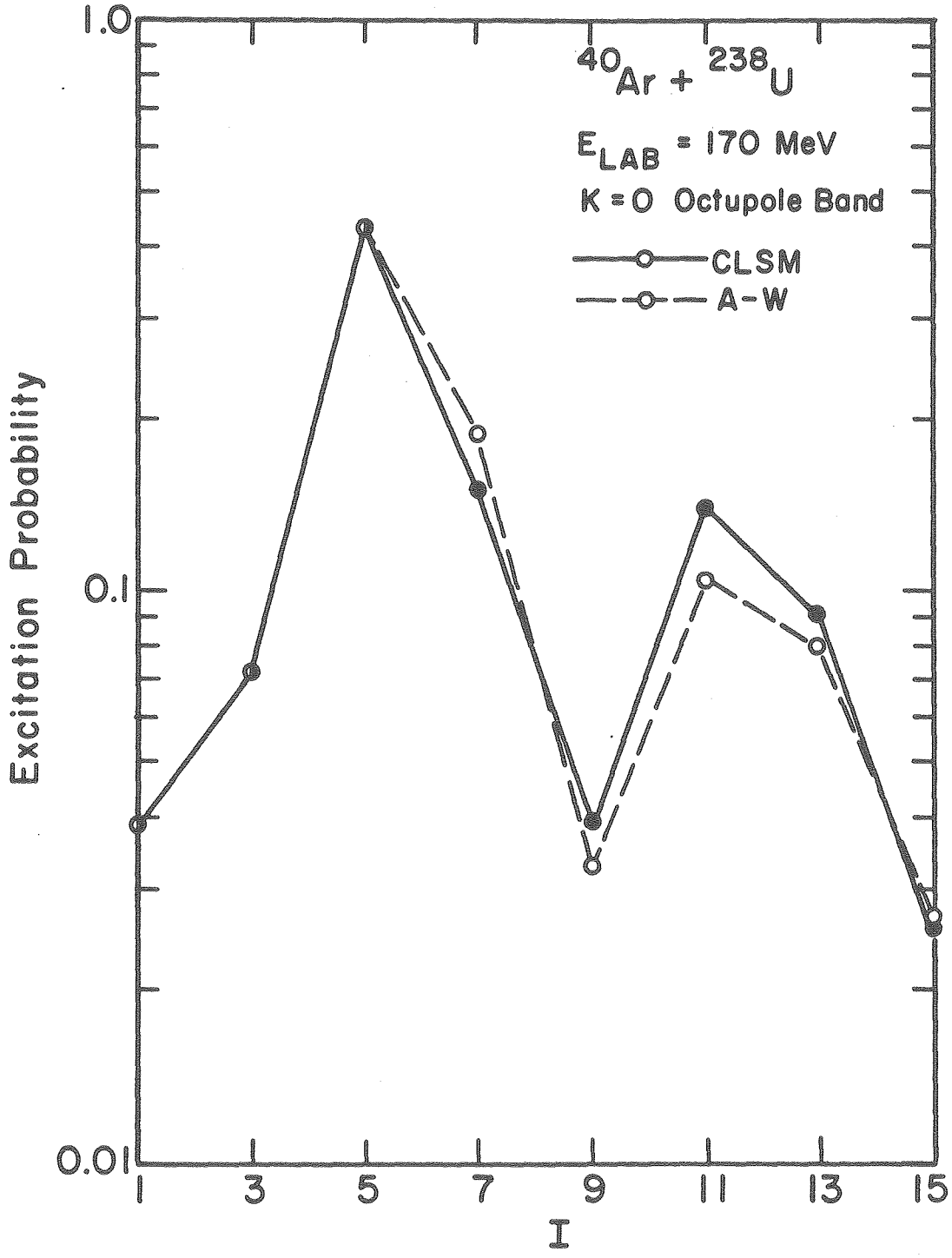

XBL 775-8591

Fig. V-6

Fig. V-6 Signature of the K = 0 octupole band excitation in ^{238}U by 170 MeV ^{40}Ar ions. The energies are taken from the rotational model with E_{1^-} = 0.7313 MeV for the octupole band and E_{2^+} = 0.0449 MeV for the ground band. The quadrupole moment of ^{238}U is taken to be 11.12b for both bands.

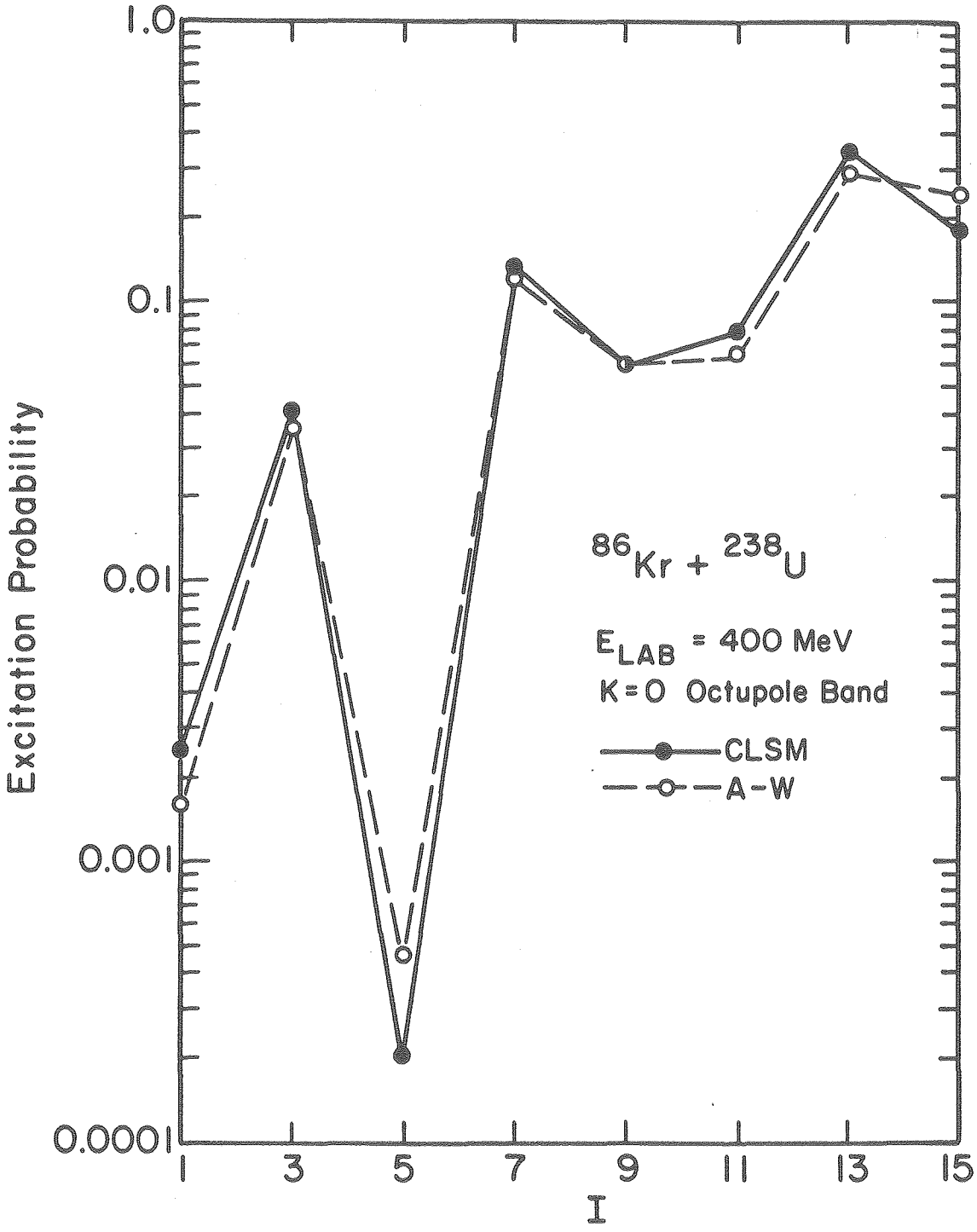

XBL 775-8589

Fig. V-7 Same as Fig. V-6 using 400 MeV ^{86}Kr ions as projectiles.

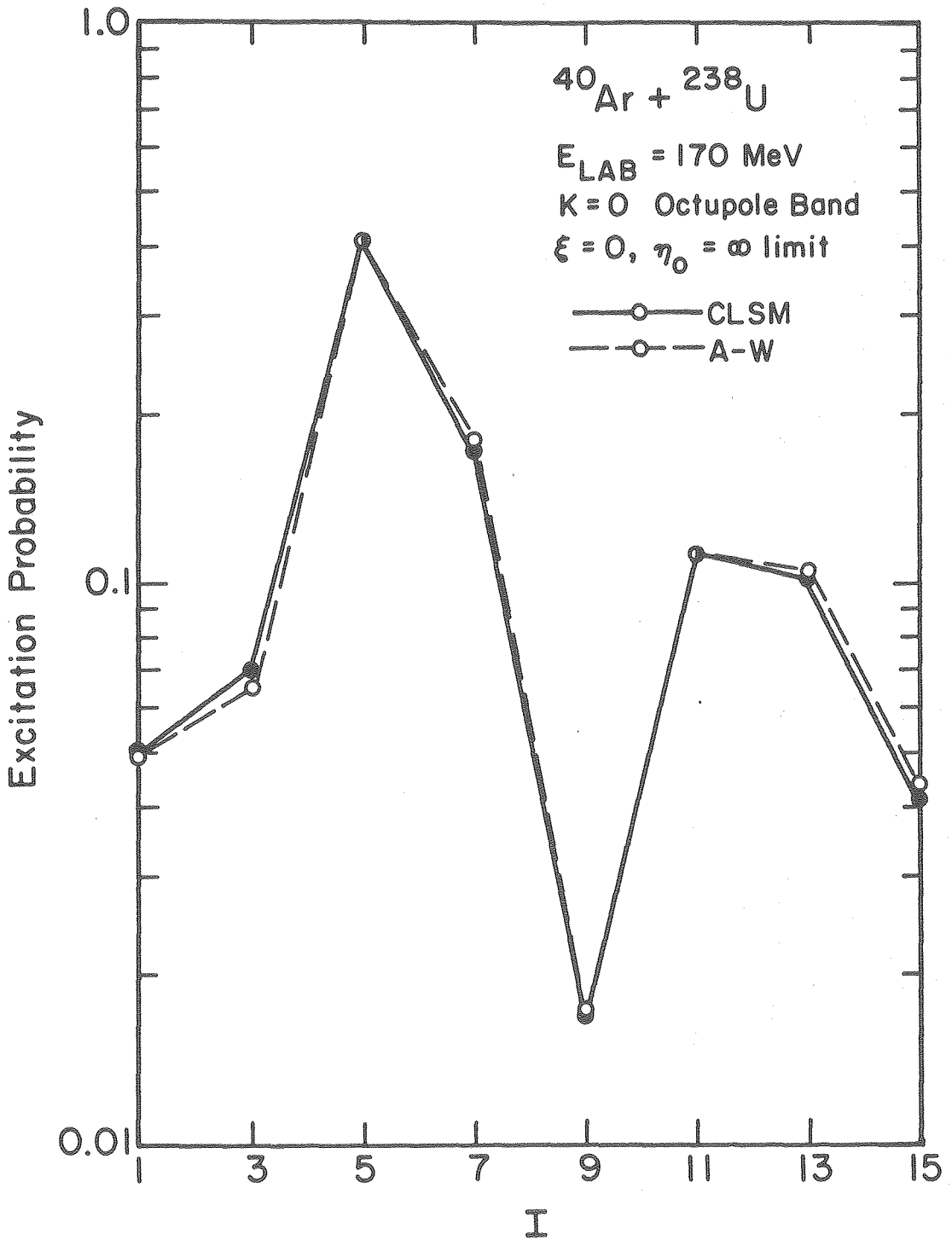

XBL 775-8592

Fig. V-8 Signature of the K = 0 octupole band excitation for the same system as in Fig. V-6 in the $\xi = 0$, $\eta_0 = \infty$ limit.

Table V-1. Coulomb excitation of the K = 0 octupole band in ^{238}U with 170 MeV ^{40}Ar ions. The quadrupole moment of ^{238}U was taken to be 11.12b for both bands for all calculations. The interband coupling was obtained from the experimental value of BE3 ($0^+ \rightarrow 3^-$) = 0.663 b^3. The rotational energies were taken from the rotational model with E_{2^+} = 0.0443 MeV for the ground band and E_{1^-} = 0.6798 MeV and E_{3^-} = 0.7313 MeV for the octupole band. This is shown to differ little from the results when the energies are those found experimentally in Ref. 63.

SPIN	EXCITATION PROBABILITIES[a]				
	CLSM	A - W Rotational Energies	A - W Experimental Energies	CLSM Sudden Limit[b]	A - W Sudden Limit[b]
1	0.039	0.039	0.039	0.050	0.049
3	0.074	0.074	0.074	0.070	0.066
5	0.435	0.446	0.452	0.410	0.410
7	0.151	0.189	0.190	0.171	0.181
9	0.039	0.033	0.032	0.017	0.017
11	0.142	0.107	0.105	0.113	0.113
13	0.091	0.080	0.077	0.102	0.105
15	0.026	0.027	0.026	0.041	0.044

a) results were normalized to have a total excitation probability for the octupole band equal to 1.

b) all energies were set equal to zero

We should remark that we have considered the excitation of the K = 0 band of the octupole vibration. Reference 63 indicates that we should expect a significant mixing of all K = 0, 1,2,3 octupole bands for high spins. Therefore the predictions of our model apply specially to the lower spins in the band. For the higher spins, where the band mixing is very important, the Coriolis coupling aligns the vibrational angular momentum along the rotation axis, producing therefore a band with energy spacings identical to those of the ground band but with spins 3 units higher.[63] The vibration deformation is now given by $Y_{33}(\theta,\phi)$, where the Z-axis is taking along the rotation axis. This vibration appears not as stationary wave, as was the case for the K = 0 band but as a wave propagating on the nuclear surface, orthogonally to the rotation axis. The excitation of the vibration in this case will be independent of the direction of approach of the projectile (except for the effects due to the change in the point of closest approach caused by the octupole moment, and which we saw was negligible in the K = 0 band case), since now we have a travelling and not a standing wave. Therefore the probability for exciting a high spin I in the octupole band will be proportional to the probability of exciting the spin I-3 in the ground band, since the form factor for exciting the vibration (and with it the 3 units of angular momentum that are added to the I-3 of the rotation) is a constant independent of the orientation χ_0.

6. Nucleon and cluster transfer on a deformed nucleus

The success found in the case just discussed suggests the possibility of studying other processes in a similar way. One problem that appears to be tractable by this method is that of the particle transfer taking place between the projectile and the deformed target brought close together in a collision at an energy about that of the Coulomb barrier.

The problem is slightly different according to the type of particle being transferred. For the case of a nucleon the orientation dependence of the transfer amplitude will be due to (1) the spatial distribution of the Nilsson orbital involved in the transfer; this will favor orientations for which the major lobe of the Nilsson wave function from or to which the transfer takes place points in the direction of the other collision partner at the point of closest approach, and (2) the fact that the tunneling probability depends strongly on the distance of closest approach, which is at its turn dependent on the particular orientation of the target. This will favor transfer for trajectories that approach the target at the poles.

Since the transfer amplitude will have a strong correlation with the relative orientation of the deformed target nucleus with respect to the impinging projectile, and therefore with the excitation of particular rotational states of the product nucleus, we expect to find, as it was the case for the octupole vibrations, a characteristic signature for the final rotational states of the target.

In the case of one-nucleon transfer the problem is complicated by the fact that this nucleon carries with it angular momentum which

has to be added to the part transferred through the electromagnetic excitation.

Therefore it will be easier to consider the transfer of a spinless particle, such as a di-neutron or an α-particle. For this case the angular dependence through the Nilsson orbital appearing in the case of nucleon transfer would be replaced by that of the probability of forming the compound particle on the nuclear surface. This problem was studied by Poggenburg[63] for the case of an α-particle.

The formalism is the same as in section 5 except that now $a(\chi_0)$ will represent the transfer amplitude. Work on this approach has already started.

VI. CONCLUSIONS

The classical-limit S-matrix formalism was shown to be a very useful tool in the understanding of the physical processes taking place in the excitation of rotational states by means of heavy ions. It is fascinating and highly instructive to see how a theory which is based upon classical dynamics can give so much insight into problems where quantum effects are very strong. This makes us wonder whether there is a much deeper connection between classical and quantum mechanics than that the former is the limit of the latter as $\hbar$ goes to zero, or in the limit of the high quantum numbers. Neither of these two limits were imposed for the problems studied here. Nevertheless the results of the CLSM theory were seen to be in quantitative agreement with the quantum-mechanical results.

Besides this theoretical question it is our opinion that the CLSM constitutes per se an important means to study the problem of rotational scattering, and it should be useful in the task of perfecting the most widely used theory of Coulomb excitation, the semiclassical method of Alder and Winther.

Until the time arrives when faster codes and computers will make possible the quantum mechanical study of heavy-ion scattering from deformed nuclei at energies at or above the Coulomb barrier, where the nuclear potential can no longer be neglected, the CLSM will play a useful role in analyzing the experimental data that is starting to appear, and which we think contains much information about the nuclear surface region.

The formalism developed here has limitations due to the existence of caustics in the family of classical trajectories for some systems. We do not think these are absolute restrictions and that they will be removed sooner or later by a more careful choice of representation. What we find to be a real limitation is that it can be used only for processes that can be classically described, such as, the excitation of collective vibrations and rotations of nuclei. Even so, this leaves a large and important region of applicability to the CLSM method. It is interesting to note that processes in this region are the ones most easy to understand in familiar terms, since their description involves concepts common in macroscopic physics and therefore in everyday life.

APPENDIX A

The Uniform Semiclassical Approximation

The quantum-mechanical propagator

$$K(q_2t_2|q_1t_1) = \langle q_2| e^{-\frac{i}{\hbar}H(t_2-t_1)} |q_1\rangle \tag{1}$$

can be written, according to Feynman, as a path integral over all possible paths $q_\alpha(t)$ satisfying the boundary conditions $q_\alpha(t_1) = q_1$, $q_\alpha(t_2) = q_2$.

The propagator K is then written as

$$K(q_2t_2|q_1t_1) = \int_\alpha D[q_\alpha(t)]\, e^{-\frac{i}{\hbar}\phi_\alpha(q_2,q_1)} \tag{2}$$

where $\phi_\alpha(q_2,q_1)$ is the classical action calculated along the path $q_\alpha(t)$. The definition of classical action is

$$\phi_\alpha(q_2,q_1) = \int_{t_1}^{t_2} dt\, \mathscr{L}(q_\alpha(t),\dot{q}_\alpha(t)) \tag{3}$$

where $\mathscr{L}(q,\dot{q})$ is the classical Lagrangian.

The integrand in Eq. (2) is a rapidly changing function of the path q_α in cases where the action $\phi_\alpha(q_2,q_1)$ is large (measured in units of $\hbar$), so that the contribution from one path is cancelled by the one of nearby paths. Therefore only those paths for which $\phi_\alpha(q_2,q_1)$ is stationary result in a net contribution to the integral in Eq. (2).

This condition can be written as

$$\delta \int_{t_1}^{t_2} dt\, \mathscr{L}(q_\alpha(t), \dot{q}_\alpha(t)) = 0 \tag{4}$$

which, as is well known in Classical Mechanics, results in the Lagrange equations of motion. We see then that the paths that make a net contribution are those classical paths which satisfy the boundary conditions $q_\alpha(t_1) = q_1$, $q_\alpha(t_2) = q_2$. If we denote by $q_c(t)$ these classical paths, by expanding $\phi_\alpha(q_2, q_1)$ to second order in the departures $\delta q(t)$ from the paths $q_c(t)$ one obtains gaussian integrals which can be evaluated to give

$$K(q_2 t_2 | q_1 t_1) \approx \sum_c \sqrt{\frac{2\pi i\hbar}{\dfrac{\partial^2 \phi_c}{\partial q_2 \partial q_1}}}\; e^{\frac{i\phi_c(q_2, q_1)}{\hbar}} \tag{5}$$

where the sum is implied over all classical trajectories $q_c(t)$ satisfying the boundary conditions mentioned before.

It is interesting to note that in the limit $\hbar \to 0$ Eq. (5) is exact and classical mechanics can thus be considered as the stationary phase approximation to quantum mechanics.

The quantity $\sum_c \dfrac{2\pi\hbar}{\left|\dfrac{\partial^2 \phi_c}{\partial q_2 \partial q_1}\right|}$ can be interpreted as the classical probability of finding at time t_2 the system at position q_2 , provided it was in position q_1 , at time t_1.

At this stage it is convenient to change towards Hamiltonian formulation. The momentum $p(t)$ conjugate to $q(t)$ is defined as

usual by:

$$p = \frac{\partial \mathscr{L}(q,\dot{q})}{\partial \dot{q}} \tag{6}$$

and the Hamiltonian H by:

$$H(p,q) = p\dot{q} - \mathscr{L}(q,\dot{q}) \tag{7}$$

(We should remark that even if we are considering only one independent coordinate q, the extension of this formalism to more degrees of freedom is quite straightforward).

In momentum representation the action integral is given by[10]

$$\phi_\alpha(p_2,p_1) = -(p_2q_2 - p_1q_1) + \int_{t_1}^{t_2} dt\left[p(t)\,\dot{q}(t) - H(p(t),\, q(t))\right] \tag{8}$$

and the propagator is then written:

$$K(p_2t_2|p_1t_1) \approx \sum_c \sqrt{\frac{2\pi i\hbar}{\dfrac{\partial^2\phi_c}{\partial p_2 \partial p_1}}}\; e^{\frac{i\phi_c(p_2,p_1)}{\hbar}} \tag{9}$$

where the sum is done over all classical trajectories that satisfy $p(t_1) = p_1$, $p(t_2) = p_2$.

The S-matrix is defined as:

$$S_{p_1 \to p_2} = \langle p_2|S|p_1\rangle \equiv \lim_{\substack{t_1 \to -\infty \\ t_2 \to +\infty}} \langle p_2|\, e^{\frac{iH_0t_2}{\hbar}}\, e^{\frac{-iH(t_2-t_1)}{\hbar}}\, e^{\frac{-iH_0t_1}{\hbar}} \,|\, p_1\rangle \tag{10}$$

where $|p_1\rangle$, $|p_2\rangle$ are the eigenstates of the unperturbed Hamiltonian H_0; they appear as the "indices" (or quantum numbers) in the S-matrix and correspond classically to the constants of motion of H_0.

We see that the S-matrix is a propagator-type quantity, and we can associate to it immediately a phase factor:

$$\phi_\alpha(p_2,p_1) = E(t_2-t_1) + \int_{\substack{t_1\to-\infty \\ t_2\to+\infty}}^{t_2} dt[p_\alpha q_\alpha - H(p_\alpha,q_\alpha)] - (p_2q_2 - p_1q_1) \qquad (11)$$

By using energy conservation, $\int_{t_1}^{t_2} H\, dt = E(t_2-t_1)$ and since

$$\int_{t_1}^{t_2} dt\; p\dot{q} - (p_2q_2 - p_1q_1) = -\int_{t_1}^{t_2} dt\; q\dot{p}$$

$$\phi_\alpha(p_2,p_1) = -\int_{\substack{t_1\to-\infty \\ t_2\to+\infty}}^{t_2} dt\; q(t)\,\dot{p}(t) \qquad (11')$$

Therefore the stationary phase approximation of the Feynman path integral corresponding to (10) is:

$$S_{p_1\to p_2} \approx \sum_c \sqrt{\frac{2\pi i\hbar}{\dfrac{\partial^2\phi_c}{\partial p_2 \partial p_1}}}\; e^{\frac{i\phi_c(p_2,p_1)}{\hbar}} \qquad (12)$$

where $\phi_c(p_2,p_1)$ is given by Eq. (11').

Equation (12) requires for it being valid, that if there is more than one stationary path they are not too close so that the second order expansion for the phase around each of these stationary points is a good approximation.

This is not the case when two or more of the stationary paths lie close to each other, and the problem of doing the stationary phase integration becomes harder to solve, and was not done in the general case. For the particular case in which there are only two stationary trajectories by mapping the phase unto a cubic polynomial in such a way that the stationary points of the phase and the polynomial correspond, the following improved expression for the S-matrix is found

$$S_{p_1 \to p_2} \approx \sqrt{2}\,\pi\, e^{\frac{i}{2}(\phi_1+\phi_2)} \left\{ \left[\frac{\left.\frac{\partial p_2}{\partial p_1}\right|_1}{\sqrt{\frac{\partial^2 \phi_1}{\partial p_2 \partial p_1}}} + \frac{\left.\frac{\partial p_2}{\partial p_1}\right|_2}{\sqrt{\frac{\partial^2 \phi_2}{\partial p_2 \partial p_1}}} \right] \xi^{1/4}\, A_i(-\xi) \right.$$

$$\left. - \left[\frac{\left.\frac{\partial p_2}{\partial p_1}\right|_1}{\sqrt{\frac{\partial^2 \phi_1}{\partial p_2 \partial p_1}}} - \frac{\left.\frac{\partial p_2}{\partial p_1}\right|_2}{\sqrt{\frac{\partial^2 \phi_2}{\partial p_2 \partial p_1}}} \right] \xi^{-1/4}\, A_i'(-\xi) \right\} \tag{13}$$

Where ϕ_1 and ϕ_2 are the phases along the two stationary trajectories; Ai(x) and Ai'(x) are the usual Airy function and its derivative, and ξ is defined by:

$$\xi = \left[\frac{3}{4}(\phi_2 - \phi_1)\right]^{2/3} \tag{14}$$

A drawback of both expressions (12) and (13) appears for cases where the action integral ϕ is not a sufficiently rapidly changing function of the path chosen, because in the derivation of both expressions the mapping chosen reproduces the region around each stationary path for Eq. (12), or also in between the two stationary paths considered in Eq. (13), but the mappings are assumed to be valid for all the space; in cases where the remaining of the space makes a significant contribution the expressions (12) and (13) are not valid and this happens in the cases where ϕ changes slowly. For this case Stine and Marcus have developed a variation of the uniform approximation, where the action ϕ is mapped onto a function of the form $-\zeta \cos y - ky + A$, with ζ and A being real numbers and k an integer, and where again the stationary points of the phase integral are mapped onto the stationary points of the function.

The resulting expression is:

$$S_{p_1 \to p_2} = \sqrt{\frac{\pi}{2}}\,\zeta^{1/2}\, e^{i\bar{A}} \left\{ (\cos\theta)^{1/2} \left[\frac{\left.\frac{\partial p_2}{\partial p_1}\right|_2}{\sqrt{-\frac{\partial^2 \phi_2}{\partial p_2 \partial p_1}}} + \frac{\left.\frac{\partial p_2}{\partial p_1}\right|_1}{\sqrt{\frac{\partial^2 \phi_1}{\partial p_2 \partial p_1}}} \right] J_k(\zeta) \right.$$

$$\left. + i\,(\cos\theta)^{-1/2} \left[\frac{\left.\frac{\partial p_2}{\partial p_1}\right|_2}{\sqrt{-\frac{\partial^2 \phi_2}{\partial p_2\, p_1}}} - \frac{\left.\frac{\partial p_2}{\partial p_1}\right|_1}{\sqrt{\frac{\partial^2 \phi_1}{\partial p_2 \partial p_1}}} \right] J_k'(\zeta) \right\} \qquad (15)$$

where $k = |p_1 - p_2|$, $\bar{A} = \frac{1}{2}[\phi_1 + \phi_2]$, $\cos\theta = \sqrt{1 - \frac{k^2}{\zeta^2}}$ and ζ is obtained from $\frac{1}{2}\left[\phi_2 - \phi_1\right] = \sqrt{\zeta^2 - k^2} - k \cos^{-1}\left(\frac{k}{\zeta}\right)$.

APPENDIX B

Semiclassical Theory of Coulomb Excitation

Since in heavy-ion Coulomb excitation projectile velocities are small compared to that of light, magnetic excitation, which goes as $(v/c)^2$, may be ignored. Therefore the Coulomb excitation process is treated as due to the interaction between the electric field of the incoming projectile with the nuclear charge density of the target.

The electromagnetic interaction between the projectile of charge $Z_p e$, with its position in space defined, at time t, by the coordinates $r(t)$, $\theta(t)$, $\phi(t)$ with respect to a laboratory fixed reference frame fixed on the target, is given by

$$H_E(t) = \sum_{\lambda=1}^{\infty} \sum_{\mu=-\lambda}^{\lambda} \frac{4\pi Z_p e}{2\lambda+1} \mathcal{M}^*(E_{\lambda,\mu}) \frac{Y_{\lambda\mu}(\theta(t),\phi(t))}{r(t)^{\lambda+1}} \tag{1}$$

where $\mathcal{M}(E_{\lambda,\mu})$ is the electric multipole moment, defined from the nuclear charge density $\rho(\vec{r})$ by the relation:

$$\mathcal{M}(E_{\lambda,\mu}) = \int r^{\lambda} Y_{\lambda\mu}(\theta,\phi)\, \rho(\vec{r})\, d^3r \tag{2}$$

The wavefunction for the target satisfies the following Schrödinger equation:

$$i\hbar \frac{\partial}{\partial t} |\psi\rangle = [H_0 + H_E(t)]|\psi\rangle \tag{3}$$

where H_0 is the Hamiltonian of the free target. We see that the interaction with the projectile is represented by the time dependent potential $H_E(t)$.

If $\{|\phi_n>\}$ is the complete set of eigenfunctions of the Hamiltonian H_0:

$$H_0|\phi_n> = E_n|\phi_n> \ , \quad n = 0,1,2,... \tag{4}$$

a standard way of solving Eq. (3) is to use the fact that $\{|\phi_n>\}$ is a basis, and expand $|\psi>$ in this basis:

$$|\psi> = \sum_m a_m(t) \ |\phi_m> \ e^{-\frac{i}{\hbar}E_m t} \tag{5}$$

Replacing (5) into (3), and applying $<\phi_n|$ to both sides of the resulting expression, we find

$$i\hbar\frac{da_n(t)}{dt} = \sum_m <\phi_n|H_E(t)|\phi_m> \ e^{\frac{i}{\hbar}(E_n-E_m)t} \ a_m(t) \tag{6}$$

Since the target is initially in its ground state, the initial conditions for this system of first-order coupled differential equation is:

$$a_n(t = -\infty) = \delta_{0n} \tag{7}$$

The wave function after the interaction is determined from the asymptotic values of the coefficients a_n for $t \to +\infty$. The excitation probabilities are given by

$$P_n = |a_n(t=+\infty)|^2 \tag{8}$$

The matrix element $\langle\phi_n|H_E(t)|\phi_m\rangle$ is evaluated by using Eq. (1):

$$\langle\phi_n|H_E(t)|\phi_m\rangle = \sum_{\lambda=1}^{\infty}\sum_{\mu=-\lambda}^{\lambda} \frac{4\pi Z_p e}{2\lambda+1}\frac{Y_{\lambda\mu}(\theta(t),\phi(t))}{r(t)^{\lambda}} \tag{9}$$

$$\times \langle\phi_m|\mathcal{M}(E_{\lambda,\mu})|\phi_n\rangle$$

The nuclear states are specified by the spin quantum numbers I and M; therefore using Wigner-Eckart's theorem

$$\langle\phi_m|\mathcal{M}(E_{\lambda,\mu})|\phi_n\rangle = \langle I_m M_m|\mathcal{M}(E_{\lambda,\mu})|I_n M_n\rangle$$

$$= (-1)^{I_m - M_m}\begin{pmatrix} I_m & \lambda & I_n \\ -M_m & \mu & M_n \end{pmatrix}\langle I_m \| \mathcal{M}(E_\lambda) \| I_n\rangle \tag{10}$$

Replacing (10) into (9), and the resulting expression into (6) we find:

$$i\hbar\frac{d}{dt}a_{I_n M_n}(t) = \sum_{\lambda=1}^{\infty}\sum_{\mu=-\lambda}^{\lambda}\sum_{I_m M_m} \frac{(-1)^{I_m - M_m}}{2\lambda+1}$$

$$\times\begin{pmatrix} I_m & \lambda & I_n \\ -M_m & \mu & M_n \end{pmatrix}\langle I_m \| \mathcal{M}(E_\lambda) \| I_n\rangle \frac{Y_{\lambda\mu}(\theta(t),\phi(t))}{r(t)^{\lambda+1}} \tag{11}$$

$$\times e^{\frac{i}{\hbar}(E_n - E_m)t} a_{I_m M_m}(t)$$

Since the target is being described in quantum mechanical terms, the uncertainty principle forbids a precise description of how the instantaneous values of the internal coordinates affect the classical trajectory of the projectile. Therefore the trajectory of the projectile is supposed to be a hyperbola in which, in order to take into account the energy transfer between target and projectile, one takes a velocity

$$v = \sqrt{v_i \, v_f} \tag{12}$$

geometric mean of the velocities in the initial and final channels. For a final scattering angle θ, the eccentricity of the hyperbolic orbit is given by:

$$\varepsilon = \frac{1}{\sin\frac{\theta}{2}} \tag{13}$$

A convenient parametrization of the hyperbolic orbit in the coordinate system in which the z axis is perpendicular to the plane of the hyperbola and the x axis bisects it is given by:

$$\begin{aligned} x(\omega) &= a\,(\cosh\omega + \varepsilon) \\ y(\omega) &= a\,\sqrt{\varepsilon^2-1}\,\sinh\omega \\ z(\omega) &= 0 \\ r(\omega) &= a\,(\varepsilon\cosh\omega + 1) \\ t &= \frac{a}{v}\,(\varepsilon\sinh\omega + \omega) \end{aligned} \tag{14}$$

Using (14) we find

$$\frac{Y_{\lambda\mu}(\theta(t),\phi(t))}{r(t)^{\lambda+1}} = Y_{\lambda\mu}(\tfrac{\pi}{2},0)\ \frac{(\cosh\omega+\varepsilon+i\sqrt{\varepsilon^2-1}\sinh\omega)^{\mu}}{a^{\lambda+1}(\varepsilon\cosh\omega+1)^{\lambda+\mu}} \tag{15}$$

$$\frac{i}{\hbar}(E_n-E_m)t \approx i(\eta_m-\eta_n)(\varepsilon\sinh\omega+\omega) = i\,\xi(\varepsilon\sinh\omega+\omega) \tag{16}$$

where η_m and η_n represent the Sommerfeld parameter in the channels m and n respectively, and ξ is usually called the adiabaticity parameters.

Substituting (15) and (16) in (11) and using the definitions:

$$\chi^{(\lambda)}_{I_nI_m} \equiv \frac{4\pi Z_p e}{2\lambda+1} < I_m \| \mathcal{M}(E\lambda) \| I_n > \frac{m}{\hbar^2 k}\ \frac{(\lambda-1)!}{(2\lambda-1)!!}\ \frac{1}{a^{\lambda}\sqrt{\pi(2I_m+1)}} \tag{17}$$

$$W^{(\lambda,\mu)}_{I_nM_n,I_mM_m} = \sqrt{\pi(2I_m+1)}\ \frac{(2\lambda-1)!!}{(\lambda-1)!}(-1)^{I_m-M_m}\begin{pmatrix} I_m & \lambda & I_n \\ -M_m & \mu & M_n \end{pmatrix} Y_{\lambda\mu}(\tfrac{\pi}{2},0) \tag{18}$$

We obtain:

$$\frac{d}{d\omega} a_{I_n M_n}(\omega) = -i \sum_{I_m, M_m} \chi^{(\lambda)}_{I_n I_m} \; W^{(\lambda,\mu)}_{I_n M_n, I_m M_m} \; e^{i\xi(\varepsilon \sinh \omega + \omega)}$$

$$\times \frac{(\cosh \omega + \varepsilon + i\sqrt{\varepsilon^2 - 1} \sinh \omega)^{\mu}}{(\varepsilon \cosh \omega + 1)^{\lambda+\mu}} \; a_{I_m M_m}(\omega) \tag{19}$$

In the particular case of a rotor, the matrix elements are given by

$$\langle I_m \| \mathcal{M}(E\lambda) \| I_n \rangle = e \, Q_0^{(2)} \sqrt{\frac{(2\lambda+1)(2I_n+1)(2I_m+1)}{16\pi}} \begin{pmatrix} I_n & \lambda & I_m \\ 0 & 0 & 0 \end{pmatrix} \tag{20}$$

where $Q_0^{(2)}$ is the intrinsic quadrupole moment of the target.

Once the amplitudes $a_{IM}(t=+\infty)$ are known, the total excitation probability of a level of spin I is given by

$$P_{I_g \to I} = \frac{1}{2I_g+1} \sum_{M=-I}^{I} |a_{IM}(+\infty)|^2 \tag{21}$$

where I_g is the spin of the ground state.

The differential scattering cross section is obtained by multiplying the Rutherford cross section by this excitation probability:

$$\left.\frac{d\sigma}{d\Omega}\right|_{I_g \to I} = P_{I_g \to I} \left.\frac{d\sigma}{d\Omega}\right|_{\text{Rutherford}} = P_{I_g \to I} \frac{a^2}{4\sin^4 \frac{\theta}{2}} \tag{22}$$

REFERENCES

1. B. Mottelson, Rept. Intern. Phys. Conf., Copenhagen, June 1952 Reprinted in K. Alder and Aa. Winther "Coulomb Excitation", Academic Press, New York, New York (1966)
2. B. Mottelson, Office of Naval Research, European Scientific Notes, No. 7-9, May 1, 1953. Reprinted in K. Ander and Aa. Winther "Coulomb Excitation", Academic Press, New York, New York (1966)
3. T. Huus and C. Zupancic, Kgl. Dan. Vid. Selsk. Mat. Fys. Medd. 28, No. 1 (1953)
4. C. L. McClelland and C. Goodman, Phys. Rev. 91 (1953) 760
5. K. Alder, Aa. Bohr, T. Huus, B. Mottelson and Aa. Winther, Rev. Mod. Phys. 28 (1956) 432
6. F. Roesel, J. X. Saladin and K. Alder, Comp. Phys. Comm. 8 (1974) 35
7. K. Alder and Aa. Winther, Mat. Fys. Medd. Dan. Vid. Selsk. 32 (8) (1960)
8. Aa. Winther and J. de Boer, California Institute of Technology Technical Report, November 18, 1965, Reprinted in K. Alder and Aa. Winther "Coulomb Excitation", Academic Press, New York, New York (1966)
9. R. P. Feynman and A. R. Hibbs, "Quantum Mechanics and Path Integrals", McGraw Hill, New York (1965)
10. W. H. Miller, J. Chem. Phys. 53 (1970) 1949
11. W. H. Miller, J. Chem. Phys. 53 (1970) 3578

12. W. H. Miller, Chem. Phys. Lett. 7 (1970) 431

13. W. H. Miller and T. F. George, J. Chem. Phys. 56 (1972) 5668

14. T. F. George and W. H. Miller, J. Chem. Phys. 57 (1972) 2458

15. J. D. Doll, T. F. George and W. H. Miller, J. Chem. Phys. 58 (1973) 1343

16. S. M. Hornstein and W. H. Miller, J. Chem. Phys. 61 (1974) 745

17. S. D. Augustin and W. H. Miller, J. Chem. Phys. 61 (1974) 3155

18. A. W. Raczkowski and W. H. Miller, J. Chem. Phys. 61 (1974) 5413

19. R. A. Malfliet, Symposium on Classical and Quantum Mechanical Aspects of Heavy Ion Collisions, Heidelberg (1974)

20. T. Koeling and R. A. Malfliet, Phys. Rep. 22C (1975) 182

21. J. Knoll and R. Schaeffer, Phys. Lett. 52B (1974) 131

22. J. Knoll and R. Schaeffer, Ann. Phys. 97 (1976) 307

23. S. Levit, V. Smilanski and D. Pelte, Phys. Lett. 53B (1974) 39

24. H. Massmann and J. O. Rasmussen, Nucl. Phys. A243 (1975) 155

25. H. Massmann, Ph.D. Thesis, University of California, Berkeley (1975) Unpublished

26. M. W. Guidry, H. Massmann, R. Donangelo and J. O. Rasmussen, Nucl. Phys. A274 (1976) 183

27. R. A. Marcus, Chem. Phys. Lett. 7 (1970) 525

28. R. A. Marcus, J. Chem. Phys. 54 (1971) 3965

29. J.N.L. Connor and R. A. Marcus, J. Chem. Phys. 55 (1971) 5636

30. W. H. Wong and R. A. Marcus, J. Chem. Phys. 55 (1971) 5663

31. R. A. Marcus, J. Chem. Phys. 56 (1972) 311

32. R. A. Marcus, J. Chem. Phys. 56 (1972) 3548

33. J. Stine and R. A. Marcus, Chem. Phys. Lett. 15 (1972) 536

34. R. A. Marcus, J. Chem. Phys. 59 (1973) 5135

35. J. R. Stine and R. A. Marcus, J. Chem. Phys. 59 (1973) 5145

36. H. Kreek, R. L. Ellis and R. A. Marcus, J. Chem. Phys. 62 (1975) 913

37. L. I. Schiff, "Quantum Mechanics", 3rd Ed., McGraw Hill, New York (1968)

38. P.A.M. Dirac, "The Principles of Quantum Mechanics", 4th Ed., Oxford University Press, New York (1958)

39. H. Goldstein, "Classical Mechanics", Addison-Wesley, Reading, Massachusetts (1950)

40. A. Messiah, "Quantum Mechanics", John Wiley & Sons, New York (1966)

41. R. Donangelo, M. W. Guidry, J. P. Boisson and J. O. Rasmussen, Phys. Lett. 64B (1976) 377

42. L. C. Biedenharn and C. M. Class, Phys. Rev. 98 (1955) 691

43. K. Alder, R. Morf and F. Roesel, Phys. Lett. 32B (1970) 645

44. K. Alder, F. Roesel, and R. Morf, Nucl. Phys. A186 (1972) 449

45. K. Alder, in Proceedings of the International Conference on Reactions between Complex Nuclei, Nashville, Tenn. 10-14 June, 1974, edited by R. L. Robinson, F. K. McGowan, J. M. Ball, and J. H. Hamilton, North-Holland, Amsterdam/American Elsevier, New York, 1974, Vol. I, p. 94ff

46. J. de Boer, H. Massmann and A. Winther, Contribution to International Workshop III, on Gross Properties of Nuclei and Nuclear Excitations, Hirschegg, Austria, Jan. 13-18 (1975) (unpublished)

47. K. Alder and A. Winther, "Electromagnetic Excitation", North-Holland, Amsterdam/American Elsevier, New York (1975)

48. W. H. Miller, Adv. Chem. Phys. 25 (1974) 69

49. S. Levit and U. Smilansky, Weizmann Institute of Science, Preprint WIS-76157-Ph.

50. J. Randrup, W. J. Swiatecki and C. F. Tsang, Lawrence Berkeley Laboratory, preprint LBL-3603

51. J. P. Blocki, J. Randrup, W. J. Swiatecki and C. F. Tsang, to be published in Ann. Phys.

52. C. Ngô, B. Tamain, M. Beiner, R. J. Lombard, D. Mar and H. H. Deubler, Nucl. Phys. A252 (1975) 237

53. C. E. Bemis, Jr., F. K. McGowan, J.L.C. Ford, Jr., W. T. Milner, P. H. Stelson and R. L. Robinson, Phys. Rev. C8 (1973) 478

54. D. L. Hendrie, Phys. Rev. Letters 31 (1973) 478

55. J. R. Birkelund, J. R. Huizenga, H. Friesleben, K. L. Wolf, J. P. Unik and V. E. Viola, Jr., Phys. Rev. C13 (1976) 133

56. I.-Yang Lee, Ph.D. Thesis, University of Pittsburgh (1974) and private communication

57. R. A. Broglia, S. Landowne, R. A. Malfliet, V. Rostokin, and Aa. Winther, Phys. Rep. 11C (1974), 1.

58. H. Massmann, P. Ring and J. O. Rasmussen, Phys. Lett. 57B (1975)

59. P. Fröbrich, Q.K.K. Liu and K. Möhring, contribution to the Conference Europeenne de Physique Nucleaire avec des Ions Lourds, Caen, France, 1976

60. P. Fröbrich, Q.K.K. Liu and K. Möhring, contribution to the 4ème Session d'Etudes Biennale de Physique Nucléaire, La Toussouire, France, 1977

61. P. Fröbrich, Q.K.K. Liu and K. Möhring, private communication

62. E. Grosse, J. de Boer, R. M. Diamond, F. S. Stephens and P. Tjøm, Phys. Rev. Letters 35 (1975) 565

63. J. K. Poggenburg, H. J. Mang and J. O. Rasmussen, Phys. Rev. 181 (1969) 1697